Publications of the
Astronomical Society of the Pacific

Vol. 107 1995 September No. 715

Publications of the Astronomical Society of the Pacific
107: 803–845, 1995 September

Invited Review Paper

Unified Schemes for Radio-Loud Active Galactic Nuclei

C. MEGAN URRY

Space Telescope Science Institute, 3700 San Martin Drive, Baltimore, Maryland, 21218
Electronic mail: cmu@stsci.edu

PAOLO PADOVANI

Dipartimento di Fisica, II Università di Roma "Tor Vergata" Via della Ricerca Scientifica 1, I-00133 Roma, Italy
Electronic mail: padovani@roma2.infn.it

Received 1995 May 26; accepted 1995 May 31

ABSTRACT. The appearance of active galactic nuclei (AGN) depends so strongly on orientation that our current classification schemes are dominated by random pointing directions instead of more interesting physical properties. Light from the centers of many AGN is obscured by optically thick circumnuclear matter, particularly at optical and ultraviolet wavelengths. In radio-loud AGN, bipolar jets emanating from the nucleus emit radio through gamma-ray light that is relativistically beamed along the jet axes. Understanding the origin and magnitude of radiation anisotropies in AGN allows us to unify different classes of AGN; that is, to identify each single, underlying AGN type that gives rise to different classes through different orientations. This review describes the unification of radio-loud AGN, which include radio galaxies, quasars, and blazars. We describe the classification and general properties of AGN. We summarize the evidence for anisotropic emission caused by circumnuclear obscuration and relativistic beaming. We outline the two most plausible unified schemes for radio-loud AGN, one linking the high-luminosity sources (quasars and luminous radio galaxies) and one the low-luminosity sources (BL Lac objects and less luminous radio galaxies). Using the formalism appropriate to samples biased by relativistic beaming, we show that the population statistics for two schemes are in accordance with available data. We analyze the possible connections between low- and high-luminosity radio-loud AGN and conclude they probably are powered by similar physical processes, at least within the relativistic jet. We review potential difficulties with unification and conclude that none currently constitutes a serious problem. We discuss likely complications to unified schemes that are suggested by realistic physical considerations; these will be important to consider when more comprehensive data for larger complete samples become available. We conclude with a list of the ten questions we believe are the most pressing in this field.

TABLE OF CONTENTS

1. INTRODUCTION

The mystery of active galactic nuclei (AGN) is that they produce very high luminosities in a very concentrated volume, probably through physical processes other than the nuclear fusion that powers stars. AGN are thus special laboratories for extreme physics which we would like to understand. They are also our principal probes of the Universe on large scales, so understanding them is essential to studying the formation and evolution of the Universe.

At present, the approximate structure of AGN is known, but much of the detailed physics is literally hidden from view because of their strongly anisotropic radiation patterns. The prevailing (but not necessarily correct) picture of the physical structure of AGN is illustrated in Fig. 1 (Holt et al. 1992). At the center is a supermassive black hole whose gravitational potential energy is the ultimate source of the AGN luminosity. Matter pulled toward the black hole loses angular momentum through viscous or turbulent processes in an accretion disk, which glows brightly at ultraviolet and perhaps soft X-ray wavelengths. Hard X-ray emission is also produced very near the black hole, perhaps in connection with a pervasive sea of hot electrons above the disk. If the black hole is spinning, energy may be extracted electromagnetically from the black hole itself.

Strong optical and ultraviolet emission lines are produced in clouds of gas moving rapidly in the potential of the black hole, the so-called "broad-line clouds" (dark blobs in Fig. 1). The optical and ultraviolet radiation is obscured along some lines of sight by a torus (as shown in Fig. 1) or warped disk of gas and dust well outside the accretion disk and

broad-line region. Beyond the torus,[1] slower moving clouds of gas produce emission lines with narrower widths (grey blobs in Fig. 1). Outflows of energetic particles occur along the poles of the disk or torus, escaping and forming collimated radio-emitting jets and sometimes giant radio sources when the host galaxy is an elliptical, but forming only very weak radio sources when the host is a gas-rich spiral. The plasma in the jets, at least on the smallest scales, streams outward at very high velocities, beaming radiation relativistically in the forward direction.

This inherently axisymmetric model of AGN implies a radically different AGN appearance at different aspect angles. In practice, AGN of different orientations will therefore be assigned to different classes. Unification of these fundamentally identical but apparently disparate classes is an essential precursor to studying the underlying physical properties of AGN. The ultimate goal is to discover which are the fundamentally important characteristics of AGN—e.g., black- hole mass, black-hole spin, accretion rate, host galaxy type, interaction with neighboring galaxies—and how they govern the accretion of matter, the formation of jets, and the production of radiation in these bizarre objects.

This review covers the unification of radio-loud AGN, i.e., those with prominent radio jet and/or lobe emission. Comparable unification schemes for radio-quiet objects (Rowan-Robinson 1977; Lawrence and Elvis 1982; Antonucci and Miller 1985), which have not been explored using the same statistical techniques, have recently been reviewed by Antonucci (1993; his review includes radio-loud AGN as well) and are not discussed here. In the following sections, we describe current AGN classification schemes (Sec. 2) and the two principal causes of anisotropic radiation, obscuration (Sec. 3) and relativistic beaming (Sec. 4). We establish the motivation for current unification schemes for high- and low-luminosity[2] radio-loud AGN (Sec. 5) and then discuss them quantitatively (Sec. 6). We discuss the possible connections among high- and low-luminosity AGN and other aspects of the unification paradigm (Sec. 7), including potential problems, complications, and future tests (Sec. 8). In the final section (Sec. 9), we briefly summarize the status of unification and pose what we believe are the ten most important questions at the current time. In the Appendices, we present equations governing the various beaming parameters (A), the Doppler enhancement (B), and the ratio of core to extended flux (C), and a glossary of acronyms used in the paper (D). Throughout this review the values $H_0=50$ km s^{-1} Mpc^{-1} and $q_0=0$ have been adopted (unless otherwise stated) and the spectral index α is defined such that $F_\nu \propto \nu^{-\alpha}$.

[1]For convenience, we tend to refer to the obscuring matter as a torus, but to date there is little to indicate whether it is actually a torus, a warped disk, or some other distribution (cf. Sec. 8.2.1).

[2]In all that follows, we compute *observed* luminosities assuming spherical symmetry, i.e., we assume uniform emission into 4π steradians. If an AGN radiates anisotropically, it may be called a "high-luminosity" source even though its intrinsic luminosity is low.

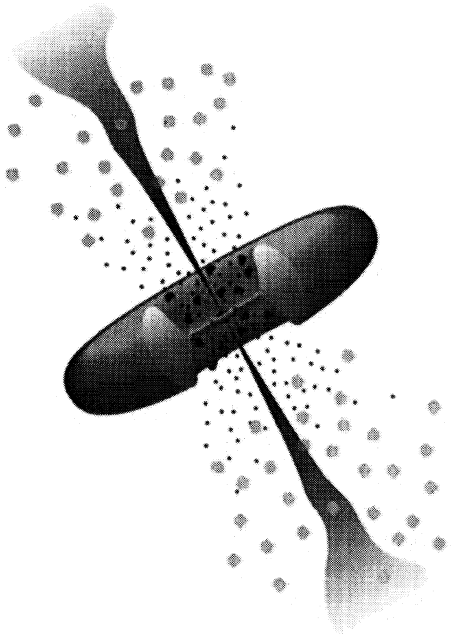

FIG. 1—A schematic diagram of the current paradigm for radio-loud AGN (not to scale). Surrounding the central black hole is a luminous accretion disk. Broad emission lines are produced in clouds orbiting above the disk and perhaps by the disk itself. A thick dusty torus (or warped disk) obscures the broad-line region from transverse lines of sight; some continuum and broad-line emission can be scattered into those lines of sight by hot electrons that pervade the region. A hot corona above the accretion disk may also play a role in producing the hard X-ray continuum. Narrow lines are produced in clouds much farther from the central source. Radio jets, shown here as the diffuse jets characteristic of low-luminosity, or FR I-type, radio sources, emanate from the region near the black hole, initially at relativistic speeds. For a $10^8 M_\odot$ black hole, the black hole radius is $\sim 3\times10^{13}$ cm, the accretion disk emits mostly from ~ 1–30×10^{14} cm, the broad-line clouds are located within ~ 2–20×10^{16} cm of the black hole, and the inner radius of the dusty torus is perhaps $\sim 10^{17}$ cm. The narrow-line region extends approximately from 10^{18}–10^{20} cm, and radio jets have been detected on scales from 10^{17} to several times 10^{24} cm, a factor of ten larger than the largest galaxies.

2. OBSERVED PROPERTIES AND EMPIRICAL CLASSIFICATION OF AGN

The full complement of active galactic nuclei constitutes a zoo of different names, detection criteria, and spectral, polarization, and variability characteristics. As in biology, however, taxonomy derived from empirical observations can impose some order on the chaos. Table 1 shows the principal classes of AGN (adapted from Lawrence 1987, 1993), organized according to their radio loudness and their optical spectra, i.e., whether they have broad emission lines (Type 1), only narrow lines (Type 2), or weak or unusual line emission. Within each of the groupings, different types of AGN are listed by increasing luminosity. We now explain Table 1 in more detail.

Roughly 15%–20% of AGN are radio-loud, meaning they have ratios of radio (5 GHz) to optical (B-band) flux $F_5/F_B \gtrsim 10$ (Kellermann et al. 1989), although this fraction increases with optical (Padovani 1993; La Franca et al. 1994) and X-ray (Della Ceca et al. 1994) luminosities, reaching, for example, $\sim$50% at $M_B \lesssim -24.5$. With few exceptions, the

TABLE 1
AGN Taxonomy

Radio Loudness	Optical Emission Line Properties: Type 2 (Narrow Line)	Type 1 (Broad Line)	Type 0 (Unusual)
Radio-quiet:	Sy 2 NELG	Sy 1	
	IR Quasar?	QSO	BAL QSO?
Radio-loud:	NLRG {FR I FR II	BLRG SSRQ FSRQ	Blazars {BL Lac Objects (FSRQ)

Black Hole Spin?

Decreasing angle to line of sight

optical and ultraviolet emission-line spectra and the infrared to soft X-ray continuum of most radio-loud and radio-quiet AGN are very similar (Sanders et al. 1989) and so must be produced in more or less the same way. The characteristic of radio loudness itself may be related in some way to host galaxy type (Smith et al. 1986) or to black hole spin (Blandford 1990; Wilson and Colbert 1995), which might enable the formation of powerful relativistic jets.

Based on the characteristics of their optical and ultraviolet spectra, AGN can be separated into the three broad types shown in Table 1.

(1) Those with bright continua and broad emission lines from hot, high-velocity gas, presumably located deep in the gravitational well of the central black hole, are known as Type 1 AGN. In the radio-quiet group, these include the Seyfert 1 galaxies, which have relatively low luminosities and therefore are seen only nearby, where the host galaxy can be resolved, and the higher-luminosity radio-quiet quasars (QSO), which are typically seen at greater distances because of their relative rarity locally and thus rarely show an obvious galaxy surrounding the bright central source. The radio-loud Type 1 AGN are called Broad-Line Radio Galaxies (BLRG) at low luminosities and radio-loud quasars at high luminosities, either Steep Spectrum Radio Quasars (SSRQ) or Flat Spectrum Radio Quasars (FSRQ) depending on radio continuum shape, with the dividing line set at $\alpha_r = 0.5$ (where the radio spectrum is measured at a few GHz). Other than luminosity, little distinguishes Seyfert 1s from radio-quiet quasars, or BLRG from radio quasars.

(2) Type 2 AGN have weak continua and only narrow emission lines, meaning either that they have no high-velocity gas or, as we now believe, the line of sight to such gas is obscured by a thick wall of absorbing material. Radio-quiet Type 2 AGN include Seyfert 2 galaxies at low luminosities, as well as the narrow-emission-line X-ray galaxies (NELG; Mushotzky 1982). The high-luminosity counterparts are not clearly identified at this point, but likely candidates are the infrared-luminous *IRAS* AGN (Sanders et al. 1988; Hough et al. 1991; Wills et al. 1992b), which may show a predominance of Type 2 optical spectra (Lawrence et al. 1995).

Radio-loud Type 2 AGN, often called Narrow-Line Radio Galaxies (NLRG), include two distinct morphological types: the low-luminosity Fanaroff–Riley type I radio galaxies (Fanaroff and Riley 1974), which have often-symmetric radio jets whose intensity falls away from the nucleus, and the high-luminosity Fanaroff–Riley type II radio galaxies, which have more highly collimated jets leading to well-defined lobes with prominent hot spots (see Sec. 5.2). Examples of FR I and FR II radio morphologies are shown in Fig. 2.

(3) A small number of AGN have very unusual spectral characteristics. Inventing a term, we call these Type 0 AGN and speculate that they are related by a small angle to the line of sight ("near 0 degrees"). These include the BL Lacertae (BL Lac) objects, which are radio-loud AGN that lack strong emission or absorption features (typical equivalent width limits are set at $W_\lambda < 5$ Å). In addition, roughly 10% of radio-quiet AGN have unusually broad P-Cygni-like absorption features in their optical and ultraviolet spectra, and so are known as BAL (Broad Absorption Line) quasars (Turnshek 1984). If BAL spectral features are caused by polar outflows at small angles to the line of sight, they too are Type 0 AGN as indicated in Table 1; alternatively, they may have edge-on disks with winds instead (Turnshek 1988). There are no known radio-quiet BL Lacs. A subset of Type 1 quasars, including those defined variously as Optically Violently Variable (OVV) quasars, Highly Polarized Quasars (HPQ),[3] Core-Dominated Quasars (CDQ), or FSRQ, are probably also found at a small angle to the line of sight. Their continuum emission strongly resembles that of BL Lac objects (apart from the presence of a blue "bump" in a few cases) and, like BL Lac objects, they are characterized by very rapid variability, unusually high and variable polarization, high brightness temperatures (often in excess of the Compton limit $T \sim 10^{12}$ K; Quirrenbach et al. 1992), and superluminal velocities of compact radio cores (Sec. 4.). Although the names OVV, HPQ, CDQ, and FSRQ reflect different empirical definitions, evidence is accumulating that they are all more or less the same thing—that is, the majority of flat-

[3]We refer here only to radio-loud HPQ. While a few radio-quiet quasars also have highly polarized optical emission, and thus fit the HPQ definition, their polarization is almost certainly caused by scattering rather than intrinsic emission processes.

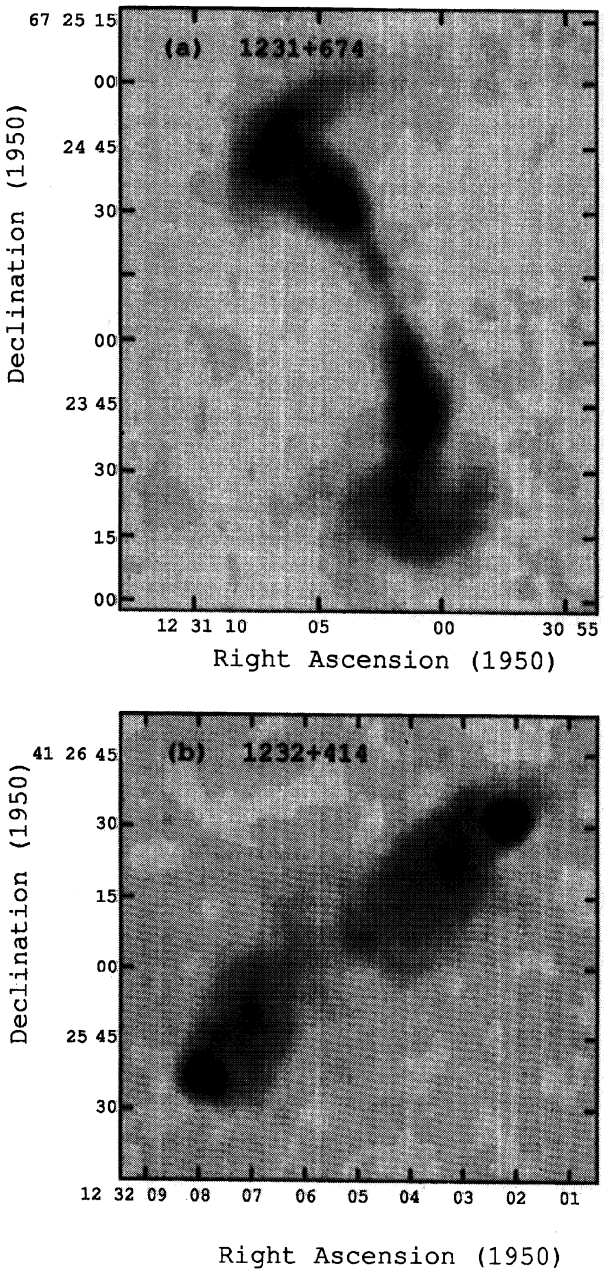

FIG. 2—Radio images of the two types of radio galaxies: (a) at low luminosity, an FR I radio galaxy, 1231+674, with diffuse, approximately symmetric jets whose surface brightness falls off away from the center, and (b) at high luminosity, an FR II radio galaxy, 1232+414, with sharp-edged lobes and bright hot spots; the jets in this case are often too faint to see. (Courtesy of Frazer Owen and Mike Ledlow.)

spectrum radio quasars tend to show rapid variability, high polarization, and radio structures dominated by compact radio cores, and *vice versa* (Fugmann 1989; Impey et al. 1991; Valtaoja et al. 1992; Wills et al. 1992a)—so hereafter we refer to them simply as FSRQ. Collectively, BL Lacs and FSRQ are called blazars. Even though the FSRQ have strong broad emission lines like Type 1 objects, they are noted in the "Type 0" column in Table 1 because they have the same blazar-like continuum emission as BL Lac objects.

We have described an empirical division of AGN according to radio and optical/ultraviolet properties. Table 1 is analogous to the Periodic Table of the Elements developed by chemists a century or so ago, when many chemical elements had been discovered and studied but the relations among them were not entirely clear. Where in chemistry it was eventually recognized that valence electrons dominate the horizontal relations and nuclear mass the vertical relations, we will argue that the categories in this "Periodic Table of the AGN" are distinguished primarily by orientation effects along the horizontal direction and by as-yet unknown physics in the vertical direction.

Whether AGN are classified Type 1 or Type 2 depends on obscuration of the luminous nucleus, and whether a radio-loud AGN is a blazar or a radio galaxy depends on the alignment of the relativistic jet with the line of sight. These two causes of anisotropy, obscuration of infrared through ultraviolet light by optically thick gas and dust, and relativistic beaming of radio jets, both important in radio-loud objects, are discussed in turn in the next two sections, which can be skipped by readers interested only in the actual unification schemes. Note that the unification of quasars with high-luminosity radio galaxies requires both kinds of anisotropy, while the unification of BL Lac objects with low-luminosity radio galaxies requires (at present) only relativistic beaming.

3. ANISOTROPIC RADIATION FROM OBSCURATION

The central regions of many AGN appear to contain obscuring material, probably in the form of dust, that prevents infrared through ultraviolet light from penetrating some lines of sight (Rowan-Robinson 1977). This dust may be distributed in a torus (Pier and Krolik 1992, 1993) or in a warped disk (Sanders et al. 1989). In either case, it causes AGN to look markedly different from different aspect angles. Direct evidence for obscuration has been found in many Type 2 AGN, although mostly in the more numerous radio-quiet objects. Those NLRG in which obscuration has been detected because of scattered broad emission lines are all FR IIs; detection of such hidden lines in FR Is would provide an intriguing connection between the high- and low-luminosity unification schemes.

3.1 Polarimetric Evidence for Hidden Nuclear Regions

The most direct evidence for circumnuclear obscuration comes from spectropolarimetry of Type 2 objects, particularly the nearby Seyfert 2 NGC 1068 (Antonucci and Miller 1985) and the radio galaxy 3C 234 (Antonucci 1984). Some fraction of the light from these objects is highly polarized, and their polarized spectra have strong broad lines like Type 1, rather than Type 2 objects. Much of the polarization is probably caused by electron scattering since it is wavelength independent; some scattering by dust clouds has also been observed (Miller et al. 1991). In 3C 234, the plane of polarization is perpendicular to the radio jet axis, as expected if a

Type 1 nucleus is at least partially obscured by a thick wall of gas and dust whose axis coincides with the radio jet axis.[4] The continuum luminosity inferred from the strength of the scattered broad lines is quasar-like.

Subsequent polarization observations generally support the picture of scattered light from a luminous, hidden continuum source in NLRG. Like 3C 234, the radio galaxy IC 5063 has polarized broad lines, indicative of scattered light from a hidden broad-line region (Inglis et al. 1993). Spectropolarimetry of three powerful radio galaxies at $z\sim1$ has shown broad polarized Mg II lines, with equivalent widths typical of those observed in radio-loud quasars (di Serego Alighieri et al. 1994a). Multiwavelength polarimetry of 3C 109 (Goodrich and Cohen 1992) suggests polarization by transmission through dust, in which case the intrinsic luminosity is also quasar-like.[5]

Recent *HST* spectra of Cygnus A show a broad Mg II emission line which appears to be reflected from the southeast knot (a region of extended featureless optical continuum; Pierce and Stockton 1986). This is a direct signature of the hidden quasar in this luminous FR II galaxy (Antonucci et al. 1994); that broad emission lines have not been detected with optical spectropolarimetry (Jackson and Tadhunter 1993) may be because of dilution by the local optical continuum at the scattering site (Antonucci et al. 1994; Sec. 8.2.6).

Imaging polarimetry of the radio galaxies PKS 2152−69 (di Serego Alighieri et al. 1988), 3C 277.2 (di Serego Alighieri et al. 1989), Cygnus A (Tadhunter et al. 1990), 3C 368 (di Serego Alighieri et al. 1989; Scarrott et al. 1990), and additional radio galaxies (Cimatti et al. 1993, and references therein) reveals extended regions of polarized continuum emission which appear to be nuclear continuum scattered by ambient dust and/or electrons. Tadhunter et al. (1989; see also Cimatti et al. 1993 and di Serego Alighieri et al. 1994a) have suggested that dust scattering of quasar radiation could also explain the so-called "alignment effect" observed in high-redshift radio galaxies (McCarthy et al. 1987; Chambers et al. 1987), i.e., the correlation between the direction of the radio axis and the optical structure (extended emission-line regions plus continuum).

3.2 Infrared and X-Ray Evidence for Hidden Nuclear Regions

Since optical depth decreases at wavelengths longer than the optical, infrared observations are potentially much deeper probes of the nuclear regions of Type 2 AGN. Compact, bright, infrared cores and/or wavelength-independent perpendicular polarization as in 3C 234 have been found in about a dozen narrow-line radio galaxies, of both high and low luminosities (Bailey et al. 1986; Fabbiano et al. 1986; Hough et al. 1987; Antonucci and Barvainis 1990; McCarthy et al. 1990; Djorgovski et al. 1991). In a few cases, infrared spectroscopy has revealed broad wings on the Paschen lines (Fabbiano et al. 1986; Hill et al. 1995), at least partially revealing the infrared high-velocity gas that is completely obscured at optical wavelengths. In others the hidden infrared–optical continuum source and broad-line region remain stubbornly hidden, suggesting the expected optical depths are quite large; for example, up to 25–50 mag of visual extinction to the nucleus are estimated in the case of Cygnus A (Ward et al. 1991; Djorgovski et al. 1991).

The weakness of the X-ray continuum from Type 2 AGN relative to Type 1s is also consistent with the idea of an obscured nucleus (Lawrence and Elvis 1982; Fabbiano et al. 1984; Fabbiano et al. 1986). The X-ray spectrum of Cygnus A, a classic high-luminosity narrow-line radio galaxy, is commensurate with a typical quasar spectrum absorbed by a high column density of cold gas along the line of sight (Arnaud et al. 1987; Ward et al. 1991; Ueno et al. 1994). Similar high column densities are deduced from X-ray measurements of a number of Type 2 AGN, exactly as expected if the central source in Type 2s is obscured from direct view (Mulchaey et al. 1992).

3.3 Anisotropic Illumination of Narrow Emission Line Gas

The presence of anisotropic continuum emission can be inferred from the extended narrow-line regions, sometimes tracing ionizing light cones, seen in direct imaging of many nearby Type 2 AGN. High-resolution *HST* images of NGC 1068 in the light of [O III] (Evans et al. 1991) confirm in exciting detail earlier ground-based evidence for an ionization cone with apex at an obscured nucleus (Pogge 1988). Figure 3 shows the *HST* image of another nearby Seyfert 2 galaxy, NGC 5728 (Wilson et al. 1993); the conical shape of the ionized gas and its filamentary structure are both apparent. In these and other cases, the biconical structure suggests that an obscured nuclear source with quasar-like luminosity is photoionizing gas in the extended narrow-line region (Robinson et al. 1987; Baum and Heckman 1989; Tadhunter and Tsvetanov 1989; Wilson et al. 1993).

At present, there is no direct evidence (i.e., from spectropolarimetry) for obscuration in low-luminosity, FR I radio galaxies, although there are strong indications of anisotropic continuum emission in some individual objects. (Indirect evidence for obscuration in FR Is as a class is discussed in Sec. 5.4.) The FR I radio galaxy PKS 2152−69 shows optical line emission from a gas cloud at a projected distance of 8 kpc from the nucleus which, if due to excitation from a beamed nuclear source, implies an ionizing beam power well within the range for BL Lacs (di Serego Alighieri et al. 1988).

Similarly, in the FR I radio galaxy Centaurus A, optical

[4]Antonucci (1984) identified 3C 234 as a narrow-line radio galaxy even though it has broad Hα (Grandi and Osterbrock 1978). His point was that 3C 234 is equivalent to a narrow-line object like NGC 1068 because its broad lines are very highly polarized and therefore must be scattered. The broad emission lines of 3C 234 were not really "hidden" prior to the spectropolarimetric observations (although they were not strong broad lines that would clearly mark it as a quasar), but spectropolarimetry indicated that a direct view to the broad-line region was obscured. The fuzzy definition of "broad-line" (Type 1) objects is discussed further in the footnote in Sec. 6.1.1.

[5]Like 3C 234, 3C 109 has strong broad lines observable in total flux, in this case Hα. While the spectral shapes of the polarized continuum in 3C 109 and 3C 234 are similar, the polarization in 3C 234 is too high to be caused by dust transmission (Goodrich, private communication).

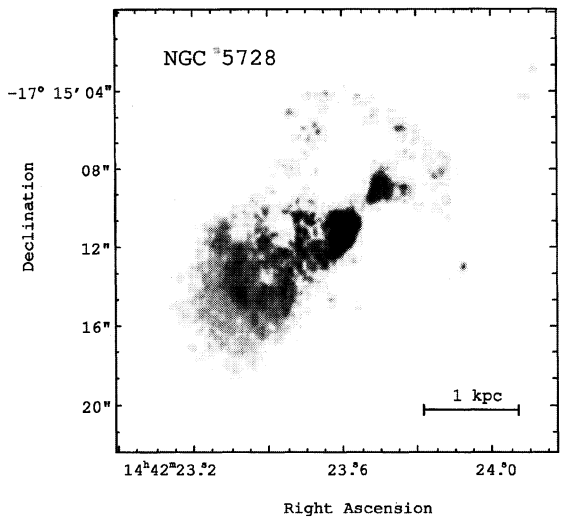

FIG. 3—*HST* WFPC image of the nearby Seyfert 2 galaxy NGC 5728 taken in the light of [O III] with resolution 0.1 arcsec (Wilson et al. 1993). The biconical structure suggests that a hidden nuclear source with quasar-like ultraviolet luminosity is photoionizing gas in the narrow-line region. (Copyright American Astronomical Society, reprinted with permission.)

emission-line filaments subtend a small projected solid angle in the northwest part of the galaxy, roughly aligned with the position of the jet-like structures found in the X-ray and radio bands (Morganti et al. 1991). A detailed analysis of the line ratios in the Cen A filaments suggests they are photoionized by strongly anisotropic radiation, about two orders of magnitude larger in the X-ray band than that observed directly (Morganti et al. 1992). Were this due to simple obscuration of an isotropic continuum by a thick torus, the obscured radiation would be reradiated in the infrared, contrary to observation. At least some of the continuum emission must be obscured, however, as the variable (i.e., nuclear) X-ray source in Cen A is heavily absorbed (Mushotzky et al. 1978). The continuum anisotropy in Centaurus A could be caused by relativistic beaming (see Sec. 4)—its inferred beam power is similar to that of BL Lacertae (Morganti et al. 1991)—or the optical filaments could be excited by local shocks where the northern radio jet interacts with a dense cloud of material (Sutherland et al. 1993). We note that illuminated clouds like those seen in Cen A and PKS 2152−69 are expected if FR Is found in cooling flow clusters contain hidden BL Lacs (Sarazin and Wise 1993).

4. ANISOTROPIC RADIATION FROM RELATIVISTIC BEAMING

When an emitting plasma has a bulk relativistic motion relative to a fixed observer, its emission is beamed in the forward direction (in the fixed frame), a direct consequence of the transformation of angles in special relativity. An observer located in or near the path of such a plasma sees much more intense emission than if the same plasma were at rest. Time scales for variability are also shorter, and this can cause the emission region to appear to move superluminally in the transverse direction (Appendix A). Strong relativistic beaming is thought to explain the rapid variations, high polarization, and high luminosities that characterize blazars (Blandford and Rees 1978), and if present in blazars, it must also be present in other radio-loud AGN. The consequences of the anisotropic beamed radiation pattern are considerable (Appendices B and C), introducing significant selection effects in almost any flux-limited sample.

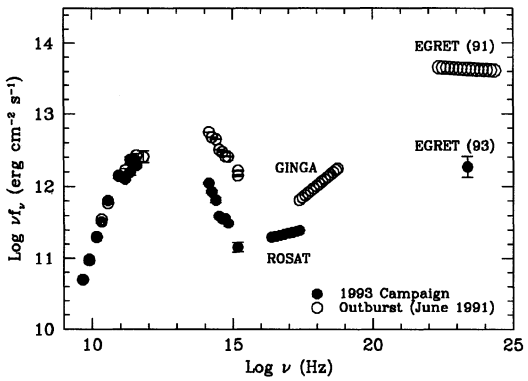

FIG. 4—Multiwavelength spectra of the gamma-ray-bright superluminal quasar 3C279 (Maraschi et al. 1994a) at two epochs, a high state in June 1991 and a low state in January 1993. In the high state, the gamma-ray luminosity is ten times the luminosity in the synchrotron component seen at lower energies, while in the low state the two are comparable. (Copyright American Astronomical Society, reproduced with permission.)

4.1 Evidence for Relativistically Beamed Gamma Rays

More than forty blazars have now been detected with the EGRET high energy experiment on the *Compton Gamma-Ray Observatory* (von Montigny et al. 1995). Without exception, all EGRET-detected extragalactic objects are radio-loud blazars, either FSRQ or BL Lac objects (primarily the former). Not only are blazars bright at $E \geq 100$ MeV, in many cases their observed gamma-ray luminosity dominates the luminosity in other wavebands by a factor between 1 and 1000. Multiwavelength spectra of the superluminal quasar 3C 279 (Fig. 4) show that the ratio of gamma-ray to bolometric luminosity increases with overall luminosity (Maraschi et al. 1994a).

In several blazars, the observed high-energy gamma rays are highly variable, on time scales of a few days.[6] For example, the intensity of 3C 279 ($z=0.538$) declined by a factor of 4–5 in less than 3 days (Fig. 5; Kniffen et al. 1993), and the blazar PKS 0528+134 ($z=2.06$) more than doubled its intensity in 5 days (Hunter et al. 1993).

This rapid variability leads to a largely model-independent argument that the gamma rays, at least, must be relativistically beamed (Maraschi et al. 1992). This argument does not depend on which physical mechanism gives rise to the gamma-ray emission, simply on the observed luminosity and variability time scales at high energies. Specifically, in

[6]The variability time scale can be defined in several ways, including the doubling time $[t_d=\langle F\rangle(dF/dt)^{-1}]$ or the e-folding time $[t_e=(d \ln F/dt)^{-1}]$. Either is fine for the rough estimates here as long as it is derived from a substantial change in flux ($\gtrsim$30%).

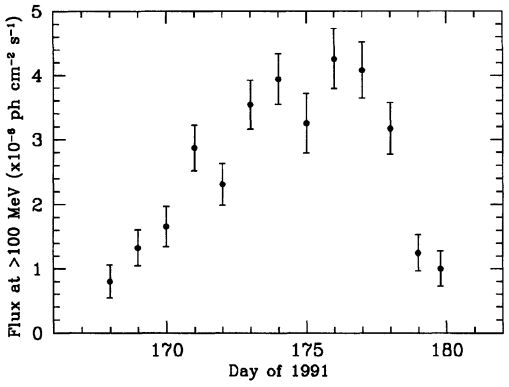

FIG. 5—Gamma-ray light curve of the superluminal quasar 3C 279 during the bright outburst in June 1991 (Kniffen et al. 1993). The combination of rapid variability and high gamma-ray luminosity strongly suggests the emission is relativistically beamed. (Copyright American Astronomical Society, reproduced with permission.)

order for gamma rays to escape the source, the optical depth to pair production, $\tau_{\gamma\gamma}$, must be of order unity or less, which is equivalent to saying the compactness, a convenient dimensionless parameter that represents source luminosity divided by dimension, must be less than about 40 at the threshold for pair production. That is, $\tau_{\gamma\gamma}\sim\ell/40\ll 1$, where $\ell=(L/r)(\sigma_T/m_e c^3)$ is the compactness, L and r are the source luminosity and dimension, respectively, and m_e and c are the usual constants (electron mass and speed of light). The Thomson cross section, σ_T, is appropriate because most pairs will be produced by X–γ interactions.

For 3C 279 and PKS 0528+134, the inferred values for the compactness are 5000 to 15,000, well in excess of the optical depth limit. In order that we observe gamma rays from these blazars, the true gamma-ray luminosity, $\mathscr{L}$, must be much smaller than observed and the true dimension much larger. Relativistic beaming has the effect that $L_{\rm obs}=\delta^4\mathscr{L}$ [Eq. (B5)], where δ is the Doppler beaming factor (Appendix A). If r is estimated from the variability time scale ($r\sim\delta c\Delta t$), then

$$\ell=\delta^{-5}\frac{L_{\rm obs}}{\Delta t_{\rm obs}}\frac{\sigma_T}{m_e c^4}. \quad (1)$$

The limit $\ell\lesssim 40$ then translates to $\delta\gtrsim 6$ for 3C 279 and $\delta\gtrsim 7$ for PKS 0528+134, where $L_{\rm obs}$ has been evaluated at X-ray energies under reasonable spectral assumptions (Maraschi et al. 1992); similar limits are obtained for all the gamma-ray blazars (Dondi and Ghisellini 1995). For comparison, the values derived in an entirely independent way from a synchrotron self-Compton calculation using radio and X-ray data (see Sec. 4.4) are $\gtrsim 18$ for 3C 279 and 3 for PKS 0528+134 (Ghisellini et al. 1993).

Note that no radio-quiet AGN have been detected so far with EGRET. One cannot rule out that, since gamma-ray power appears to correlate with radio power (Padovani et al. 1993), radio-quiet AGN might still have blazar-like spectra with high-energy (>50 MeV) emission well below the sensitivity of EGRET. This is unlikely, however, because OSSE observations of Seyfert 1 galaxies show steep cutoffs above ~50 keV, in sharp contrast to the hard spectra of radio-loud objects (Kurfess et al. 1994). The difference in gamma-ray properties may then be related to radio loudness, which in turn must be closely associated with relativistic beaming.

4.2 Superluminal Motion in Radio Jets

The term "superluminal motion" describes proper motion of source structure (traditionally mapped at radio wavelengths) that, when converted to an apparent speed v_a, gives $v_a>c$. This phenomenon occurs for emitting regions moving at very high (but still subluminal) speeds at small angles to the line of sight (Rees 1966). Relativistically moving sources "run after" the photons they emit, strongly reducing the time interval separating any two events in the observer's frame and giving the impression of faster than light motion (Appendix A).

Typical proper motions observed with Very Long Baseline Interferometry (VLBI) are in the range 0.1 to 1 milliarcsec yr^{-1} and imply apparent velocities up to $\sim 30c/(H_0/50)$ (Vermeulen and Cohen 1994). The majority of superluminal sources are FSRQ and BL Lacs, although this is in part a selection effect since these objects have the brightest cores and so are more easily observed with VLBI. Blazars do tend to have the largest apparent velocities (Ghisellini et al. 1993; Vermeulen and Cohen 1994), in agreement with the idea that their jets are more aligned with the line of sight than other classes of radio-loud AGN.

Detection of superluminal motion does not necessarily imply that the source of radiation is moving at near-relativistic speeds. For example, the tip of a rotating beam of light moves faster than light at a distance $r>c/\omega$, where ω is the angular speed. If the beam ionizes material that re-emits the radiation, the observer will detect superluminal motion even though the ionized material is not moving at all. (Of course, a simple rotating-beam model would predict some cases of superluminal contractions, i.e., negative values of v_a, contrary to observation; Vermeulen and Cohen 1994.) Apparent superluminal motion requires only a relativistic phase or pattern speed, which could be different from the bulk velocity of the radiating plasma itself.

Whether the pattern speed inferred from superluminal motion differs from the bulk motion of the plasma, as predicted by jet models that include relativistic shocks (Lind and Blandford 1985), is a matter of current debate (Ghisellini et al. 1993; Vermeulen and Cohen 1994; Kollgaard 1994). There is an observed correlation between the apparent superluminal velocity and the Doppler beaming factor (Ghisellini et al. 1993), thus connecting superluminal motion directly to bulk relativistic motion (Sec. 6.3). A particularly nice local laboratory has been found by Mirabel and Rodriguez (1994), who discovered a galactic superluminal source for which both jet and counterjet are seen and the two expansion velocities and luminosities are measured. In this case the pattern and bulk velocity are probably quite similar, with $\beta_{\rm bulk}/\beta_{\rm pattern}\sim 0.8$ (Appendix B; Bodo and Ghisellini 1995). A second galactic superluminal source has since been discovered, with similar bulk velocity and lying roughly in the

plane of the sky, but with significant intrinsic jet asymmetries (Tingay et al. 1995; Hjellming and Rupen 1995).

4.3 Observed Radio Jet Asymmetries

One of the intriguing characteristics of jets imaged on the sky is that they are often one-sided, almost exclusively so for the high-luminosity AGN (Bridle and Perley 1984), for the parsec scale jets measured with VLBI (Cawthorne 1991), and even at the base of the symmetric jets in low-luminosity objects (Bridle and Perley 1984; Parma et al. 1987). This raises the key question of whether jets are intrinsically one-sided or have one of two intrinsically equal jets brightened by relativistic beaming. If observed superluminal velocities on parsec scales are due to bulk relativistic motion of the emitting plasma, the enormous intensity enhancement from relativistic aberration would inevitably cause jet one-sidedness [Eq. (A8)]. The continuity of sidedness between parsec and kiloparsec scales would then argue for large-scale superluminal motions, which in turn implies kinetic energies many orders of magnitude larger than required by the parsec-scale jets.

The evidence for relativistic speeds on the larger scales is largely circumstantial but not easily dismissed. Wherever one-sided jets are seen on the small scale, they are on the same side as those seen on the large scale, strongly suggesting a connection between the two (Bridle 1992). Studies of the nearby FR I radio galaxy M87 support the hypothesis that its jets are intrinsically two-sided: first, modest superluminal motion has been detected on kiloparsec scales (Biretta et al. 1995) and second, an invisible counterjet has been inferred from the optically polarized hot spot in the extended radio lobe on the counterjet side (Stiavelli et al. 1992; Sparks et al. 1992). Similarly, optical evidence for an invisible counterjet was seen in the superluminal BLRG 3C 120 (Axon et al. 1989).

More general evidence for Doppler enhancement of large-scale jets is found in the depolarization asymmetry in radio lobes (Laing 1988; Garrington and Conway 1991). If jet one-sidedness indicates an oncoming high-velocity jet, then the extended radio lobe on the jet side should be closer to us than the lobe on the opposite side. In 49 of the 69 sources studied by Garrington and Conway (1991), the lobe on the counterjet side is more depolarized than the one on the jet side, exactly as expected if it were further away and had more depolarizing material along the line of sight. The differential depolarization is explained well by a hot gaseous halo surrounding the radio source (Tribble 1992). It may be possible to ascertain the characteristics of the depolarizing gas independently through sensitive X-ray observations with *AXAF*, which would confirm that the one-sidedness of most kpc-scale jets is caused by relativistic beaming. We note that in some cases asymmetric radio jet emission correlates spatially with the extended optical emission line gas, which is clearly not beamed, indicating that intrinsic asymmetries are also present at some level in radio sources (McCarthy et al. 1991).

Finally, supporting evidence for the preponderance of relativistic jets comes from large surveys of radio-loud AGN (Hough and Readhead 1989; Impey et al. 1991). Just as one would expect if all jets were relativistic, the ratio of core radio emission (presumably relativistically beamed) to extended (clearly unbeamed) radio emission is correlated with optical polarization, optical power-law fraction, degree/rapidity of variability, jet curvature, and superluminal motion, and is inversely correlated with linear size.[7]

4.4 Brightness Temperature Calculations and SSC Models

The smooth nonthermal radio-through-infrared continuum emission in radio-loud AGN is probably synchrotron radiation, i.e., emission from relativistic electrons moving in a magnetic field. Some of the synchrotron photons will be inverse Compton scattered to higher energies by the relativistic electrons, which is known as the synchrotron self-Compton (SSC) process. For some radio-loud AGN the synchrotron radiation density inferred from the observed radio power and angular size predicts SSC X rays well in excess of the observed X-ray flux (Marscher et al. 1979; Ghisellini et al. 1993), which is called the "Compton catastrophe" (Hoyle et al. 1966). A related (but not equivalent) statement is that extremely rapid radio variability in some blazars (Quirrenbach et al. 1992) implies brightness temperatures, $T_B = I_\nu c^2/(2k\nu^2)$, where k is Boltzmann's constant, larger than the 10^{12} K limit (Kellermann and Pauliny-Toth 1969; see also Singal and Gopal-Krishna 1985 and Readhead 1994, who suggest a limit $T_B \lesssim 10^{11}$ K appropriate to the equipartition of magnetic field and relativistic electron energy densities).

It follows that the true synchrotron photon density must be lower than observers infer by assuming isotropy. The strong anisotropy and shortened time scales caused by relativistic beaming can account naturally for the Compton catastrophe (or noncatastrophe, as it happens). A lower limit to the Doppler factor, δ, which characterizes these effects (Appendix B) can be estimated from the ratio of predicted to observed SSC flux (Jones et al. 1974; Marscher et al. 1979). In the case of a spherical emission region of observed angular diameter ϕ_d, moving with Doppler factor $\delta_{\rm sphere}$, the limit is (Ghisellini et al. 1993)

$$\delta_{\rm sphere} > f(\alpha) F_m \left(\frac{\ln(\nu_b/\nu_m)}{F_x \phi_d^{6+4\alpha} E_x^{\alpha} \nu_m^{5+3\alpha}} \right)^{1/(4+2\alpha)} (1+z), \quad (2)$$

where ϕ_d is in milliarcseconds, ν_m is the observed self-absorption frequency of the synchrotron spectrum in GHz, F_m is the observed radio flux at ν_m in Jy, E_x and F_x are the observed X-ray energy and flux in keV and Jy, respectively, and ν_b is the observed synchrotron high frequency cutoff. The function $f(\alpha)$, where α is the spectral index of the optically thin synchrotron emission, depends only weakly on the various assumptions used by different authors (see discussion in Urry 1984) and has the approximate value $f(\alpha)$

[7] Lister et al. (1994a) found no correlation between the ratio of core flux to total flux and other beaming indicators, but this may be in part because for that particular ratio, core-dominated objects (those with $R > 1$; Appendix C) are restricted to the limited range $0.5 \leq f_{\rm core}/f_{\rm total} \leq 1$.

$\simeq 0.08\alpha + 0.14$ (Ghisellini 1987). If the radio source is a continuous jet, which is perhaps more realistic (Appendix B, case $p = 2 + \alpha$), then (Ghisellini et al. 1993)

$$\delta_{\rm jet} = \delta_{\rm sphere}^{(4+2\alpha)/(3+2\alpha)}. \quad (3)$$

For a continuous jet compared to a single blob, therefore, the same observed quantities imply a higher Doppler beaming factor (for $\delta > 1$).

The limit in Eq. (2) has been calculated for many radio-loud AGN (Marscher et al. 1979; Madejski and Schwartz 1983; Madau et al. 1987), with the result that δ has lower limits both larger and smaller than unity, depending on the AGN. One complication is that the angular size (ϕ_d) is a function of observation frequency and so is to some extent arbitrary. A self-consistent approach is to use, in Eq. (2), the observing frequency as ν_m and the flux and angular size (preferably measured with VLBI) at that frequency as F_m and ϕ_d, respectively.

For ~100 radio sources for which the VLBI size of the radio-emitting core is published, Eq. (2) gives $\delta > 1$ for a large fraction of BL Lacs and essentially all FSRQ (Ghisellini et al. 1993). That is, blazars for which appropriate data exist do appear to have relativistically beamed emission. Similarly, using variability time scales to infer Doppler factors from the condition $T_{B,\rm max} < 10^{12}$ K gives $\delta > 1$ for a number of blazars (Teräsranta and Valtaoja 1994). The latter values for BL Lacs are somewhat low compared to the SSC calculation, but if the equipartition brightness temperature is more appropriate (Singal and Gopal-Krishna 1985; Readhead 1994), the derived Doppler factors increase by a factor of 2–3, since $\delta = [T_{B,\rm obs}/T_{B,\rm max}]^{1/3}$.

5. BASIS FOR UNIFICATION SCHEMES

The previous two sections described the abundant evidence for strongly anisotropic radiation from radio-loud AGN. Their appearance therefore depends strongly on orientation, and unification schemes are inevitable. The light from some AGN must be directed toward the observer, whether by relativistic beaming or by obscuration, and the remaining misaligned AGN must constitute the so-called "parent population."[8] The known properties of radio-loud AGN—radio galaxies, quasars, and BL Lac objects—are key to identifying the correct parent and beamed populations.

Here we describe the basic unification schemes that have been proposed to date (Sec. 5.1), and how the isotropic properties of radio-loud AGN support or undermine these schemes. Both FR I and FR II radio galaxies tend to have pairs of jets more or less in the plane of the sky and thus are candidates for misoriented blazars. We discuss the FR I/FR II distinction (Sec. 5.2) and then pursue the two most viable unification schemes, linking quasars with FR II galaxies (Sec. 5.3) and BL Lac objects with FR I galaxies (Sec. 5.4). Specifically, we summarize the principal matching criteria, which include the isotropic properties of extended radio power and morphologies, optical narrow line emission, far-infrared continuum emission, host galaxies, environments external to the AGN, and evolution over cosmic time. Finally, we argue that statistical treatment of proper unbiased samples is not currently possible (Sec. 5.5) and we review the method for incorporating the selection effects introduced by relativistic beaming (Sec. 5.6).

We note that all of the comparisons of FR II galaxies and radio-loud quasars ignored the existence of a separate class of FR IIs with low-excitation optical emission lines (Hine and Longair 1979; Laing et al. 1994). Since the low-excitation FR IIs tend to have lower radio luminosities than the high-excitation FR IIs (Laing et al. 1995), as well as more complex radio morphologies (Laing et al. 1994), the comparisons of isotropic properties described below could be affected in a systematic way. In particular, the low-excitation FR IIs may be more closely associated with BL Lac objects than with quasars. Reanalyzing existing data in the light of this alternative classification would be very interesting.

5.1 History of Radio-Loud Unification Schemes

The suggestion that radio-loud quasars were an aligned version of radio-quiet quasars (Scheuer and Readhead 1979) was an early attempt to unify quasars, but was ruled out by the lack of strong large-scale, diffuse radio emission in the radio-quiet sources. An alternative suggestion was that flat-spectrum radio quasars were aligned versions of steep-spectrum radio quasars (Orr and Browne 1982). This satisfies the requirement for equivalent large-scale radio structures and has not been ruled out. However, a third suggestion, that the SSRQ and FSRQ are increasingly aligned versions of FR II galaxies (Peacock 1987; Scheuer 1987; Barthel 1989) appears to fit the data better (Padovani and Urry 1992).

Since BL Lac objects are also blazars but have much lower equivalent-width lines than FSRQ, it was originally suggested that they could be still more aligned versions of quasars (Blandford and Rees 1978). The intrinsic BL Lac luminosities are much smaller than quasar luminosities (for well defined samples), however, and crude estimates of the number densities of parents required are more consistent with low-luminosity radio galaxies (Schwartz and Ku 1983; Browne 1983; Pérez-Fournon and Biermann 1984), as are quantitative estimates of the number densities and luminosities of BL Lacs and FR I galaxies (Ulrich 1989; Browne 1989; Padovani and Urry 1990; Urry et al. 1991a).

5.2 Distinction between FR I and FR II Radio Galaxies

Two decades ago, Fanaroff and Riley (1974) recognized that radio galaxies separate into two distinct luminosity classes, each with its own morphology. As described in Sec. 2, radio emission in the low-luminosity FR Is peaks near the nucleus, while the high-luminosity FR IIs have radio lobes with prominent hot spots and bright outer edges. Jets, when seen, tend to be more collimated in the FR IIs. Examples of both morphological types are shown in Fig. 2.

[8]There is a difference between what should really be called the parent population, which is to say all intrinsically identical objects regardless of orientation, and the misaligned subclass, which is the parents minus the aligned objects. In most cases involving relativistic beaming, however, the relative number of aligned objects is small and there is little difference between the two.

The luminosity distinction is fairly sharp at 178 MHz, with FR Is and FR IIs lying below and above, respectively, the fiducial luminosity $L_{178} \approx 2 \times 10^{25}$ W Hz^{-1}. The separation is cleanest in the two-dimensional optical–radio luminosity plane, where each class follows a separate, approximately linear, $L_r - L_0$ correlation (Owen and White 1991; Owen and Ledlow 1994), implying the FR I/FR II break depends on optical as well as radio luminosity. At a given radio luminosity, FR Is are more luminous optically than FR IIs, although both classes span the same range in optical luminosity overall (Owen and Ledlow 1994).

At higher radio frequencies, the luminosity ranges for each class do overlap by as much as two orders of magnitude, with FR Is having 2.7 GHz luminosities as high as $L_{2.7} \sim 6 \times 10^{26}$ W Hz^{-1}, while FR IIs have luminosities as low as $L_{2.7} \sim 2 \times 10^{25}$ W Hz^{-1} for the 3CR sample (Laing et al. 1983) and even $L_{2.7} \sim 3 \times 10^{24}$ W Hz^{-1} for the 2 Jy sample (Morganti et al. 1993).

FR I and FR II galaxies differ systematically in several ways in addition to host galaxy magnitude. At the same radio luminosity or host galaxy magnitude, FR IIs have optical emission lines about an order of magnitude stronger than those of FR Is (Rawlings et al. 1989; Baum and Heckman 1989; Zirbel and Baum 1995). FR Is tend to inhabit moderately rich cluster environments (Prestage and Peacock 1988; Hill and Lilly 1991) in which they are sometimes the first-ranked ellipticals (Owen and Laing 1989), while FR IIs are more isolated.

Classification of radio galaxies is surely more complicated than a simple bifurcation. While FR II morphologies are well defined by their clear outer hotspots and/or bright edges, the FR I class includes many disturbed and atypical radio structures (Parma et al. 1992). At the same time, optical spectra of FR IIs are quite heterogeneous, with some having strong emission lines and others having only very weak, low-excitation emission lines (Hine and Longair 1979; Laing et al. 1994). An alternative classification of radio galaxies by optical spectra might group the low-excitation FR IIs with the (weak-lined) FR Is. The physical connection between FR I and FR II radio galaxies is a clue to the formation of jets and the extraction of energy from the black hole (Baum et al. 1995).

The blurry line between FR types does affect the proposed AGN unification schemes, but only as a perturbation on the basic picture. In terms of statistical analysis, it affects the details of the low-luminosity end of the FR II luminosity function and the high-luminosity end of the FR I luminosity function but has no major impact because what matters in a quantitative analysis (Sec. 6) is the knee of the parent luminosity function.

5.3 Isotropic Properties of Quasars and FR II Galaxies

5.3.1 Extended radio emission

FR II radio galaxies are dominated by emission from large, diffuse radio lobes which is almost certainly unbeamed, especially at low frequencies where the contribution from flat-spectrum hot spots is minimal. The radio luminosities of the extended structures of FR II galaxies and quasars should therefore be comparable if the unified scheme is right. The fact that most compact radio sources have substantial extended radio power has been known for more than a decade (Ulvestad et al. 1981) and the distributions of $P_{\rm ext}$ for compact radio sources (largely quasars) and 3CR/B2 radio galaxies (at 1.5 GHz) do overlap (Antonucci and Ulvestad 1985).

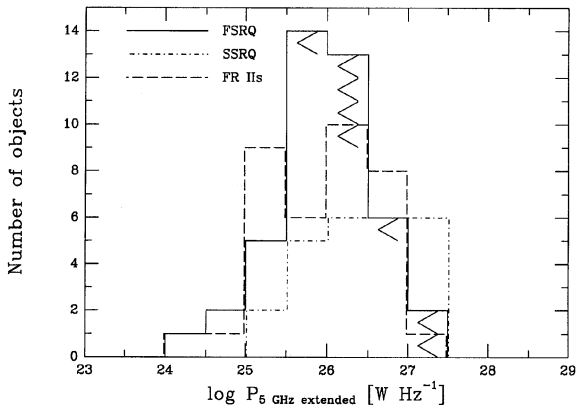

FIG. 6—A comparison of the extended radio powers at 5 GHz for FR II radio galaxies (*dashed line*), steep-spectrum radio quasars (*dot-dashed line*), and flat-spectrum radio quasars (*solid line*) from the 2 Jy sample (Wall and Peacock 1985; di Serego Alighieri et al. 1994a,b). Data for the FR IIs come from Morganti et al. (1993), those for FSRQ have been derived from the R values (Appendix C) given by Padovani (1992b), updated with lower limits from Ulvestad et al. (1981), while extended radio powers for SSRQ have been collected from the literature (mostly from Browne and Murphy 1987). Upper limits on extended power for FSRQ are indicated with the symbol "<". Radio powers have been de-evolved using the best-fit evolution for each class (Table 2).

In terms of the quasar–FR II unification scheme in particular, the extended radio luminosities at a few GHz of complete samples of FSRQ and SSRQ are typical of those for complete samples of FR II radio galaxies, as shown in Fig. 6 for the 2 Jy sample. (All radio powers have been de-evolved using the best-fit evolution appropriate for that class; see Sec. 6.1.) We note that it is not appropriate to use the Kolmogorov–Smirnov (KS) statistic to test whether these distributions are compatible—or similarly, whether the distributions of redshift or narrow-line luminosity are comparable for blazars and radio galaxies—because the sample identification itself involves strong selection effects from relativistic beaming and thus one should not expect the *shape* of the distributions to be the same. For example, since beamed objects can be detected to higher redshifts, in a flux-limited sample they will be intrinsically more luminous as well. The histograms in Fig. 6 demonstrate only that the range in unbeamed radio luminosity overlaps completely, not that the distributions have the same shape.

5.3.2 Narrow emission lines

Assuming the narrow emission lines are emitted isotropically, unification schemes predict similar narrow-line luminosities in quasars and FR II radio galaxies. Due to the intrinsic correlation between narrow-line luminosity and extended radio emission (Baum and Heckman 1989; Rawl-

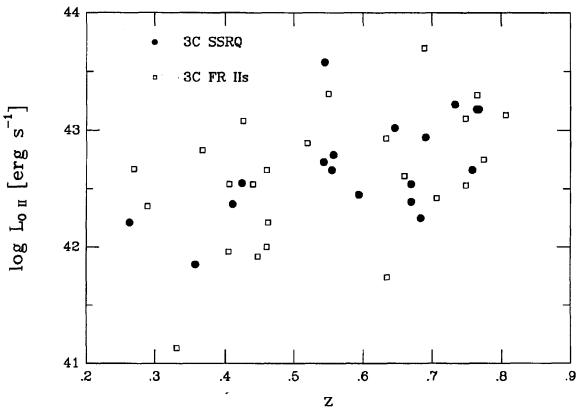

FIG. 7—The [O II] emission-line luminosity for quasars (*filled circles*) and powerful (FR II) radio galaxies (*open squares*) in the 3CR sample, plotted vs. redshift to allow comparisons at similar radio luminosity (which is well correlated with redshift in a radio-flux-limited sample) and/or observed wavelength of [O II]. The narrow-emission-line luminosities of radio galaxies and quasars, which should be unaffected by obscuration or relativistic beaming, span the same values over the full redshift range. (Data from Hes et al. 1993.)

ings and Saunders 1991; Zirbel and Baum 1995), the comparison has to be done matching objects of similar extended radio luminosity. For flux-limited samples, this is roughly equivalent to matching in redshift (although the scatter in the redshift–P_{ext} correlation can be large for core-dominated objects since it is an induced correlation). Also, matching the objects in redshift will exclude the effects of cosmological evolution, as well as observational selection effects due to the bandpass used.

Quasars do have systematically higher [O III] λ5007 luminosities than radio galaxies (Jackson and Browne 1990), but this line appears to be emitted anisotropically when compared to [O II] λ3727 (McCarthy 1989; Hes et al. 1993), possibly due to contribution to [O III] from the broad-line region (although there is no sign of broad wings on the [O III] line) and/or partial obscuration by the thick torus. (Excluding the low-excitation FR II galaxies also reduces the discrepancy in [O III] luminosities: Laing et al. 1994.) As shown in Fig. 7, the [O II] λ3727 line luminosities of 3CR steep-spectrum quasars and FR II radio galaxies matched in radio power are completely overlapping (Hes et al. 1993), as expected from the unification scheme.[9]

5.3.3 *Infrared properties*

Models for the obscuring torus suggest it becomes transparent in the far-infrared (Pier and Krolik 1993), where the radiation, possibly thermal emission by dust grains (Sanders et al. 1989), therefore becomes isotropic. To date, the only bulk measurements of AGN at far-infrared wavelengths come from *IRAS*, which was not sensitive enough to detect most radio galaxies individually. Separate coadds of *IRAS* data for radio galaxies and quasars, including many nondetections, do show that quasars are systematically more luminous at all observed wavelengths from 12 to 100 μm. This suggests that there is a fundamental difference between the two populations, or there is a significant contribution from beamed far-infrared continuum in the quasars, or the torus is still radiating anisotropically at ~50 μm in the rest frame (Heckman et al. 1994). The ratio of 60 μm to 178 MHz flux appears to correlate with core to extended flux ratio, which suggests that far-infrared emission is enhanced in core-dominated objects and therefore is likely beamed (Hes et al. 1995). *ISO* observations will be fundamental in addressing this issue further.

In AGN for which the optical depth to the nucleus is not too high, detection of broad Paschen lines may be possible. To date, Paα has been seen in some broad-line radio galaxies and also in a few narrow-line radio galaxies, and in all cases the reddening to the broad-line region was larger than the reddening to the narrow-line region (Hill et al. 1995). With more sensitive instruments, the expectation is that infrared broad lines will be found in a number of Type 2 radio galaxies. The torus is likely quite thick in the equatorial plane, so it is only at intermediate angles that the extinction would be small enough for Paα photons to escape. Interestingly, radio galaxies appear to have nuclear sources stronger in the infrared than in the optical, exactly as expected for a reddened, hidden nucleus (Dunlop et al. 1993).

5.3.4 *Host galaxies*

A simple test of unification is that the morphology and magnitude of radio galaxies and quasar host galaxies be comparable. At present, the observational situation for quasars and FR II radio galaxies is not entirely clear, as comparisons of their mean host galaxy luminosities have led to conflicting conclusions. Some studies have found radio galaxies to be fainter by ~0.5–1 mag (Hutchings 1987; Smith and Heckman 1989), while others concluded the mean magnitudes (and dispersions) were comparable (Véron-Cetty and Woltjer 1990; Lehnert et al. 1992). In part, determining quasar host-galaxy magnitudes is difficult, and in part the differences between the conflicting results may be explained by systematic effects (Abraham et al. 1992) and/or by incomplete or heterogeneous samples. For example, in the present unification scheme the parent population consists of luminous narrow-line radio galaxies, yet samples of "powerful radio galaxies" used to test unification sometimes include broad-line radio galaxies (the local counterpart of quasars) and FR Is.

With high-resolution ground-based imaging, host galaxies have been detected in quasars out to a couple of gigaparsecs. Figure 8 shows a CFHT image of the radio-loud quasar 2135−147, which has redshift $z=0.2$. Even though the quasar nucleus is very bright, the host galaxy is clearly visible, as are companion objects ~2 arcsec and ~5 arcsec to the east (Hutchings and Neff 1992). Most quasars are at higher redshift, so determining whether they are in ellipticals requires high resolution imaging of the kind now available with *HST* (Hutchings et al. 1994; Hutchings and Morris 1995; Bahcall et al. 1995). Such studies of the galaxy morphologies of large, complete samples of quasars and radio

[9]Any trend with redshift is induced through the correlation of luminosity and redshift in flux-limited samples, and should therefore be ignored in this and similar plots.

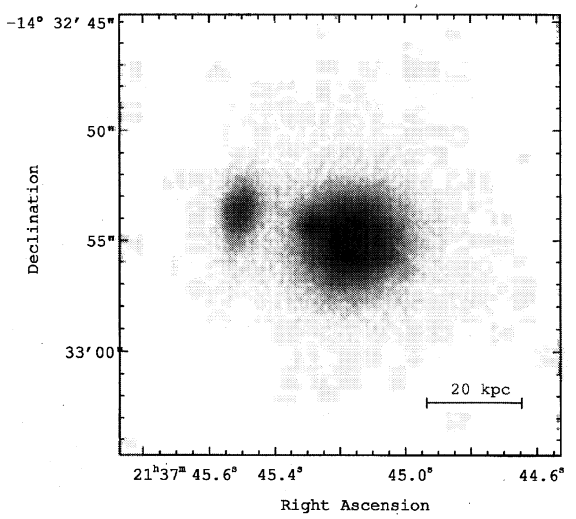

FIG. 8—Optical image of the radio-loud quasar 2135−147 obtained with the CFHT with resolution 0.5 arcsec. The host galaxy is clearly visible, as are two close companions ~2 and ~5 arcsec to the east (Hutchings and Neff 1992; copyright American Astronomical Society, reproduced with permission).

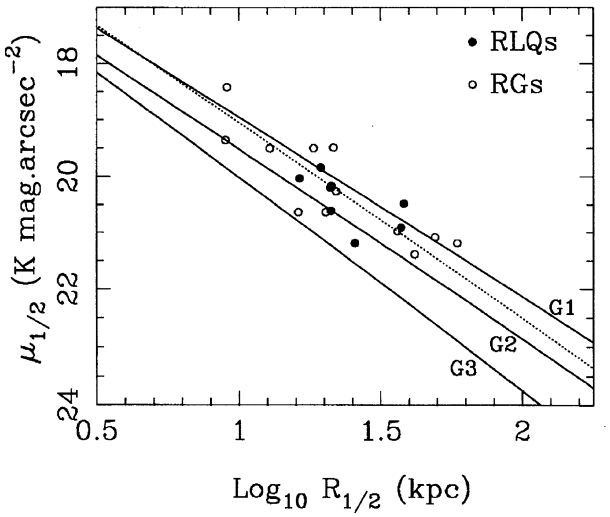

FIG. 9—The distribution of radio galaxies and the host galaxies of radio-loud quasars on the K-band $\mu_{1/2}$, $\log R_{1/2}$ plane, where $\mu_{1/2}$ is the K-band surface brightness at the half-light radius, $R_{1/2}$, for samples matched statistically in redshift and radio power to minimize selection effects. Both radio galaxies and quasar hosts are very luminous and have large scale lengths; the best-fit correlation for the combined dataset (dotted line) is very similar, in both slope and normalization, to those for brightest cluster galaxies (solid lines; from Schneider et al. 1983, shifted to the K band by the observed mean zero-redshift color of the radio galaxies in the sample, $B-K=3.75$). The properties of radio galaxies and quasar hosts on this diagram are statistically indistinguishable, lending strong support to unified schemes, at least for $z<0.4$ (Taylor et al. 1995; figure courtesy of James Dunlop).

galaxies will be important for testing unified schemes.

Most host galaxy studies have been done at optical wavelengths, where the ratio of nuclear to galaxy flux is relatively high. Diffuse stellar light surrounding bright AGN is more easily detected in the infrared; for example, the K-band images of 2135−147, the quasar in Fig. 8, also show the diffuse galaxy emission and companion objects quite clearly, if not at the same resolution (Dunlop et al. 1993). A recent infrared comparison of radio galaxies and radio-loud quasars at $z \lesssim 0.4$, matched in radio power and redshift, shows that the host galaxies of both classes appear to be luminous ellipticals, have the same average half-light radii, and have the same mean absolute magnitudes (Dunlop et al. 1993; Taylor et al. 1995). For both the radio galaxies and quasars, infrared galaxy surface brightness and scale length are well correlated (Fig. 9), with the same slope and normalization as for brightest cluster galaxies (Schneider et al. 1983). This gives strong support to the unified scheme, at least for relatively nearby quasars.

5.3.5 *Environments*

For a unification scheme to be correct, the environments of the unified classes—here, FR IIs and radio quasars—have to match.[10] The observational situation here is unclear. In an oft-quoted study, Prestage and Peacock (1988) found that compact/flat-spectrum radio sources appear to lie in regions of galaxy density a factor of ~2 lower than those typical of FR Is and possibly even lower than for FR II sources. However, this was based on small samples of only ~10 compact flat-spectrum sources, which included BL Lacs, local FSRQ, and even some radio galaxies. The Prestage and Peacock (1988) data on FSRQ alone are too limited to derive a spatial correlation amplitude for comparison to the FR IIs.

Other studies at low redshift showed either no significant difference in environment (Smith and Heckman 1990), or only a marginal difference (Yates et al. 1989) that disappears when the radio galaxies without definite FR II structure are excluded. At higher redshift ($0.35 \lesssim z \lesssim 0.5$), the environments of powerful radio galaxies are as rich as those observed around radio-loud quasars in the same redshift interval (Yates et al. 1989).

Thus, there is no evidence for concluding that the environments of FR IIs and radio quasars differ. Obviously, additional data for larger samples covering a range in redshift are needed to confirm that the environments are similar.

5.3.6 *Cosmic evolution*

If radio galaxies and quasars are related strictly through aspect, then the relative numbers and luminosities of each class should be broadly comparable at all cosmological epochs. Indeed, the cosmological evolution of steep-spectrum radio quasars, flat-spectrum radio quasars, and radio galaxies can be described in each case by luminosity increasing with redshift roughly as $(1+z)^3$ out to $z \sim 2$, followed by a comparable decline in comoving density at higher redshifts

[10]Even within the unified scheme, environment may have an effect on the relative numbers of radio galaxies and blazars. For example, the opening angle of the torus might depend on gas density external to the active nucleus. In that case, the number ratio of blazars to radio galaxies could differ between cluster and field. If the opening angle were smaller in clusters due to extra quenching, for example, radio galaxies would be found more often in clusters than are blazars. This is a matter of degree, however; the fact that both radio galaxies and blazars should be found in clusters and in the field would not change.

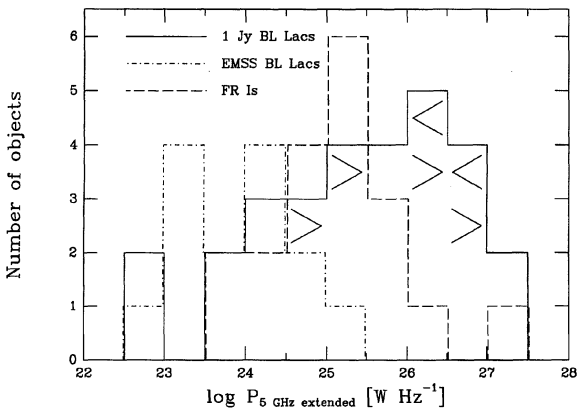

FIG. 10—A comparison of the extended radio powers at 5 GHz for FR I radio galaxies (*dashed line*) from the 2 Jy sample (Wall and Peacock 1985; di Serego Alighieri et al. 1994b), radio-selected BL Lac objects (*solid line*) from the 1 Jy sample (Stickel et al. 1991) and X-ray-selected BL Lacs (*dot-dashed line*) from the EMSS sample (Stocke et al. 1991). Data for the FR Is come from Morganti et al. (1993); those for RBL have been derived from the R values (Appendix C) given by Padovani (1992a), updated with data from Kollgaard et al. (1992) and Murphy et al. (1993) plus lower limits from Ulvestad et al. (1981); data for the XBL are taken from Perlman and Stocke (1993). Upper limits on extended power (<) and lower limits on redshift (>) for BL Lac objects are indicated.

(Dunlop and Peacock 1990). This means current samples are broadly consistent with unification independent of redshift.

Over cosmic time, changes in the relative strengths of beamed and unbeamed components in individual sources, or in the opening angle of an obscuring torus (Lawrence 1991), might be expected. In either of those cases, the observed evolution would be different depending on orientation angle. The magnitude of this effect is clearly model-dependent, but if the unification of radio galaxies and quasars is correct, it cannot be large given the observed similarity in their evolutionary properties.

5.4 Isotropic Properties of BL Lac Objects and FR I Galaxies

5.4.1 Extended radio emission

More than ten years ago it was noted that the extended radio emission of BL Lacs was comparable to that of low-luminosity (i.e., FR I) radio galaxies (Browne 1983; Wardle et al. 1984; Antonucci and Ulvestad 1985), although these early studies were hampered by the lack of redshift information and small and incomplete samples. Now that sizeable complete BL Lac samples are available, indeed the mean extended radio powers at 5 GHz for the 1 Jy radio-selected BL Lac sample (Stickel et al. 1991) and a subsample of the 3CR FR Is are essentially the same, $\langle P_{\rm ext}\rangle \sim 10^{25}$ W Hz^{-1} (Padovani 1992a). Figure 10 shows the overlapping histograms of $P_{\rm ext}$ observed for the 1 Jy BL Lacs and the 2 Jy FR Is (Wall and Peacock 1985; di Serego Alighieri et al. 1994b), which have similar flux limits and selection frequencies. It is not clear whether the BL Lac morphologies are consistent with FR I morphologies seen at small angles; if the angle separating the two classes is large enough, one might expect to see more double-jet structures in BL Lacs, although the FR I morphologies are quite varied (Parma et al. 1992).

There is similar agreement between B2 FR Is and X-ray selected BL Lac objects (XBL) from the *Einstein* Medium Sensitivity Survey (EMSS; Perlman and Stocke 1993) or 3CR and B2 FR Is and XBL from the *HEAO-1* Large Area Sky Survey (LASS; Laurent-Muehleisen et al. 1993). Figure 10 includes the distribution of $P_{\rm ext}$ for the EMSS XBL; both the 3CR and B2 samples have slightly lower fluxes at 5 GHz than the 2 Jy sample, which results in their extended powers reaching smaller values.

It is notable that the mean extended radio power of XBL is more than an order of magnitude lower than for radio-selected BL Lacs (RBL; see also Laurent-Muehleisen et al. 1993). Moreover, the weak radio cores of XBL appear relatively unbeamed, as if they are "off-axis" in the radio band (Padovani 1992a; Perlman and Stocke 1993) or intrinsically less luminous (Giommi and Padovani 1994; Padovani and Giommi 1995a). The large difference in extended power supports the latter interpretation (see Secs. 6.2.5, 6.2.6).

Some of the 1 Jy RBL, which extend to higher redshifts and thus to higher luminosities, appear to have radio morphologies more consistent with FR IIs than with FR Is (or rather, with what FR IIs would look like at a small angle with the line of sight; Kollgaard et al. 1992; Murphy et al. 1993). This is not a serious challenge to the idea of FR Is being the parent population of BL Lac objects (see also Maraschi and Rovetti 1994, who consider the continuity explicitly), as it affects only a relatively few objects at the high end of the FR I luminosity function, but it reinforces the blurriness of the distinction between FR Is and FR IIs in the overlapping luminosity range. Just as the luminosities overlap at high frequencies, perhaps the clear morphological separation breaks down in higher frequency maps (which are needed to get high spatial resolution in the more luminous, higher redshift objects). Also, none of the BL Lacs observed by Kollgaard et al. (1992) displays FR II characteristics as clearly as some core-dominated quasars observed by the same group (albeit with somewhat better resolution; Kollgaard et al. 1990). Finally, a substantial number of 3CR FR II sources have low-excitation optical spectra, i.e., with lines such as [O III] that are very weak (or undetectable) in comparison to the hydrogen lines (Laing et al. 1994). Since the narrow-line spectra of these objects are clearly different from those of classical FR II radio galaxies and radio quasars, instead resembling those of FR Is, it is possible that the low-excitation sources, despite their FR II morphology, could well belong to the low-power unification scheme. It would then follow that some BL Lacs are *expected* to display FR II morphology and also that that does not necessarily associate them with all the high-power sources.

5.4.2 Narrow emission lines

It is not yet clear whether the narrow-line luminosities of BL Lac objects, in the few cases when such lines can be observed, are consistent with those of FR I galaxies. [O III] luminosities are available for 8 of the 11 1 Jy BL Lac objects with certain redshift $z \lesssim 0.5$ (Stickel et al. 1993). The mean emission line luminosity is $L_{\rm O\,III} = 10^{41.30\pm0.11}$ erg s^{-1},

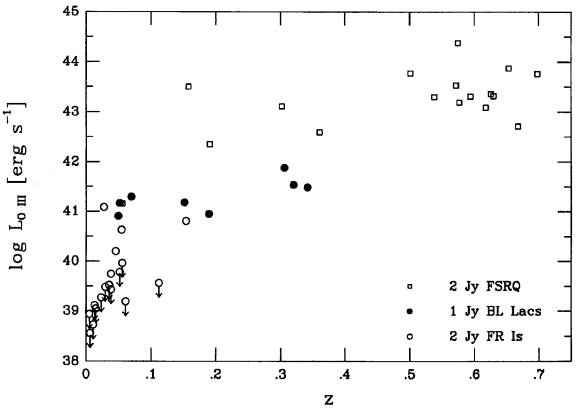

FIG. 11—The [O III] emission-line luminosity for the 1 Jy BL Lacs (*filled circles*), 2 Jy FR Is (*open circles*), and 2 Jy flat-spectrum radio quasars (*open squares*), including some upper limits for the FR Is, plotted vs. redshift to allow comparisons at similar radio luminosity (which is well correlated with redshift in radio-flux-limited samples) and/or observed wavelength. At a given redshift, the line luminosities of FR Is are generally smaller than those of BL Lacs, although the highest FR I [O III] luminosities are comparable. The line luminosities of quasars are larger than those of BL Lacs by more than a factor of ten. (The one quasar located in the BL Lac region, PKS 0521−365, is discussed in the text; Sec. 7.1.) This argues against the idea that the high-redshift, high-luminosity BL Lac objects are more closely related to flat-spectrum radio quasars than to low-redshift, low-luminosity BL Lacs, although the BL Lac data extend only to $z\sim0.4$.

with a spread of less than an order of magnitude. Figure 11 shows these values compared to the available [O III] luminosities for the FR I galaxies in the 2 Jy sample (Tadhunter et al. 1993), plotted vs. redshift to compensate simultaneously for any trends with observed wavelength range or luminosity (which correlates well with redshift in flux-limited samples).

For $z\lesssim0.2$, the maximum redshift of the FR Is, and excluding nondetections, the mean [O III] luminosities are $L_{O\,III} = 10^{41.10\pm0.07}$ and $10^{40.49\pm0.24}$ erg s^{-1} for five BL Lacs and five FR Is, respectively. The difference is a factor of ~4, significant at the ~94% level, and is more than an order of magnitude if one includes the upper limits. However, the FR I line fluxes may be underestimated due to small slits and/or contamination from a strong stellar continuum (Tadhunter et al. 1993). Also, a comparable set of uniform upper limits for BL Lac objects is not available for comparison; possibly, the [O III] luminosity in most BL Lac objects is well below the few detections available. High signal-to-noise-ratio spectra through large apertures of a reasonably large sample of FR I radio galaxies (and BL Lac objects) are needed to determine whether $L_{O\,III}$ in FR Is is really smaller than in BL Lacs.

The apparent difference in [O III] luminosities for BL Lacs and FR Is could also arise if [O III] were emitted anisotropically, as for radio quasars and FR II radio galaxies (Sec. 5.3). The fact that broad Mg II emission lines are seen in some BL Lac objects (Stickel et al. 1993) means that for unification to be correct, some FR Is (albeit high-redshift ones) must have obscured broad-line regions. By analogy to quasars (Sec. 5.3.2), the obscuring matter could affect the [O III] emission more than the [O II], thus explaining the apparent discrepancy. While there is no direct evidence for an obscuring torus surrounding the [O III]-emitting clouds in BL Lac objects or FR Is, neither is there evidence against it.

Recent *HST* spectra of the nucleus of M87, a nearby FR I galaxy of modest luminosity (Harms et al. 1994), do show relatively broad emission lines, ranging from FWHM ~1400 km s^{-1} for Hβ up to ~1900 km s^{-1} for [O I]. These lines are broader than the typical widths for Seyfert 2 galaxies (FWHM ~250–1200 km s^{-1}; Osterbrock 1989) and the [O III]/Hβ ratio is much larger than 1, unlike the typical case for Seyfert 1 galaxies. If M87 has a hidden nuclear broad-line region, further spectroscopic investigation of this and other FR Is is obviously of great interest.

Unlike the quasar–FR II unification scheme, where SSRQ appear at intermediate angles, the BL Lac–FR I scheme has essentially no transition objects (the low-luminosity BLRG 3C 120 might be an exception). These would be FR I-like radio sources, with steep radio spectra and FR I-like morphologies because they are oriented outside the relativistic beaming cone, but would show BL Lac-like emission lines (possibly broad lines) because they are oriented inside any obscuration cone. It may be that BL Lacs just do not have any appreciable emission, lines or continuum, beyond that relativistically beamed from the jet. Alternatively, broad lines could be hidden in FR Is, a phenomenon implied by unification with the high-redshift BL Lac objects, in which case there should be (as for quasars) broad-line FR Is. The lack of such objects could be explained if the opening angle of the obscuring torus is narrower at lower powers (Lawrence 1991; Falcke et al. 1995; see also Baum et al. 1995). Far infrared observations of BL Lacs and FR Is with *ISO* should indicate whether or not there is obscuring matter in low-luminosity radio sources.

5.4.3 Host galaxies

There is good observational evidence that low-redshift BL Lacs reside in giant ellipticals as FR Is do. The host galaxy of the BL Lac object PKS 0548−322 (Fig. 12, center) has a de Vaucouleurs $r^{1/4}$ law profile (Falomo et al. 1995), as do the point-source-subtracted optical profiles of many low-redshift BL Lacs (Ulrich 1989; Stickel et al. 1991, 1993). The distribution of host galaxy absolute magnitudes peaks around $M_V\sim-23$, which is comparable to the brightest galaxies in clusters (Kristian et al. 1978). The mean host galaxy magnitude for the seven 1 Jy BL Lac objects with $z<0.2$ is $\langle M_V\rangle=-22.9\pm0.3$ (Stickel et al. 1991, 1993), in excellent agreement with the mean value for FR Is, $\langle M_V\rangle=-23.1\pm0.1$ (derived from Smith and Heckman 1989, converting to $H_0=50$ km s^{-1} Mpc^{-1}). There is no useful imaging information available for the BL Lacs at higher redshifts ($z\gtrsim0.2$), a project now underway with *HST*.

A few of the 20 or so BL Lac host galaxies classified in the literature show evidence for disks, but this is far from conclusive. The surface brightness profile of PKS 1413+135 appears to be better fitted by an exponential law than by a de Vaucouleurs law (Abraham et al. 1991), suggesting a disk host, while for OQ 530 the results are mixed (Abraham et al. 1991, Stickel et al. 1991, 1993). Stocke et al. (1992; see also Perlman et al. 1994) have suggested that PKS 1413+135, an

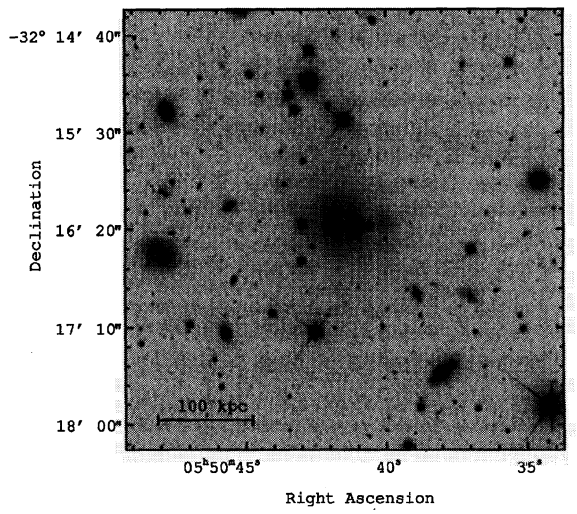

FIG. 12—The central part of an NTT R-band image of the BL Lac object PKS 0548−322 (center) and its environment (Falomo et al. 1995). The host galaxy has the $r^{1/4}$ profile typical of an elliptical. Numerous other galaxies visible in the field have the same redshift as the BL Lac ($z=0.069$), indicating this BL Lac object lies in a rich cluster (Abell richness class 2; Falomo et al. 1995). A number of these galaxies are distorted or otherwise unusual; for example, the bright galaxy at the left edge of the image has a small jet-like structure extending to the southeast. (Copyright American Astronomical Society, reproduced with permission.)

unusually reddened BL Lac object, may lie behind a spiral galaxy rather than within it (cf. McHardy et al. 1994). Finally, while Halpern et al. (1986) reported a disk host in 1E 1415.6+2257, Romanishin (1992) found the brightness profile to be consistent with an elliptical galaxy, with the possible presence of a jet-like feature that went unnoticed by Halpern et al. About 10% of FR Is are known to have some sort of morphological peculiarity in the optical (Smith and Heckman 1989). This could complicate the surface brightness profile analysis for BL Lac host galaxies, although to our knowledge there is no FR I radio galaxy whose optical surface brightness profile is better fitted by an exponential law than a de Vaucouleurs law. It would be useful to have higher resolution imaging of both BL Lacs and FR Is to explore this further.

5.4.4 Environments

The systematic study of the environment of BL Lacs is relatively recent. The work of Prestage and Peacock (1988), discussed in Sec. 5.3, is usually quoted (wrongly) as evidence that BL Lacs avoid rich environments; it actually shows that (within large uncertainties) the spatial correlation amplitude of (4) BL Lacs is consistent with that of FR I radio galaxies.

Fields of low-redshift BL Lac objects that have been studied intensively tend to show statistically significant excesses of galaxies, compatible with clusters of galaxies of Abell richness class 0 and 1 (Falomo et al. 1993; Pesce et al. 1994; Fried et al. 1993; Wurtz et al. 1993; Smith et al. 1995), in good agreement with the environments of FR I type radio galaxies (Hill and Lilly 1991). The environment of PKS 0548−322 (Fig. 12) is clearly rich in galaxies, including two companion elliptical galaxies within ~40 kpc projected distance (if at the redshift of the BL Lac, $z=0.069$) and numerous other galaxies with brightnesses appropriate for a cluster at $z=0.069$. Some nearby BL Lacs lie in somewhat poorer clusters, as do some FR Is (Wurtz et al. 1993; Laurent-Muehleisen et al. 1993). In short, BL Lacs and FR Is do appear to have similar environments.

Reversing the question leads to an unexplained discrepancy. A spectroscopic survey of 193 radio sources found in Abell clusters revealed 186 FR I galaxies but no BL Lac objects, when according to beaming models roughly 8 would have been expected in the observed luminosity range, a discrepancy significant at the >99% level (Owen et al. 1995). That is, this unbiased cluster-selected survey for BL Lac objects suggests they occur preferentially outside of normal FR I environments. We note that the FR I luminosities observed by Owen et al. (1995), $L_{1.4}<10^{26}$ W Hz^{-1}, and the observed BL Lac radio luminosity function, for which $L_5>10^{25}$ W Hz^{-1} (Fig. 17; Urry et al. 1991a), overlap by less than one decade. In this interval there are only 18 FR Is and the absence of BL Lacs is only marginally significant (95% confidence; Owen et al. 1995). Furthermore, the conflict in number density is actually between the *observed* BL Lac and FR I luminosity functions, rather than with the predictions of the beaming model. It is possible that since the redshift limit of the cluster sample is low, $z<0.09$, recognition effects (Browne and Marchã 1993) could be important.

At higher redshifts ($z\sim1$) there is no indication of a density enhancement near the BL Lacs, as expected because cluster galaxies at these redshifts would be well below the typical detection limits (Fried et al. 1993). It is important to study blazar environments at high redshifts because it is there that quasar environments appear to undergo significant evolution. At $z\sim0.6$, radio quasars are often found in clusters of galaxies, while locally they are in regions of lower galaxy density (Yee and Ellingson 1993). Furthermore, if there were a connection between the more luminous BL Lac objects and radio quasars (see Sec. 7.2), it would only be apparent at higher redshift.

5.5 The Myth of Unbiased Selection

Given the strong selection effects introduced by relativistic beaming and obscuration, it is very difficult to find useful unbiased samples. In the ideal case, surveys would be designed to select AGN by some completely isotropic property. Since surveys are generally flux-limited, this effectively means selecting sources at a wavelength not strongly affected by obscuration or beaming, such as in the low-frequency radio, far-infrared, or hard X-ray bands.

At present, however, it is not possible to select a useful AGN sample in an unbiased way. The 3CR radio sample, selected at 178 MHz where steep-spectrum emission from the lobes dominates, contains only a few core-dominated objects (i.e., blazars); in the 3CR catalog (Spinrad et al. 1985), only 2/298 (0.7%) objects are BL Lac objects (0% in the complete subsample of Laing et al. 1983). That is, the 3CR catalog may be (essentially) unbiased by beaming, but it does not include enough blazars to test their participation in

unified schemes. In contrast, in the 1 Jy radio source catalog (Stickel et al. 1994), selected at 5 GHz, there are 37/527 BL Lacs (7%; there are 34 in the complete sample, with $V \leqslant 20$), and 214/527 (41%) FSRQ, i.e., about 50% of the sources are blazars. Low-frequency-selected samples that are larger than the 3CR, like the Molonglo or B2 surveys, are still not completely identified: a complete sample of 550 sources selected from the Molonglo catalog is in the process of being identified (Kapahi et al. 1994), while two relatively small but completely identified subsamples of the B2 catalog exist (Fanti et al. 1987) but are defined by a cut in optical magnitude, which is certainly not an isotropic property. Finally, the emission at low radio frequencies need not be entirely isotropic, as it can be affected somewhat by beaming in the cores and radio-lobe hot spots.

Far-infrared selection does avoid the bias introduced by dust obscuration of optical/ultraviolet emission but introduces a bias against dust-free AGN. Furthermore, the selection effects at far-infrared wavelengths depend on the properties of the obscuring torus or other dusty structures, which may not generate isotropic emission (Pier and Krolik 1992) and which may differ from source to source by more than just orientation. The far infrared may also be affected by beaming insofar as there is a contribution from an infrared nonthermal source. Finally, the sample identification for the *IRAS* survey is a major burden, not to mention that AGN are not found efficiently (less than 1% of the high-latitude sources are AGN).

Hard-X-ray surveys are theoretically useful, but no deep large-area surveys are currently planned. Also, X-ray spatial resolution at 10 keV is not as good as radio or infrared resolution, making the confusion limit correspond to an effectively higher flux; i.e., hard X-ray surveys cannot go as deep. The lower resolution also makes optical identification of the sample more difficult. In the future, an all-sky survey with arcsecond resolution at 10–20 keV would be very valuable for evaluating unified schemes in a model-independent way.

In short, to address the key question of unified schemes—whether the numbers and luminosities of objects in the classes one proposes to unify are as expected by the scheme—means using well-defined (i.e., flux-limited) samples with known biases, and accounting for those selection effects quantitatively. This allows us to comment on whether a specific unified scheme is plausible and what parameter values are needed to make it so. It also avoids the pitfall of defining samples *post facto*, based on "isotropic quantities" like narrow-line emission or host galaxy type, which may well be incomplete because the detection threshold is not related to the sample definition. Fortunately, allowing for selection bias head-on, at least in the case of relativistic beaming, is a robust process which is not terribly sensitive to the details of the beaming model.

5.6 Effect of Relativistic Beaming on Number Statistics

AGN with anisotropic emission patterns will be boosted into and shifted out of flux-limited samples according to their orientation. For some radiation patterns, including those caused by relativistic beaming (Urry and Shafer 1984) and thick accretion disks (Urry et al. 1991b), a narrow distribution in intrinsic luminosity is broadened into a flat distribution over a wide range of observed luminosities (which follows from the probability function for flux enhancement). This leads to a distortion in the measured shape of the luminosity function of the boosted AGN relative to their intrinsic luminosity function (Urry and Shafer 1984; Urry and Padovani 1991).

More specifically, under the basic assumption that AGN are randomly oriented on the sky, and assuming a radiation pattern, we can predict the exact numbers of AGN with a given observed luminosity relative to their intrinsic luminosity (summed over all angles). Given the luminosity function (LF) of the misaligned AGN, then, one can predict the LF of the aligned AGN, subject to the form of the radiation pattern. In practice, the pattern for relativistic beaming depends on the assumed distribution of Lorentz factors and on whether one assumes a unidirectional jet or a fan beam; the pattern for obscuration depends on the size and optical depth of the torus; the pattern for thick disks depends primarily on the funnel geometry.

To evaluate the number statistics of radio-loud unification schemes we incorporate the effect of relativistic beaming on the observed LFs (Urry and Shafer 1984). Consider an ensemble of emitters all having the same intrinsic luminosity ($\mathscr{L}$) and all moving with the same relativistic bulk speed (β) at random angles (θ) to the line of sight. Given that $L = \delta^p \mathscr{L}$ [Eq. (B7)], the probability of having a particular Doppler factor $\delta = [\gamma(1-\beta\cos\theta)]^{-1}$ (Appendix A) is $P(\delta) = d(\cos\theta)/d\delta = (\beta\gamma\delta^2)^{-1}$. The probability of observing luminosity L given intrinsic (emitted) luminosity $\mathscr{L}$ is

$$P(L|\mathscr{L}) = P(\delta)\frac{d\delta}{dL} = \frac{1}{\beta\gamma\delta}\mathscr{L}^{1/p}L^{-(p+1)/p}. \qquad (4)$$

For fixed $\mathscr{L}$, the distribution of observed luminosities is a flat power law (with index in the range 1–1.5 for likely values of p; Appendix B) extending from $L \sim (2\gamma)^{-p}\mathscr{L}$ to $L \sim (2\gamma)^p\mathscr{L}$. The observed luminosity distributions are illustrated in Fig. 13(a) (thick dashed lines) for three different intrinsic luminosities (thin dashed lines). The low-luminosity cutoff corresponds to an emitter moving directly away from us ($\theta = 180°$) and the high-luminosity cutoff to an approaching emitter perfectly aligned ($\theta = 0°$). The normalization of this flat power law decreases with increasing beaming (higher β, γ, or p) because the beaming cone angle gets smaller.

For a distribution of intrinsic luminosities (i.e., a luminosity function), the observed LF is just the integral of the intrinsic luminosity distribution times the conditional probability function in Eq. (4):

$$\Phi_{\rm obs}(L) = \int d\mathscr{L}\, P(L|\mathscr{L})\Phi_{\rm intr}(\mathscr{L}). \qquad (5)$$

This integral [thick solid line in Fig. 13(a)] is basically the envelope of the beamed LFs for fixed intrinsic luminosities (the intrinsic LF is shown as a thin solid line). For simple power-law luminosity functions, Eq. (5) can be integrated analytically (Urry and Shafer 1984).

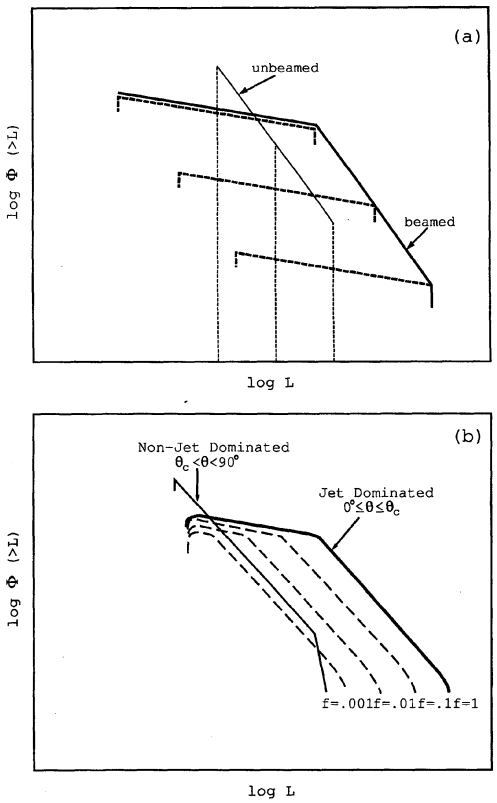

FIG. 13—The effect of relativistic beaming on observed luminosity functions. (a) Simple case where all emitted flux comes from a randomly oriented relativistic jet. For a delta-function intrinsic luminosity (*thin dashed line*), the observed luminosity function after beaming (*thick dashed line*) is a flat power law of differential slope $1 \lesssim (p+1)/p \lesssim 1.5$ [Eq. (4)]. A power-law intrinsic luminosity function (*thin solid line*), after integration of Eq. (5), gives rise to an observed luminosity function that is a double power law (*thick solid line*), with flat slope $(p+1)/p$ at low luminosities and the same slope as the intrinsic power law at high luminosities. (b) Case where the intrinsic luminosity in the jet is a fraction $f=0.001$, 0.01, 0.1, or 1 of the unbeamed luminosity. As in (a), the beamed luminosity function has slope $(p+1)/p$ below the break and the parent luminosity function slope above the break. In both (a) and (b), the high luminosity objects (those in the steep part of the beamed luminosity function) are oriented close to the line of sight ($\theta \sim 0°$).

In practice, one expects an unbeamed component (e.g., radio lobes) to be present in addition to a beamed component (jet). We use the simple parametrization that the intrinsic luminosity in the jet is a fixed fraction of the unbeamed luminosity, $\mathscr{L}_j = f\mathscr{L}_u$, so the total observed luminosity is

$$L_T = \mathscr{L}_u + L_j = \mathscr{L}_u(1 + f\delta^p). \quad (6)$$

This takes account of the approaching jet only; it can be shown that if jets come in oppositely directed pairs of similar intrinsic power, the receding beamed component (with Doppler factor equal to $\delta = [\gamma(1+\beta\cos\theta)]^{-1}$) will have a negligible contribution for likely values of the Lorentz factor and approaching jets within $\sim 60°$ of the line of sight (Appendix C). As before, the conditional probability is derived from Eq. (6), but in this case Eq. (5) is integrated numerically. A (likely) distribution of Lorentz factors can also be included (Urry and Padovani 1991). If we define the critical angle, θ_c, to be where the beamed and unbeamed luminosities are comparable (i.e., $f\delta^p = 1$), then for $\theta < \theta_c$ the luminosity will be dominated by beamed emission and we can identify these sources as blazars. The observed parent and beamed LFs for the case of a single-power-law intrinsic LF are shown in Fig. 13(b), for four values of f.

The key point is that the luminosity function of the beamed population has a characteristic broken-power-law form, flat at the low luminosity end and steep at the high luminosity end (Urry and Shafer 1984). This remains approximately the case even when the intrinsic luminosity function has a more complicated form, without sharp cutoffs (Urry and Padovani 1991). This means that the comparison of the number densities of beamed and parent populations is a strong function of luminosity, and for samples biased by relativistic beaming can be evaluated only by measuring the luminosity functions for each.

Since radio maps of blazars show the presence of a diffuse component we consider the two-component model for which $L_T = \mathscr{L}(1 + f\delta^p)$ (Eq. 6). The assumption that the intrinsic jet power is linearly proportional to the extended power may not be consistent with observations. Observed core power and total radio power are well correlated but apparently not linearly (Feretti et al. 1984; Giovannini et al. 1988; Jones et al. 1994). Although results vary, all seem to find that observed core power has a less than linear dependence on total radio power. (Since their samples include mainly radio galaxies, total power is essentially the same as extended power.) For example, Jones et al. (1994) find that $P_{\rm core} \propto P_{\rm total}^{0.8}$. The range of observed slopes, generally calculated taking upper limits into account, is 0.4–0.8. Calculating the regression with $P_{\rm core}$ as the dependent parameter will lead to a systematically different slope and indeed treating the variables symmetrically would be the appropriate approach (Isobe et al. 1990).

We note that the observed nonlinearity does not immediately conflict with the assumption that $\mathscr{L}_{\rm jet} = f\mathscr{L}_{\rm ext}$. First, beaming will cause large scatter in the observed $P_c - P_{\rm ext}$ plane due to the spread in viewing angles and possibly Lorentz factors. Second, selection effects could influence the slope of the correlation, although we do not immediately see why it should be flatter than unity. If the intrinsic relation is nonlinear (e.g., $\mathscr{L}_{\rm jet} = f\mathscr{L}_{\rm ext}^{x}$), then the calculation described here [represented by Eqs. (5) and (6)] would need to be modified. This would change the derived parameter values, but as long as x is reasonably close to 1, it should not be a major effect.

Radio-loud unification schemes, which involve primarily relativistic beaming, have been verified with the luminosity function approach just described. Radio-quiet schemes have not been tested this way because the radiation patterns are still very uncertain and the radiation anisotropy is probably much more draconian at the usual (blue) selection wavelengths (Pier and Krolik 1992; Ward et al. 1991; Djorgovski et al. 1991). For the high-power radio-loud scheme, obscuration is needed to explain the optical properties (namely, to allow for the fact that we do not have a direct view of the broad-line region in FR II radio galaxies), but it is not important for statistical arguments based on radio luminosities

alone. In the next section we outline the quantitative evaluation of the observed and beamed luminosity functions for radio-loud AGN.

6. STATISTICAL UNIFICATION OF RADIO-LOUD AGN

A fundamental test of the proposed unification of blazars and radio galaxies is whether the number statistics of the populations agree with the relativistic beaming hypothesis. The total number of beamed objects (here, blazars) must be small compared to the number of parent objects (radio galaxies), as they are presumably oriented at small angles to the line of sight. This ratio depends only on the critical angle dividing blazars and radio galaxies, which in turn depends on the amount of beaming (essentially, the Lorentz factor and the relative luminosities of beamed and unbeamed components). The critical angle is therefore central to unification.

In recent years it has become possible to test unified schemes via the number statistics of complete samples of blazars and radio galaxies. This section describes separately the statistics of the unification of quasars and FR II radio galaxies (Sec. 6.1) and of BL Lac objects and FR I radio galaxies (Sec. 6.2). Since relativistic beaming is best constrained by radio observations (thanks to VLBI), we compare in Sec. 6.3 the Lorentz factors from superluminal motion, SSC calculations, and jet/counterjet ratios with those derived from number statistics.

6.1 Unification of Radio Quasars and FR II Galaxies

We start by deriving the luminosity function of FR II radio galaxies, then we beam it according to the prescription outlined in Sec. 5.6 and compare the beamed and observed radio luminosity functions for quasars. The free parameters are γ, the bulk Lorentz factor of the jet, and f, the fractional luminosity of the jet. One can further constrain these two parameters from R, the ratio of beamed to unbeamed flux (core to extended flux in high-resolution radio maps; Appendix C).

6.1.1 Content of the 2 Jy sample of radio sources

As in Padovani and Urry (1992), we derive quasar and radio galaxy luminosity functions from the 2 Jy sample (Wall and Peacock 1985), a complete flux-limited sample of 233 sources with flux at 2.7 GHz $F_{2.7} \geq 2$ Jy. Redshifts and optical spectroscopic identifications have been updated using the latest version of the 1 Jy catalog (Stickel et al. 1994) and new optical spectra for sources with declination $d<10°$ (di Serego Alighieri et al. 1994b).

Quasars (and BLRG) are distinguished from radio galaxies (NLRG) by whether they have broad optical/ultraviolet emission lines or not. This criterion might not be as straightforward to apply as it sounds: recent papers (Laing et al. 1994; Economou et al. 1995; Hill et al. 1995) have pointed out that some objects classified as narrow-line galaxies actually show broad Hα emission. This is particularly likely for high-redshift sources classified on the basis of an Hβ line, for which the broad wings can be extinguished by modest reddening, thus introducing a redshift dependence (in practice) to the definition of Type 1 vs. Type 2 AGN.[11]

Only 3 of the 2 Jy sources (1% of the sample) have no optical counterpart, while 14 more (6%) have no redshift information. The great majority of the objects without redshifts are classified as galaxies, i.e., they appear extended, and based on their visual magnitudes they have estimated redshifts larger than 0.7.

Morphological classifications as FR I or FR II for the galaxies in the 2 Jy sample have been updated according to new radio maps for objects with $d<10°$ and $z<0.7$ (Morganti et al. 1993), and using additional information as available (Zirbel and Baum 1995, and references therein). 15 galaxies are classified as compact or unresolved, while 7 more are, to the best of our knowledge, unclassified. The division between steep- and flat-spectrum quasars was made at a radio spectral index between 2.7 and 5 GHz of $\alpha=0.5$.

These updates have essentially no effect on the FSRQ and SSRQ luminosity functions. For FR II radio galaxies, the luminosity function was originally derived (Padovani and Urry 1992) from a different sample, the 3CR catalog (Laing et al. 1983), because at the time a large fraction (nearly one third) of FR II galaxies in the 2 Jy sample had uncertain redshift estimates and their estimated evolution differed from that of radio galaxies in other samples.[12] While neither the different selection frequency nor the different flux limit of the 3CR appeared to affect the resulting luminosity function substantially, the 2 Jy FR II sample is now much better defined, so we revisit the question of using it.

The new 2 Jy FR II galaxies still exhibit less evolution than the 3CR FR II galaxies, although the evolutionary properties of the two samples are consistent at the 1σ level. Using only the definite FR II radio galaxies with $z<0.7$ (the completeness limit of the spectroscopic subsample of di Serego

[11]The precise meaning of "narrow-line" AGN, particularly if every Type 2 AGN harbors a hidden Type 1 nucleus, is not well-defined. For some astronomers it means AGN completely devoid of high-velocity ionized gas, while for others it means that broad lines are simply not detectable in the best spectrum to date. To rule out the presence of a hidden broad-line region in every Type 2 AGN would require spectropolarimetry more sensitive than that currently available, not to mention more observing time. It is also not particularly useful to have objects changing type based on the latest best observations. Thus, we favor a definition based on fixed observational criteria; for example, a given signal-to-noise ratio in a given wavelength range (perhaps out to Hα in the rest frame but excluding the Paschen lines). Based on spectra meeting these criteria, all AGN could be categorized definitely as Type 1 or Type 2. One would then have to devise other names to represent objects with similar intrinsic (as opposed to observed) properties. For example, 3C 234 would be called a Type 1 object because it has strong broad lines but at the same time it would belong with NGC 1068 (a Type 2 AGN) in some new category because both have hidden broad-line regions.

[12]The evolutionary properties of a sample can be characterized by the mean value of the ratio between V, the volume enclosed by an object, and $V_{\max}$, the maximum accessible volume within which the object could have been detected above the flux limit of the sample. In a Euclidean geometry, then, $V/V_{\max}=(F/F_{\lim})^{-3/2}$, where F is the observed flux of an object and $F_{\lim}$ is the flux limit of the survey. In the absence of evolution $V/V_{\max}$ has the property of being uniformly distributed between 0 and 1, with a mean value of 0.5 (Rowan-Robinson 1968; Schmidt 1968). When the survey is made up of separate fields with different flux limits, as is the case for the EMSS, it is more appropriate to use V_e/V_a, that is the ratio between *enclosed* and *available* volume (Avni and Bahcall 1980).

Alighieri et al. 1994b), one obtains $\langle V/V_{max}\rangle=0.55\pm0.04$, where the quoted error is $1/\sqrt{12N}$, appropriate for a uniform distribution. The best-fit evolution parameter[13] is $\tau=0.26$ and the associated 1σ interval is [0.16, 1.0]. This evolution is consistent with the earlier estimate (Padovani and Urry 1992) and is within 1σ uncertainty of the value for the 3CR FR II galaxies, for which the corresponding number is $\tau=0.17$ with 1σ interval of [0.15, 0.19]. If there is significant contamination of the 3CR NLRG sample with BLRG, as mentioned above, this could make their observed evolution too high (more like quasars). The two FR II luminosity functions, for the 2 Jy and 3CR galaxies, are in good agreement, although due to the smaller evolution, the 2 Jy one is somewhat flatter at higher powers. For consistency with the FSRQ and SSRQ samples, we now use the 2 Jy FR II LF (with $\tau=0.26$) in the calculations that follow.

The 2 Jy sample includes, as do other radio samples, a sizeable fraction of compact steep-spectrum (CSS) and gigahertz peaked-spectrum (GPS) sources (~20% CSS; Morganti et al. 1993). We exclude galaxies classified by Morganti et al. (1993) as compact or with unresolved radio structures, so no CSS or GPS objects should be in our FR II (or FR I) samples. However, since 2 Jy objects with broad optical line emission and unresolved radio emission are classified as quasars (FSRQ or SSRQ depending on radio spectral index), some SSRQ could actually be CSS sources and some FSRQ could actually be GPS sources. The place of CSS and GPS sources in the unified scheme is discussed further in Sec. 8.2.4. Even if they should be excluded from the unified scheme, which is not necessarily the case, they are unlikely to have "contaminated" the quasar sample because the fraction of such sources is not large; the derived luminosity functions will be distorted only if there are systematic trends with luminosity or redshift.

6.1.2 Observed LFs of high-luminosity radio sources

Given the 2 Jy sample as defined, we calculate the luminosity functions of high-power radio sources as follows. First, we fit an exponential pure luminosity evolution model to each sample, by finding the evolutionary parameter which makes $\langle V/V_{max}\rangle=0.5$ and then testing the goodness of fit via a KS test. The best-fit values of τ for each sample are listed in Table 2, along with median redshifts and $\langle V/V_{max}\rangle$ values. Each luminosity function was de-evolved using the appropriate best-fit evolution. Figure 14 shows the resulting local luminosity functions at 2.7 GHz for FR IIs, SSRQ, and FSRQ.[14]

TABLE 2
Evolution of AGN Samples

Class	Sample	N	median z	$\langle V/V_m\rangle$	τ
FR I galaxies	2 Jy	29	0.02	0.42 ± 0.05	...[a]
FR II galaxies[b]	2 Jy	61	0.15	0.55 ± 0.04	$0.26^{+0.74}_{-0.10}$
SSRQ . . .	2 Jy	37	0.76	0.64 ± 0.05	$0.15^{+0.05}_{-0.02}$
FSRQ . .	2 Jy	52	0.91	0.64 ± 0.04	$0.23^{+0.07}_{-0.04}$
RBL . . .	1 Jy	34	0.55	0.60 ± 0.05	$0.32^{+0.27}_{-0.08}$
XBL . . .	EMSS	30	0.30	0.36 ± 0.05[c]	$-0.14^{+0.05}_{-0.12}$

a – No evolution assumed.
b – $\langle V/V_m\rangle$ and τ calculated for the 57 objects with $z\leq0.7$.
c – Excluding the objects with $f_x<10^{-12}$ erg cm^{-2} s^{-1}, $\langle V/V_m\rangle=0.48\pm0.06$.

The luminosity function of FSRQ LF (filled circles) is flattest and extends to the highest luminosities. The luminosity functions of SSRQ (open triangles; Fig. 14) and FR II galaxies (open squares) are similar in shape over the common range of powers, but the SSRQ are lower in number density: the number ratio of the two classes for $P_{2.7}\gtrsim5\times10^{25}$ W Hz^{-1} is 6.4. This is larger than in Padovani and Urry (1992), due to the different LF used for the FR II galaxies.

6.1.3 Beamed LFs of high-luminosity radio sources

The beaming calculation is as follows. We start with the derived parent luminosity function, then calculate the effect of beaming it [Eqs. (4)–(6)], adjusting free parameters γ (the Lorentz factor) and f (the fraction of luminosity intrinsic to the jet) to match the observed luminosity function of FSRQ. It was not possible to fit the observed FSRQ luminosity function with a single Lorentz factor; it required instead a distribution in the range $5\lesssim\gamma\lesssim40$, weighted toward low values: $n(\gamma)\propto\gamma^{-2.3}$, with a mean value $\langle\gamma\rangle\simeq11$ and $f\simeq5\times10^{-3}$. [Note that this last parameter is fixed by the largest γ and by the maximum value of the ratio between beamed and unbeamed radio flux, R; Eq. (C5).]

Figure 14 shows the beamed (solid line) and observed (filled circles) radio LFs of FSRQ, which are in very good agreement. The ratio between FSRQ and parents, integrated over the full luminosity function, assuming that of the FR IIs cuts off at the low luminosity end, is ~2%. (Because of the flat LF slope at low luminosities, this percentage is not too sensitive to the cutoff.) The critical angle separating FSRQ from SSRQ and FR IIs[15] is $\theta_c(\gamma_1)\sim14°$. The fitted parameters of this beaming model are summarized in Table 3.

According to the beaming hypothesis, the steep-spectrum radio quasars are supposed to be at intermediate angles and their intrinsic properties—in particular, the value(s) of γ and f—must be identical to those of the FSRQ. Therefore, these parameters are already fixed. The method of calculation is similar to the one used in the previous section; however, since SSRQ are supposed to be misaligned objects, $\theta_{min}\neq0°$. We take $\theta_{min}=14°$, and the observed value of $R_{min}\sim0.002$ is used to constrain θ_{max} for SSRQ [Eq. (C4)]. With no free

[13]Here we characterize evolution in terms of exponential luminosity evolution, $P(z)=P(0)\exp[T(z)/\tau]$, where $T(z)$ is the look-back time and τ is the time scale of evolution in units of the Hubble time.

[14]The FSRQ luminosity function includes PKS 0521−365, which was inadvertently excluded by Padovani and Urry (1992). This is a low-redshift, highly polarized object (Angel and Stockman 1980), classified as a galaxy by Wall and Peacock (1985) and as a BL Lac by Véron-Cetty and Véron (1993), but showing broad Balmer lines (see Sec. 7.2). It was not included in the 1 Jy BL Lac sample (Stickel et al. 1991) because two emission lines exceeded the equivalent width criterion, but its [O III] luminosity is more typical of BL Lacs than of FSRQ, so it could be a transitional object (see Sec. 7.1).

[15]There is actually a range of critical angles, one for each γ [Eq. (C4)]. The larger the Lorentz factor, the smaller the critical angle; $\theta_c(\gamma_1)=14°$ is the largest angle within which an FR II would be identified as an FSRQ. Using this angle is appropriate for our purposes because the fitted distribution of Lorentz factors is skewed to low values.

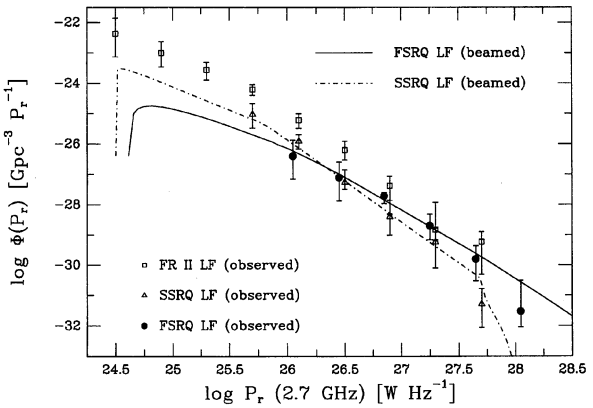

FIG. 14—Local differential radio luminosity functions for high-luminosity radio sources: flat-spectrum radio quasars (*filled circles*), steep-spectrum radio quasars (*open triangles*), and FR II galaxies (*open squares*). The error bars represent the sum in quadrature of the 1σ Poisson errors (Gehrels 1986) and the variations of the number density associated with a 1σ change in the evolutionary parameter τ (see Padovani and Urry 1992 for details). The luminosity functions of FR IIs and SSRQ have similar slopes and extend to the same luminosity at the bright end, although the FR IIs extend a decade lower at the faint end. The FSRQ luminosity function is distinctly flatter and extends to higher luminosities. This agrees well with the predictions of a beaming model calculated for FSRQ (*solid line*) and SSRQ (*dot-dashed line*); see Sec. 6.1.3 (Table 3) for details of the model parameters.

parameters, then, we calculate the beamed luminosity function of SSRQ.

The comparison between observations (open triangles) and the beaming model (dashed line) for SSRQ is shown in Fig. 14. The agreement is quite good, especially considering we did not adjust the parameters to optimize the FSRQ and SSRQ fits jointly. The angle dividing SSRQ from FR IIs is $\theta\sim 38°$ (Table 3).

The same distribution of Lorentz factors produces a good fit to both the luminosity functions of FSRQ and SSRQ. The value of $\theta\sim 38°$ for the angle separating SSRQ from FR II galaxies is in reasonable agreement with the angle derived from the number density ratio in the observed range of overlapping luminosity, $\theta=\arccos(1+1/6.4)^{-1}\simeq 30°$. The latter estimate is valid only when dealing with unbeamed luminosities or (in an approximate way) when the effect of beaming is not very strong because the objects are viewed off-axis, as in this case. For the 3CR sample, in which beaming is unimportant, Barthel (1989) found $\theta=44^{\circ}_{.}4$ from the ratio of quasars to radio galaxies in the interval $0.5<z<1$.

Table 3 summarizes the beaming parameters for the radio band for different classes of objects (see Sec. 6.2 for a discussion of the parameters for the BL Lac class). Note that we have used $p=3+\alpha$ (see Appendix B); using instead $p=2+\alpha$ results in the Lorentz factors extending to higher values (Padovani and Urry 1992), and in a slightly larger critical angle.

From the observed values of R we can estimate a lower limit to the maximum Lorentz factor (Appendix C). The FR II galaxy OD-159 is the most lobe-dominated source in the 2 Jy sample. The most core-dominated FSRQ known is 0400+258, which does not actually belong to the 2 Jy sample (its 2.7 GHz flux $\sim$1.5 Jy); its measured R is comparable to the lower limits (when no extended emission was detected) for some of the 2 Jy FSRQ. For these two objects, the R values, K corrected [Eq. (C2)] and extrapolated (when necessary) to 2.7 GHz rest frequency assuming $\alpha_{\rm core}-\alpha_{\rm ext}=-1$, are $R_{\rm min,FR\ IIs}<6\times10^{-5}$ (OD-159; Morganti et al. 1993) and $R_{\rm max,FSRQ}\simeq 1000$ (0400+258; Murphy et al. 1993). Using Eq. (C8), we find $\gamma_{\rm max}>(1.7\times10^{7}2^{1-p})^{1/2p}\sim 13$ for $p=3$.

TABLE 3
Beaming Model Parameters

Class	γ_1	γ_2	$\langle\gamma\rangle$	G	f	θ_c	% Total
FSRQ	5	40	11	−2.3	0.5×10^{-2}	14°	2%
SSRQ[a]	5	40	11	−2.3	0.5×10^{-2}	38°	10%
RBL	5	32	7	−4.0	1.3×10^{-2}	12°	2%
RBL[b]	2	20	3	−4.0	4.8×10^{-2}	19°	5%
XBL	...	...	3	...	1.0×10^{-1}	30°	14%

a – By assumption there are no free parameters for this fit; θ_c is determined by $R_{\rm min}$ and the rest are fixed at the best-fit values for FSRQ.
b – Alternative fit with lower γ_1.

For these observed R values, small values of p imply high values for the largest Lorentz factor (here, for $p=2$, $\gamma_{\rm max}\gtrsim 54$). More precisely, $\alpha_r\simeq -0.3$ for the 2 Jy FSRQ (Padovani and Urry 1992), so $p\simeq 1.7-2.7$ if p ranges between $2+\alpha$ and $3+\alpha$. Then $\gamma_{\rm max}\gtrsim 17$ (for $p=2.7$) or $\gtrsim 120$ (for $p=1.7$). The need for quite high values of the largest γs for smaller values of p was noted by Urry et al. (1991a) and Padovani and Urry (1992) from their fits to the observed LFs.

While the SSRQ–FSRQ-only scheme (ignoring the radio galaxies; Orr and Browne 1982) cannot be ruled out, it is much harder to reconcile with the available data, mainly because there seem to be too few SSRQ for them to be the parents of FSRQ (Padovani and Urry 1992). The FR II–SSRQ–FSRQ scheme, illustrated by the curves in Fig. 14, can be tested further via the predicted radio counts of flat- and steep-spectrum quasars, which converge at easily accessible levels (Padovani and Urry 1992).

6.2 Unification of BL Lac Objects and FR I Galaxies

The unification of low-luminosity radio-loud AGN can be tested in the same way, by comparing the observed number densities of BL Lac objects and FR I radio galaxies. We derive the FR I luminosity function (Padovani and Urry 1990; Urry et al. 1991a), beam it according to the prescription outlined in Sec. 5.6, and fit it to the observed BL Lac luminosity functions (Padovani and Urry 1990; Urry et al. 1991a; Celotti et al. 1993). The free parameters are γ, the bulk Lorentz factor of the jet, and f, the fractional luminosity of the jet. We further constrain these two parameters either from R, the ratio of beamed to unbeamed flux (that is, the core to extended flux in high resolution radio maps), as was done for quasars and FR IIs (Sec. 6.1), or from the ratio of maximum BL Lac luminosity to maximum FR I luminosity. The former approach is used for the radio comparison (Sec. 6.2.4) and the latter approach is used for the X-ray comparison (Sec. 6.2.3) because X-ray spatial resolution is insufficient to measure R. Some separation of beamed and unbeamed components is now becoming possible for radio

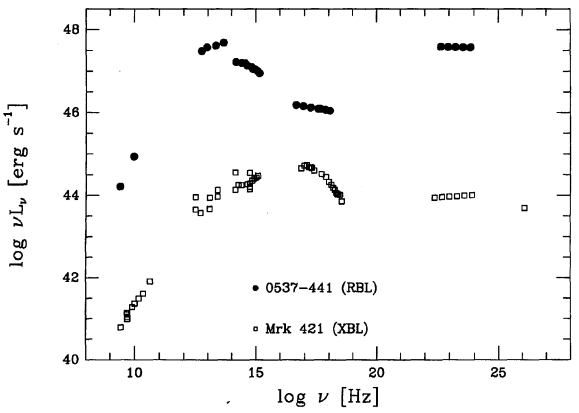

FIG. 15—Multiwavelength spectra of a low-energy cutoff BL Lac (LBL) (PKS 0537−441; *filled circles*) and a high-energy cutoff BL Lac (HBL) (Mrk 421; *open squares*). The peak synchrotron luminosity occurs at infrared/optical wavelengths for the LBL and at soft X-ray wavelengths for the HBL. In this example, the HBL is both an XBL and an RBL, and (as in most cases) the LBL is an RBL. A value of $q_0=0.5$ has been assumed. (Following Maraschi et al. 1994b; figure courtesy of Rita Sambruna.)

galaxies with *ROSAT* (Worrall and Birkinshaw 1994) and in the future, we expect X-ray measurements of R for large samples of BL Lacs will be possible with *AXAF*.

6.2.1 X-ray and radio samples of BL Lac objects

Sizeable well-defined samples of BL Lac objects are now available. X-ray surveys have produced a number of samples, including the *HEAO-1* A-2 all-sky survey (only 5 BL Lac objects; Piccinotti et al. 1982), the EMSS (36 BL Lacs; Stocke et al. 1991), and the *EXOSAT* High Galactic Latitude Survey (HGLS: 11 BL Lacs; Giommi et al. 1991). The last two go down to fairly low X-ray fluxes, $\sim 2\times 10^{-13}$ erg cm^{-2} s^{-1} in the 0.3–3.5 keV band. Redshifts are available for most EMSS BL Lacs.

The 1 Jy sample of BL Lac objects, a radio-selected sample of size comparable to the EMSS X-ray-selected sample, has also become available recently (Stickel et al. 1991). These BL Lac objects were selected from a catalog of 518 radio sources with 5 GHz fluxes ≥ 1 Jy on the basis of their flat radio spectra ($\alpha_r \leq 0.5$), weak or absent emission lines (rest-frame equivalent widths $W_\lambda \leq 5$ Å), and optical magnitudes (brighter than $V=20$). Of the 34 1 Jy BL Lacs in the complete sample, 26 have redshift information from emission lines (Stickel et al. 1991; Stickel et al. 1994), 4 have lower limits to their redshifts from absorption lines, while in 4 objects neither emission or absorption lines have been detected, but a lower limit of $z>0.2$ can be estimated from their stellar appearance (Stickel et al. 1993).

6.2.2 Properties of X-ray-selected and radio-selected BL Lac objects

The properties of X-ray-selected and radio-selected BL Lac objects are systematically different (Ledden and O'Dell 1985; Stocke et al. 1985; Maraschi et al. 1986; Padovani 1992a; Laurent-Muehleisen et al. 1993). On average, XBL have lower polarization, less variability, higher starlight fractions, and are less luminous and less core-dominated than RBLs (Stocke et al. 1985; Morris et al. 1991; Perlman and Stocke 1993; Jannuzi et al. 1994).

The two classes occupy different regions on the $\alpha_{ro}-\alpha_{ox}$ plane, which is indicative of different broadband energy distributions (Stocke et al. 1985; Ledden and O'Dell 1985). This is illustrated in Fig. 15 (Maraschi et al. 1994b), which shows the multiwavelength spectra of a radio-selected BL Lac (PKS 0537−441) and an X-ray-selected BL Lac (Mrk 421). The overall shape of the RBL spectrum, notably the wavelength of the peak of the synchrotron emission and the relative strength of the gamma-ray emission, is similar to that of the flat-spectrum radio quasar 3C 279 (Fig. 4), as is true for RBLs and FSRQ in general (Maraschi et al. 1994b). The peak of the synchrotron component is typically at infrared/optical wavelengths for the RBL (and FSRQ) and in the soft X-rays for the XBL. If the peak wavelength changes smoothly and continuously from short (ultraviolet/X-ray) to long (infrared/optical) wavelengths for BL Lac objects as a whole, the radio/optical/X-ray colors of RBL and XBL can be reproduced easily (Padovani and Giommi 1995a).

The 1 Jy sample of RBL shows a weak *positive* evolution, consistent at the 2σ level with no evolution ($\langle V/V_{\rm max}\rangle=0.60\pm0.05$; Stickel et al. 1991), while the EMSS XBL display a *negative* evolution, appearing less abundant and/or less luminous at higher redshifts, ($\langle V_e/V_a\rangle=0.36\pm0.05$; Wolter et al. 1994). For luminosity evolution of the form $L_x(z)=L_x(0)\exp[c_x T(z)]$, where $T(z)$ is the look-back time, the best-fit evolution for the EMSS sample is $c_x=-7.0$, with a 2σ range of -15.9 to -1.3 (Wolter et al. 1994), nearly consistent (at the $\sim 2\sigma$ level) with zero evolution. For the 1 Jy RBL sample, $c_r=3.1$ with a 1σ range of 1.7 to 4.2 (Stickel et al. 1991, with $c=1/\tau$), also consistent with zero evolution at the 2σ level.

Both samples are still relatively small (30 and 34 objects for XBL and RBL, respectively), so it is premature to draw any conclusion regarding the supposedly different evolutionary behaviors of the two classes. This is confirmed by two additional results. First, for the 14 RBL of the S4 survey ($f_r \geq 0.5$ Jy at 5 GHz; Stickel and Kühr 1994), $\langle V/V_{\rm max}\rangle=0.44\pm0.08$ (Padovani and Giommi 1995a), more like the EMSS XBL. Second, for the EMSS, raising the flux limit only slightly, to 10^{-12} erg cm^{-2} s^{-1}, changes the mean V_e/V_a from 0.33 ± 0.06 to 0.48 ± 0.06 (Della Ceca 1993). These results for RBL and XBL are completely consistent with no evolution.

6.2.3 Population statistics for X-ray samples

The EMSS and HGLS XBL samples, which went down to fairly low X-ray fluxes, $\sim 2\times 10^{-13}$ erg cm^{-2} s^{-1} in the 0.3–3.5 keV band, revealed a decided flattening of the counts at low flux, in marked contrast to the steep X-ray $\log N-\log S$ curves for other kinds of AGN. Padovani and Urry (1990) compared predictions of the FR I unified scheme with the X-ray counts from these two samples (plus the *HEAO-1* A-2 sample) and found good agreement for a bulk Lorentz factor $\gamma_x \sim 3$ and a ratio of intrinsic jet luminosity to unbeamed luminosity $f \approx 0.1$. The total number of BL Lac objects was $\sim$14% of the number of FR I galaxies, with more than 90%

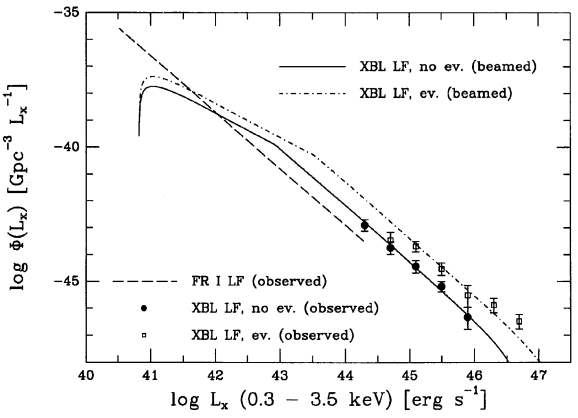

FIG. 16—The local differential X-ray luminosity functions of low-luminosity radio-loud AGN. The observed LF of FR I galaxies is represented by a broken power law (*dashed line*). The observed LFs for the EMSS XBL sample (no evolution: *filled circles*; anti-evolution: *open squares*) are fitted by beaming models for the non-evolving case (*solid line*) and the anti-evolving case (*dash-dotted line*); data and evolution estimate from Wolter et al. (1994). Error bars correspond to 1σ Poisson errors (Gehrels 1986).

of the BL Lacs at lower X-ray luminosities than currently observed, and the critical angle separating BL Lacs from FR Is was $\theta_c \sim 30°$.

Since then, the EMSS-derived X-ray luminosity function of BL Lac objects has been published (Morris et al. 1991; Wolter et al. 1994) and now we can fit it directly. We compare our beaming predictions with the X-ray luminosity function for the EMSS subsample of 30 BL Lacs with $f_x \geq 2\times10^{-13}$ erg cm^{-2} s^{-1}, assuming no evolution (which is consistent at the $\sim 2\sigma$ level with the observational data; Wolter et al. 1994; see also Sec. 6.2.2). We follow the method of Avni and Bahcall (1980) to take into account the fact that the volume surveyed in the EMSS is a function of limiting flux. Redshifts, fluxes, and sky coverage were taken from Wolter et al. (1994). Five objects in the sample have no redshift determination; these were initially excluded from the sample but their presence was taken into account by multiplying the normalization of the resulting luminosity function by 30/25.

Figure 16 shows the luminosity function (solid line) from the fitted beaming model of Padovani and Urry (1990) compared to the observed LF for the EMSS sample for no evolution (filled circles). The model agrees very well with the data ($\chi^2_\nu \simeq 0.3$), especially considering that the parameters for the model were optimized for the number counts. If instead we use the anti-evolving X-ray luminosity function of Wolter et al. (1994), with $\tau = -0.14$, then by increasing $R_{\max}$ (the ratio between the maximum luminosities of the parent and beamed populations) from 250 (as in Padovani and Urry 1990) to 1000 we get the dot-dashed line in Fig. 16. The ratio between BL Lacs and FR Is increases to about 30%, $\gamma_x \sim 2.9$, $f \sim 1.1$, and $\theta_c \sim 47°$. This is a much poorer fit to the data ($\chi^2_\nu \simeq 2.5$) but given the uncertainties in the X-ray luminosity function of FR Is (see below), one cannot definitely rule out this case.

The redshift distribution of the EMSS is difficult to reproduce. Despite the fact that beaming in the zero evolution case fits the observed LF better, it cannot reproduce the peak in $N(z)$ at $z \sim 0.2-0.3$, whereas our fit to the anti-evolving LF does. Browne and Marchã (1993) have suggested that recognition problems affecting low-luminosity BL Lacs whose light is swamped by the host galaxy, typically a bright elliptical (Sec. 5.4), might explain the unusual redshift distribution and anti-evolution of the EMSS XBL. Padovani and Giommi (1995) have shown through numerical simulations, however, that although recognition problems have some effect, they are probably not strong enough to affect these properties so drastically.

A complication in applying beaming models to the X-ray band stems from the uncertainties in the X-ray luminosity function of FR Is. These are due to its bivariate nature, small statistics, and the nondetection in X rays of ~30% of the complete radio-selected sample (which was already small). *ROSAT* will eventually produce an X-ray-selected sample of FR Is, or at least complete X-ray data on a sizeable radio-selected sample of these objects. Already one interesting *ROSAT* result is the identification of resolved (thermal) and unresolved X-ray emission in radio galaxies, as assumed by Padovani and Urry (1990). The beaming model discussed in this section predicts ratios of intrinsic-jet to extended X-ray flux in the range 0.1–1, marginally inconsistent with the observed ratios of nonthermal to thermal emission for six low-luminosity radio galaxies of 1–5 (Worrall and Birkinshaw 1994). The disagreement is even worse because in radio galaxies the jets should be de-amplified (for $\gamma \sim 3$, $\delta < 1$ for $\theta > 45°$; Appendix A). Further high-resolution X-ray observations will put more constraints on the f parameter.

The XBL samples are still relatively small. Larger XBL samples are now being optically identified, including the *HEAO-1* LASS sample (Schwartz et al. 1989; Laurent-Muehleisen et al. 1993) and the *Einstein* Slew Survey Sample (Elvis et al. 1992; Schachter et al. 1993; Perlman et al. 1995). In addition, the *ROSAT* All-Sky Survey should produce large numbers of new BL Lac objects—our beaming model for the X-ray samples predicts roughly two objects per square degree down to $F_x = 10^{-14}$ erg cm^{-2} s^{-1} in the 0.3–3.5 keV band—some of which have already been identified (Bade et al. 1994). With these new data we will be able to address the beaming hypothesis with better statistics.

6.2.4 Population statistics for radio samples

The radio data are better suited than the X-ray data for testing the beaming hypothesis for BL Lac objects. One reason is that the radio sample of FR I galaxies is larger than the X-ray sample. In addition, the higher spatial resolution available with radio interferometry allows estimates of the ratio between beamed and unbeamed radio flux (Antonucci and Ulvestad 1985), thus adding an important constraint to the combination of the parameters γ and f (Appendix C).

The radio luminosity function of FR I radio galaxies was derived by Urry et al. (1991a) from the 2 Jy catalog (and converted to 5 GHz) and then extended to lower radio powers using the radio LF of elliptical galaxies of Franceschini et al. (1988). Here we choose *not* to include the low-luminosity radio ellipticals, but restrict ourselves only to sources classi-

fied explicitly as FR Is (some of the lowest luminosity ellipticals could in fact have radio emission dominated by thermal emission rather than the nonthermal BL Lac nucleus; Phillips et al. 1986). Our results, however, are basically unchanged, since the beamed LF for BL Lacs at $P_5 \gtrsim 5\times10^{25}$ W Hz^{-1} (i.e., where it overlaps with the observed LF) is largely unaffected by the behavior of the FR I LF at such low powers. The new optical identifications (di Serego Alighieri et al. 1994b) and radio maps (Morganti et al. 1993) also have little effect on the FR I luminosity function; the fit to the new LF used here is consistent with the one in Urry et al. (1991a). The evolutionary properties of FR I radio galaxies are consistent with no evolution, with $\langle V/V_{\max}\rangle = 0.42\pm0.05$.

We can compare our FR I luminosity function, derived from the 2 Jy sample (selected at 2.7 GHz), with that of de Ruiter et al. (1990), based on the B2 sample (selected at 408 MHz) plus nearby ($z<0.2$) 3CR radio galaxies (selected at 178 MHz). Converting our Fr I LF to $H_0 = 100$ km s^{-1} Mpc^{-1} and $\nu = 408$ MHz (assuming $\alpha_r = 0.7$), we find excellent agreement from $P_{408}\sim6\times10^{23}$ W Hz^{-1} up to the break at $P_{408}\sim3\times10^{25}$ W Hz^{-1} (see Fig. 13 of de Ruiter et al. 1990). Above the break our LF is steeper, not surprisingly, since they did not exclude FR II sources. The two lowest luminosity bins in our LF ($P_5 \lesssim 2\times10^{23}$ W Hz^{-1}), lie a factor of 2–3 above the De Ruiter et al. LF. This disagreement is not surprising, as our two points are highly uncertain, with only one object in each bin. Also, the two objects, M82[16] and M84, are nearby ($z = 0.0014$ and 0.0028, respectively) and so sample the local overdensity, whereas the B2 sample, being deeper than the 2 Jy, averages over a larger volume of space. (The equivalent flux limit of the B2 survey translated to 2.7 GHz with $\alpha = 0.7$ is 130 mJy.) In any case, excluding the first two bins does not alter our fitted beamed LF significantly.

Using a two-power-law approximation to our FR I luminosity function, we fitted a beamed LF to the observed LF for the 1 Jy BL Lacs. The latter was obtained as described in Stickel et al. (1991) with the addition of S5 0454+844, which had no redshift at the time. It is impossible to fit the data with a single Lorentz factor; instead, an acceptable fit to the LF and the observed R values is obtained for Lorentz factors distributed in the range $5 \lesssim \gamma_r \lesssim 32$. While the form of the distribution is not well constrained, it is weighted toward lower values; e.g., for a power law of the form $N(\gamma_r) \propto \gamma_r^G$, the best-fit index is $G\sim-4$.

Figure 17 shows the excellent agreement between beamed (solid line) and observed (filled circles) radio luminosity functions for the 1 Jy sample of BL Lacs. The mean Lorentz factor, which is approximately independent of the exact shape of the distribution, is $\langle\gamma_r\rangle\sim7$, corresponding to a ratio between BL Lacs and FR Is of ~1:50, about an order of magnitude smaller than in the X-ray case (Sec. 6.2.3). The total number of BL Lacs is most sensitive to the lowest value of γ_r, while the maximum ratio of beamed to unbeamed flux is sensitive to the highest value. Our fitted model predicts

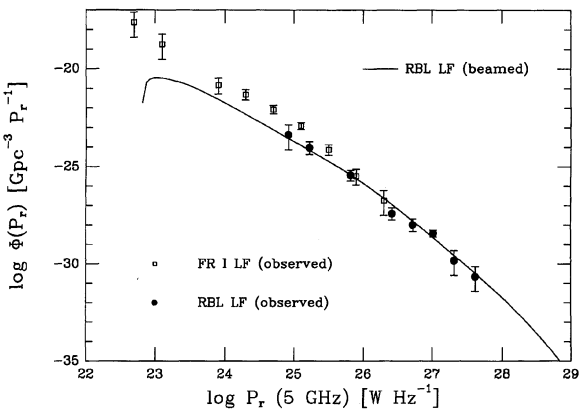

FIG. 17—The local differential radio luminosity functions of radio-selected BL Lac objects (*filled circles*; Stickel et al. 1991) and FR I radio galaxies (*open squares*; Sec. 6.2.4), compared to the fitted beaming model (*solid line*; first set of RBL parameters in Table 3). Error bars correspond to 1σ Poisson errors (Gehrels 1986).

that radio-selected BL Lacs are aligned within $\theta_c\sim12°$ of the line of sight. The fitted beaming parameters for radio-selected BL Lacs are summarized in Table 3.

As we did for quasars, we can estimate a lower limit to the maximum Lorentz factor from the observed maximum and minimum values of R for BL Lacs and FR Is, respectively (Appendix C). OJ 287 is the most core-dominated BL Lac in the 2 Jy sample (and in the 1 Jy sample), excluding those cases where no extended emission has been detected, and Fornax A is the most lobe-dominated FR I. The corresponding values of R, K corrected [Eq. (C2)] and extrapolated (when necessary) to 5 GHz rest frequency assuming $\alpha_{\rm core}-\alpha_{\rm ext}=-1$, are $R_{\rm min,FR\ I}\simeq4\times10^{-4}$ (Fornax A; Morganti et al. 1993) and $R_{\rm max,BL\ Lac}\simeq780$ (OJ 287; Kollgaard et al. 1992). Using Eq. (C8) as before, $\gamma_{\max}\gtrsim(2.0\times10^6 2^{1-p})^{1/2p}\sim9$ for $p=3$.

As was the case for the quasars, small values of p imply high values for the largest Lorentz factor (for $p=2$, $\gamma_{\max}\gtrsim30$). More precisely, since $\alpha_r\simeq-0.1$ for the 1 Jy BL Lacs (Stickel et al. 1991), $p\simeq1.9$–2.9 for p between $2+\alpha$ and $3+\alpha$. Then $\gamma_{\max}\gtrsim10$ (for $p=2.9$) or $\gtrsim38$ (for $p=1.9$).

The value of H_0 does affect the luminosity functions but has no direct effect on the derived beaming parameters. The fitted Lorentz factor, which is inversely proportional to the normalization of the beamed luminosity function, depends only on the ratio between the total numbers of objects (the integrals of the parent and beamed LFs). H_0 enters only because we constrain γ to some extent with the observed values of superluminal motion (for BL Lacs and for quasars separately; see Sec. 6.3). A higher H_0 would mean lower superluminal velocities, and in general, fits with lower γ_1 are possible. We did not explore parameter space exhaustively but we show an example of a low-γ fit for RBL in Table 3.

It is interesting that the luminosity functions of FR I and FR II galaxies overlap smoothly, as do those of BL Lac objects and FSRQ (Figs. 14 and 17). Possibly, they represent different manifestations of the same basic central engine, in which case the different radio morphologies and emission-

[16]Although M82 is classified as an FR I galaxy, its strong starburst component makes it an unlikely BL Lac parent; however, its inclusion does not change our results significantly.

line strengths would have to be closely linked to observed radio power (Maraschi and Rovetti 1994).

6.2.5 Relation of X-ray- and radio-selected BL Lac objects

The difference between XBL and RBL is surely a fundamental issue in understanding the BL Lac phenomenon. Our beaming results indicate that radio-selected BL Lac objects constitute a smaller fraction of FR I radio galaxies than do X-ray-selected BL Lacs (Table 3). This can lead to a higher fitted Lorentz factor in the radio calculation, since γ is inversely proportional to the normalization of the beamed luminosity function. The values from our published calculations are $\langle \gamma_r \rangle \sim 7$ (Urry et al. 1991a) and $\gamma_x \sim 3$ (Padovani and Urry 1990), in effect suggesting the radio emission is more collimated than the X-ray.

This result was exciting because it suggested XBL and RBL might represent slightly different orientations of the same underlying relativistic jet. Problems with this interpretation have recently emerged, as discussed below, but first we summarize the original argument. The apparent difference in Lorentz factors was interpreted (Urry et al. 1991a) in terms of an accelerating jet model (suggested for other reasons by Ghisellini and Maraschi 1989) in which the X-ray emission from the most compact region would have a smaller γ than the more extended radio-emitting region. In addition to explaining the apparent difference in number densities of XBL and RBL, the accelerating jet explained naturally the lower variability, polarization, and luminosities of XBL (Sec. 6.2.2, and references therein).

The original number density argument was actually independent of the Lorentz factors obtained from beaming calculations. Because XBL and RBL have similar X-ray luminosities, X-ray selection should be relatively unbiased (Maraschi et al. 1986). Since X-ray surveys detected very few known RBL, they must be relatively rare, exactly as expected if the radio emission is more beamed than the X-ray. This was supported by the X-ray number counts of RBL and XBL (Urry et al. 1991a). If, as our beaming results implied, RBL are viewed within $\sim 12°$ of the jet axis while XBL are between $\sim 12°$ and 30°, then RBL are a factor of ~ 7 less numerous than XBL (Table 3).

An alternative explanation of the same data was that the physical collimation itself increased along the jet, so that the narrower radio beams made it less likely that our line of sight would intercept their emission. This was commensurate with the X-ray and radio luminosity functions of RBL and XBL (Celotti et al. 1993). For this kind of fan beam, the luminosity function calculation (Celotti et al. 1993) implied a Lorentz factor that was quite high, $\gamma = 29$ (with $\theta_{c,r} = 2/\gamma \simeq 4°$, $\theta_{c,x} = 13°$, $f_r = 6 \times 10^{-3}$, and $f_x = 5 \times 10^{-3}$, assuming no evolution for both XBL and RBL), but it could be reduced if, for example, only 10% of FR Is were parents of BL Lacs ($\gamma = 10$, $\theta_{c,r} \simeq 11°$, $\theta_{c,x} = 41°$, $f_r = 0.2$, and $f_x = 0.5$).

This simple and satisfying picture based on jet collimation is now in doubt. Most significantly, the accelerating jet and the fan-beam jet are both contradicted by analysis of the multiwavelength spectra of complete samples of XBL and RBL (Sambruna 1994; Sec. 7.2.2). In addition, the fitted γ for RBL can actually be pushed to lower values, reducing the apparent difference between XBL and RBL (Sec. 6.3 and Table 3; but note that the fraction of beamed objects still remains smaller for RBL than for XBL). Finally, it is important to remember that the X-ray unification calculation is more poorly constrained than the radio calculation because the FR I samples contain fewer objects with X-ray data and because of the less extensive imaging information; thus, interpreting any difference in fitted Lorentz factors was premature.

6.2.6 New terminology and a new connection between BL Lac classes

There is now a viable interpretation of the observational data that is unrelated to jet collimation (Giommi and Padovani 1994; Padovani and Giommi 1995a). It is based on a single population of BL Lac objects characterized by a wide range of multiwavelength spectral shapes, with bolometric luminosities peaking at infrared/optical wavelengths for most RBL and at ultraviolet/X-ray for most XBL, as is observed (Giommi et al. 1995; Sambruna 1994). Before discussing this scenario further, we discuss new terminology that distinguishes clearly between the selection method used to find BL Lacs and the spectral characteristics of the sources themselves.

The new terms are motivated by the fact that the division of BL Lac objects into RBL and XBL can get garbled or confused. Strictly speaking, those terms are based on selection band rather than intrinsic physical properties, in which case some BL Lac objects already qualify as both RBL and XBL (e.g., Mrk 501), and many more "double agents" will appear as deeper radio and X-ray samples become available (Elvis et al. 1992). This leads to awkward terminology such as "XBL-like RBL" and "RBI-like XBL" when discussing the strong differences between the broadband spectral properties of RBL and XBL in the historical samples. Since we wish to explore these differences—notably the peak luminosities in the infrared/optical or ultraviolet/X-ray, respectively—it is useful to define categories in terms of the ratio of X-ray to radio flux (Ledden and O'Dell 1985).

Padovani and Giommi (1995) have suggested dividing RBL-like and XBL-like objects into LBL and HBL, respectively (for "low-energy-cutoff BL Lacs" and "high-energy-cutoff BL Lacs"), according to whether α_{rx} (between 5 GHz and 1 keV) is greater (LBL) than or less (HBL) than 0.75. These names reflect the actual spectral characteristics of the two types of BL Lacs, allowing the terms "XBL" and "RBL" to be reserved strictly for sample membership (which is well-defined). BL Lac objects like Mrk 501 or OJ 287 which appear in both radio- and X-ray-selected samples can be uniquely categorized as HBL or LBL, respectively. Most XBL are HBL (OJ 287 is an exception) and most RBL are LBL (Mrk 501 is an exception). The lack of precision of "high" and "low" reflects the possibility that the synchrotron peak in BL Lacs occurs at a wide range of wavelengths, perhaps not fully probed in current samples, from infrared through X-ray.

The essence of the argument of Padovani and Giommi (1995a) is that X-ray selection favors objects with a peak at

ultraviolet/X-ray wavelengths and thus finds fewer with peak at infrared/optical wavelengths. If radio rather than X-ray surveys are unbiased (because the radio emission does not "know" the wavelength of the peak luminosity), then HBL are relatively rare, about 10% in the 1 Jy plus S4 plus S5 radio-selected samples (Padovani and Giommi 1995). In effect, Giommi and Padovani take the opposite approach from Maraschi et al. (1986), assuming radio selection rather than X-ray selection is unbiased, and they find the opposite result: in complete contrast to the accelerating jet picture, they conclude that HBL constitute a minority of the BL Lac population.

Specifically, Giommi and Padovani (1994) argue that HBL outnumber LBL at a given X-ray flux, even though they are intrinsically less numerous, because the two classes sample different parts of the BL Lac radio counts (Giommi and Padovani 1994). As a consequence of their higher f_x/f_r ratios, HBL have lower radio fluxes ($\sim$10 mJy) and since fainter objects are more numerous than brighter ones (the radio counts are rising), their surface density is higher. Stated differently, X-ray surveys sample the BL Lac radio counts at low fluxes and mostly detect the $\sim$10% of objects with high f_x/f_r ratios. This holds down to quite faint X-ray fluxes, well below the *ROSAT* deep survey limit, below which the fraction of LBL should increase slowly and eventually dominate by a factor of 10 (Padovani and Giommi 1995a). The Giommi and Padovani hypothesis explains most of the properties of HBL—e.g., X-ray luminosity function, X-ray number counts, and radio flux distribution—using only the observed properties of RBL (and no free parameters).

There are at present insufficient data to determine whether the number ratio of HBL to LBL (integrated over all luminosities) is $\sim$0.1, as Giommi and Padovani conclude, or roughly the opposite! One persistent objection to the Giommi and Padovani picture is that the polarization characteristics of LBL and HBL differ in a way not obviously explained by a change in break frequency. Specifically, the LBL have higher polarization which varies more in both degree and position angle. According to Giommi and Padovani, the HBL are intrinsically less luminous—less extreme—so they should have lower polarization, but why the polarization angle is more stable is not obvious in their picture.

The beaming picture, comparing BL Lacs and FR I LFs, suggests that HBL are more numerous than LBL by at least a factor of 3. It does seem intuitive that more luminous objects are more rare, i.e., that luminosity functions rise to low luminosities (which they do for all known galaxies, active or not). Thus, one could ask how the bolometric luminosity functions of LBL and HBL compare; i.e., what the relative number densities are, at least in the range of overlapping luminosities. Using data from Giommi et al. (1995), we formed a close approximation to the bolometric LF using the luminosities at the peak of the emission in νL_ν. Figure 18 shows this pseudobolometric LF for the 1 Jy LBL (excluding the two HBL in the 1 Jy RBL sample) and the EMSS HBL (this sample includes no LBL). *This is a bivariate LF so it does not compensate for the selection effects inherent in the 1 Jy and EMSS samples.* The HBL appear to be more numerous in the range of overlap with number densities systematically above the LBL points. We note that the EMSS is effectively much deeper than the 1 Jy survey (its equivalent radio flux limit is $\sim$1 mJy; Padovani and Giommi 1995a). We also note the uncertainties are very large. This kind of figure will be very useful to rederive when larger samples of LBL and HBL are available.

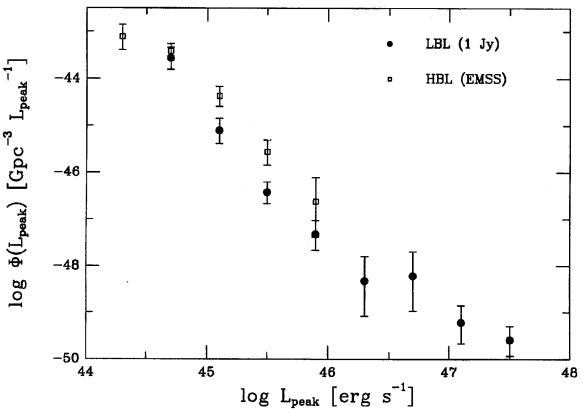

FIG. 18—The "approximate bolometric" luminosity function for 1 Jy LBL (*filled circles*) and EMSS HBL (*open squares*). This is the bivariate peak luminosity function, where the peak luminosity has been defined as the maximum in νL_ν from the data of Giommi et al. (1995) and no evolution has been assumed. Error bars correspond to 1σ Poisson errors (Gehrels 1986). The HBL appear to be more numerous in the range of overlapping luminosity, but selection effects inherent in the 1 Jy and EMSS samples are already present in these luminosity functions.

Clearly one would like to select samples in an unbiased way. Somewhere between the wavelengths where LBL and HBL have their spectral peaks, they must have roughly comparable fluxes. The optical has to be less biased than the X-ray or radio band, and indeed the optically brightest BL Lacs in the 1 Jy and Slew Survey samples have comparable optical magnitudes (Stickel et al. 1991; Perlman et al. 1995). The relative numbers of LBL and HBL in an optically selected sample, then, should reflect their relative numbers globally, at least better than radio or X-ray surveys do. Unfortunately, the best optically selected sample, the complete PG sample, has only six BL Lac objects (Green et al. 1986; Fleming et al. 1993). Of these, 1/3 are LBL and 2/3 are HBL, but the statistics are obviously poor. While formally there are more HBL than LBL in the PG sample, the observed ratio actually agrees well with what the Giommi and Padovani scenario would predict in the optical band (Padovani and Giommi 1995b). Larger optical samples of BL Lac objects are important for addressing the fundamental differences between LBL and HBL.

6.3 Independent Estimates of Relativistic Beaming Parameters

Independent estimates of Lorentz factors and angles to the line of sight are available, mostly from VLBI data. In VLBI observations of 12 FSRQ in the 2 Jy sample (Vermeulen and Cohen 1994, and references therein), all but one FSRQ show evidence of superluminal motion ($\beta_a > 1$). The apparent separation of radio components gives a lower limit to the Lorentz factor, $\gamma_{\min} = \sqrt{\beta_a^2 + 1}$ (Appendix A); the distribution

of $\gamma_{\min}$ for the fastest superluminal components in FSRQ covers the range 5–35, roughly the same as that necessary to explain the observed luminosity function (Sec. 6.1).

The observed β_a distribution can in principle be compared with that predicted using the LF-derived beaming parameters. Vermeulen and Cohen (1994) determined that a distribution of Lorentz factors peaked at high values best fit the observed β_a distribution for a small heterogeneous sample defined by a *post-facto* flux limit. (They calculated the expected distribution of β_a for naked jets without extended emission, which is appropriate to their sample of core-dominated objects and which is straightforward to calculate.) This is quite different from the steep distribution of Lorentz factors we found from fitting luminosity functions (Sec. 6.1.3). Whether these two results can be reconciled remains to be seen, but we note that our calculation is most sensitive to low values of γ, which yield the largest number of beamed objects, while superluminal motion statistics (particularly for samples of "favorite objects" studied in the past) are most sensitive to high values. Alternatively, one can compare the results from the recent VLBI surveys of well-defined flux limited samples (Pearson and Readhead 1988; Polatidis et al. 1995; Thakkar et al. 1995; Taylor et al. 1994) to the β_a distribution predicted by a more-difficult calculation incorporating selection effects appropriate to jets plus extended emission, but this calculation has not yet been done.

As is the case for emission-line blazars, all 13 1 Jy BL Lac objects observed more than once with VLBI techniques appear to show superluminal motion (Vermeulen and Cohen 1994; Gabuzda et al. 1994). For all but two objects, $\gamma_{\min}$ is higher than $\sim$4, and reaches at least $\sim$15. These results agree roughly with the distribution in γ_r required to fit the luminosity function and the core–halo ratios of radio-selected BL Lacs (Sec. 6.2).

Since two BL Lac objects have $\gamma_{\min}$ as low as 1.5, we tried a fit to the radio LF of BL Lacs with $\gamma_1=2$, leaving all other parameters unchanged. The resulting beamed LF is still in good agreement with the observed one, although the Lorentz factors are now lower, $2\lesssim\gamma_r\lesssim 20$ with an average value $\langle\gamma_r\rangle\sim 3$, corresponding to a ratio between BL Lacs and FR Is of 5% (Table 3). This shows that a scenario where the Lorentz factors are lower for BL Lacs than for FSRQ (Gabuzda et al. 1994; Morganti et al. 1995), although not required by our fits, is consistent with the luminosity function and VLBI data.

The SSC formalism (Sec. 4.4) can be used to estimate the Doppler factor independent of superluminal motion or luminosity functions, via comparison of the predicted and observed X-ray fluxes. For a sample of $\sim$100 radio sources with published VLBI measurements of the core angular size, lower limits to the Doppler factor correlate well with the apparent velocity β_a obtained from multi-epoch VLBI maps (Ghisellini et al. 1993; Sec. 4.2.). This result suggests superluminal motion is related to bulk motion of the emitting plasma and is not simply an illusion. The Doppler factor, δ, can be combined with the measured superluminal speed, β_a, where available, to constrain γ and the angle to the line of sight, θ [Eqs. (A6) and (A7)]; the mean values of these parameters for the different classes (BL Lacs, FSRQ, and SSRQ; Ghisellini et al. 1993) are in good agreement with those derived from the radio luminosity function studies (Secs. 6.1, 6.2).

Similarly, the jet velocities and orientations of radio galaxies, derived from the jet to counterjet brightness ratio [Eq. (A10)] and the SSC formalism, are broadly consistent with those derived from luminosity function studies (Giovannini et al. 1994). Their Doppler factors are also much lower than for BL Lacs and FSRQ, as expected if the radio jets are closer to the plane of the sky.

7. RELATION OF QUASARS AND BL Lac OBJECTS

7.1 Low- and High-Redshift BL Lac Objects

The high-redshift members of any flux-limited sample tend to be systematically more luminous than the low-redshift members because of the induced correlation of luminosity and redshift. Among BL Lac objects, such differences have been interpreted as evidence for a "true" (Type 0) BL Lac class at low redshift and a "quasar-like" (Type 1) BL Lac class at high redshift (Burbidge and Hewitt 1989). A particular motivation for this division (Antonucci 1993) is the fact that broad emission lines, occasionally with large equivalent widths, have been seen in some high-redshift but not low-redshift BL Lac objects. (Here "high-redshift" essentially means the distant half of the 1 Jy RBLs, which extend to $z\sim 1$; few members of any complete XBL sample have $z\gtrsim 0.5$.) In this section we review whether existing data support and/or require a bifurcation via redshift for BL Lacs.

One of the defining features of BL Lac objects is their weak or absent emission lines. For the complete 1 Jy radio-selected sample (Stickel et al. 1991), BL Lacs are defined in part by rest-frame equivalent widths of optical emission lines less than 5 Å. The EMSS and Slew Surveys are defined in a similar way, although using the observed equivalent widths (Stocke et al. 1991; Perlman et al. 1995). With this equivalent-width limit, there can in principle be cross-over objects—for example, for fixed emission-line luminosities, the equivalent widths can change when the continuum varies.

Emission line types and strengths are central to the question of whether nearby and distant BL Lacs constitute distinct populations. The nearby BL Lacs, which are associated with nearby ellipticals (typically at $z\lesssim 0.2$) with typical galaxy absorption spectra, sometimes have weak narrow emission lines (typically [O III]), while the more distant BL Lacs, around which host galaxies have never been detected, sometimes have weak but broad emission lines (typically Mg II; Stickel et al. 1991, 1993). Observational limitations (and sometimes habits), however, militate against uniform information on emission-line properties across the full redshift range. In particular, to detect broad Mg II in the nearby BL Lacs requires high signal-to-noise ultraviolet spectra, and to detect [O III] in the distant BL Lacs requires fairly red spectra.

With available data we first ask whether BL Lac objects have line luminosities comparable to or clearly distinct from FSRQ, for samples selected in the same way (therefore, the

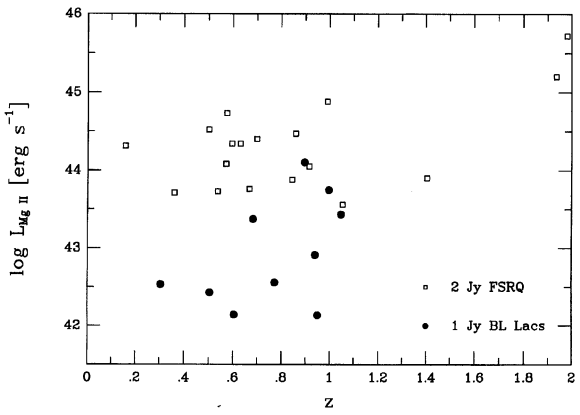

FIG. 19—The available Mg II emission-line luminosities for 1 Jy BL Lac objects (*filled circles*) and 2 Jy flat-spectrum radio quasars (*open squares*) plotted vs. redshift so that comparisons at similar luminosity (which is well correlated with redshift in flux-limited samples) and/or observed wavelength are possible. BL Lacs and FSRQ line luminosities differ by more than one order of magnitude up to $z\sim0.8$, above which some of the high-redshift BL Lacs have line luminosities comparable to the lower-luminosity quasars.

1 Jy BL Lacs and the 2 Jy FSRQ, both selected at high radio frequencies). Figure 11 shows [O III] line luminosities as a function of redshift, which removes observational selection effects due to spectral bandpass and at the same time effectively matches objects for luminosity in the selection band (which should be unbiased with respect to the optical line emission). We found [O III] data in the literature for all the 2 Jy FSRQ with $z<0.7$ and for 8 of the 12 1 Jy BL Lacs sources with certain $z<0.5$; the other four BL Lac objects have much weaker [O III] lines (Stickel et al. 1993).

Figure 11 shows that the [O III] luminosities of BL Lac objects are systematically lower than those of FSRQ. Inclusion of upper limits for BL Lacs, were they available, would exacerbate the difference. There are not enough data points, however, to determine whether the two classes actually have distinct narrow-emission-line properties.

The one BL Lac with quasar-like [O III] luminosity is PKS 0521−365, a nearby low-luminosity object which had been previously classified as a BL Lac (Véron-Cetty and Véron 1993) but which was not included in the 1 Jy BL Lac sample (Stickel et al. 1991) because the equivalent width of two lines was larger than the 5 Å limit (specifically, $W_{H\beta}\simeq9$ Å and $W_{[O\ II]}\simeq7$ Å; this object also has broad Hα; Ulrich 1981; Stickel and Kühr 1993). Figure 11 suggests that PKS 0521−365 has BL Lac-like line luminosity but qualifies as a quasar because its continuum emission was unusually faint (exactly as found earlier by Ulrich 1981) when Stickel et al. classified it.

Broad emission lines are perhaps more crucial to the comparison of high-redshift BL Lac objects and quasars. We collected from the literature all available Mg II λ2798 fluxes for the 2 Jy FSRQ and the 1 Jy BL Lacs, plotted in Fig. 19 vs. redshift to facilitate comparisons at similar luminosities and observed wavelengths. Roughly 35% of the 2 Jy FSRQ and 30% of the 1 Jy BL Lacs are represented in the figure, including six of the seven BL Lac objects with $z>0.7$. Additional data for the FSRQ would be relatively easy to obtain, but for the BL Lacs, which by definition have very weak spectral features (in fact ~1/3 do not have a firm redshift determination), spectra with higher signal-to-noise ratios are needed. Because of the low mean redshift of BL Lac samples, the Mg II line usually lies in the ultraviolet, accessible at the required signal to noise only with *HST*.

In contrast to the [O III] plot, Fig. 19 shows that a few 1 Jy BL Lacs have Mg II luminosities as high as those of the weaker-lined FSRQ. In particular, two BL Lacs have $L_{Mg\ II}>3\times10^{43}$ erg s^{-1} (the luminosity for the faintest FSRQ), namely PKS 0537−441 and B2 1308+326, both at $z\gtrsim0.7$. The equivalent width of Mg II in PKS 0537−441 was on at least one occasion larger than 5 Å (Wilkes 1986), though not when the 1 Jy sample was being defined. This object has also been suggested as a lensing candidate, meaning it might actually be a quasar, although recent observations do not confirm this (see Sec. 7.2.3). B2 1308+326 may have an FR II radio morphology (Kollgaard et al. 1992), while its VLBI polarization properties seem to be more similar to those of quasars than of BL Lacs (Gabuzda et al. 1993).

Apart from these two cases, the Mg II luminosities of BL Lac objects are clearly lower than for FSRQ across the entire redshift range sampled. Still, we cannot exclude a continuous distribution of line luminosities from BL Lacs to quasars, which could result simply from the definition of BL Lacs in terms of their low equivalent widths. In particular, the radio selection in the 1 Jy and 2 Jy samples is similar, so the radio luminosity distributions of these BL Lacs and FSRQ at a given redshift must be similar, suggesting their total luminosities may be comparable. Division in terms of equivalent width would then translate into the observed division in line luminosity. It remains to be seen if this explanation is viable quantitatively when more line luminosities become available.

The apparent difference between the evolutionary properties of radio-selected BL Lacs ($V/V_{max}=0.60\pm0.05$) and X-ray-selected BL Lacs ($V_e/V_a=0.36\pm0.05$) has been ascribed to contamination of the RBL sample from strongly evolving FSRQ (Morris et al. 1991). The comparison of line luminosities in Figs. 11 and 19 shows that RBL are clearly not quasar-like for $z\lesssim0.5$. If we divide the 24 1 Jy BL Lac objects having certain redshift information at $z=0.5$, there is no evidence that the V/V_{max} distributions or mean values for the low- and high-redshift subsamples are different, as shown by a KS and Student's t-test, respectively. More simply, there is no significant correlation between V/V_{max} and redshift in the 1 Jy sample. For the five objects with FR II or FR I/II morphology (Kollgaard et al. 1992), which might be considered the most quasar-like, $\langle V/V_{max}\rangle$ is also not significantly different from the $\langle V/V_{max}\rangle$ for the rest of the sample. In short, the evolutionary properties of BL Lac objects do not depend on redshift and do not indicate contamination by strongly evolving quasars.

A number of other results suggest that low- and high-redshift BL Lacs are more alike than the latter are like FSRQ. In particular:

(1) The distributions of extended radio power for low- and high-redshift BL Lacs are not significantly different, while those of high-redshift BL Lacs (the 1 Jy with $z>0.3$;

the largest measured redshift is $z=1.048$; Stickel et al. 1991) and FSRQ (the 2 Jy sample from Wall and Peacock 1985) differ at the 99.9% confidence level (Padovani 1992b).

(2) The ratio between compact and extended radio emission is not significantly different for low- and high-redshift BL Lac objects. This is in spite of the possibility that some high-redshift BL Lacs are FR IIs with low-excitation optical spectra (Sec. 5.4), and therefore might have systematically different radio properties.

(3) The X-ray spectral shapes of quasars and of BL Lac objects observed with the *Einstein* Observatory (Worrall and Wilkes 1990) and with *ROSAT* (Urry et al. 1995) are systematically different, with the FSRQ having flatter spectral indices. Even BL Lacs with faint but broad emission lines have X-ray spectra more similar to the other BL Lacs than to the FSRQ (Worrall and Wilkes 1990), although those with the broad lines tend to have flatter-than-average (i.e., more FSRQ-like) X-ray spectra (Urry et al. 1995).

(4) The characteristic VLBI polarization structure of BL Lac objects, which implies a magnetic field perpendicular to the jet axis, is quite different from that of quasars, which have a magnetic field parallel to the jet (Gabuzda et al. 1992), with one possible exception (the 1 Jy BL Lac B2 1308+326; Gabuzda et al. 1993). Furthermore, the milliarcsecond polarization structures of low- and high-redshift BL Lacs, divided at $z=0.3$ as suggested by Burbidge and Hewitt (1989), are indistinguishable. It is perhaps possible to create the distinction between quasars and BL Lacs if the latter are systematically more aligned with the line of sight because of the sensitive dependence of polarization on aspect at small angles (Gopal-Krishna and Wiita 1993).

We have asked two simple questions: (1) whether there is any evidence requiring separate high- and low-redshift BL Lac populations, and (2) whether the evidence shows that high-redshift BL Lacs are similar to quasars. We believe that, based on presently available data, the answer to both questions is "no." BL Lacs selected on the basis of their equivalent width represent a fairly homogeneous class, with no strong differences between objects with redshift below and above $z\sim0.3$, $z\sim0.5$ or other, or between objects with broad and with narrow emission lines. There may be a few intermediate objects, characterized by FR II radio morphology, high emission-line luminosities, unusually weak continuum, or quasar-like VLBI polarization, but their small number is unlikely to affect unified schemes significantly.

7.2 Possible Connections between BL Lac Objects and FSRQ

Because of their similar continuum properties, BL Lac objects and FSRQ are collectively called blazars, yet we saw in the previous section that there are also considerable differences between them. What is the relationship between the two blazar classes? Three suggestions—that FSRQ evolve into BL Lacs, that they are different manifestations of the same physical process, and that BL Lacs are gravitationally microlensed FSRQ—are discussed in this section (some of these points were originally discussed by Padovani 1992b).

7.2.1 The evolutionary connection

The de-evolved number densities of FSRQ and BL Lacs are similar (correcting for evolution, FSRQ are about twice as numerous at $z=0$; Padovani 1992b), but the FSRQ are distributed to much higher redshift. It is a well-known problem that high-redshift quasars must disappear and/or become considerably less luminous by the present epoch (Schmidt 1968). Here we consider the suggestion that FSRQ evolve into BL Lac objects, becoming weak-lined objects by virtue of increased beaming of the continuum, that is, a Lorentz factor increasing with cosmic time (decreasing with redshift; Vagnetti et al. 1991). The merit of this approach is that it includes evolution more directly than usual and it attempts to link the (at present) separate unified schemes for high- and low-luminosity radio-loud AGN. It also predicts the evolution of the critical angle separating blazars from radio galaxies (Vagnetti and Spera 1994). Specific predictions of distributions of jet/counterjet ratios and superluminal velocities are also possible (Vagnetti 1995).

The results in Sec. 7.1, however, demonstrate the lack of continuity in redshift between FSRQ and BL Lac objects. For example, their extended radio powers and line luminosities are very different—by 1–2 orders of magnitude at comparable redshifts. Figures 11 and 19 show that BL Lacs and FSRQ occupy separate, approximately parallel, regions in the $L_{[\mathrm{O\,III}]}-z$ and $L_{\mathrm{Mg\,II}}-z$ planes, which is more suggestive of related but distinct histories than of evolution from high-luminosity to low-luminosity blazar.

The strongest objection to the suggestion that strong-lined objects evolve into weak-lined ones because of increased beaming is the fact that BL Lacs have intrinsically weak lines. That is, the equivalent widths are not small because the optical continuum is stronger but because the lines are weaker. There is no evidence that the Lorentz factor, and to first order the Doppler factor, is larger in BL Lacs than in FSRQ. If anything, the limits on Doppler factors derived from SSC arguments are smaller for BL Lacs than for FSRQ (Sec. 6.3). Furthermore, superluminal motion data might actually support an increase with redshift of the Lorentz factor for low values of q_0 (Vermeulen and Cohen 1994).

In the context of the radio-galaxy/blazar unified scheme, an evolutionary connection between FSRQ and BL Lac objects has strong implications for the parent populations. If (some) FSRQ evolve into BL Lacs, then (some) FR IIs should evolve into FR Is. Possible mechanisms for this transition exist, like the deceleration of the high-velocity jets that give rise to an FR II radio source by an increase in the density of the intergalactic medium (De Young 1993) or a decrease in the mass accretion rate onto the central engine (Baum et al. 1995). The connection between FR I and FR II radio galaxies is still not fully understood (Owen and Laing 1989; Owen and Ledlow 1994; Baum et al. 1995), but it is interesting to note that studies of cluster environments of radio sources do suggest both FR IIs and radio quasars could evolve into FR Is (Hill and Lilly 1991; Yee and Ellingson 1993).

7.2.2 Multiwavelength spectral continuity of BL Lac objects and FSRQ

The multiwavelength spectra of HBL, LBL, and FSRQ form a continuous sequence that suggests a common physical mechanism (Sambruna 1994; Sambruna et al. 1995; Maraschi et al. 1995). The spectra of LBL (RBL) and FSRQ have relatively low peak wavelengths, while the HBL (XBL) have higher peak wavelengths. Very roughly, along the sequence from HBL to LBL to FSRQ, the wavelength of the peak synchrotron emission decreases,[17] the X-ray spectral index flattens, the ratio of gamma-ray to bolometric luminosity increases, the bolometric luminosity itself increases, and the mean redshift increases (luminosity and redshift are automatically correlated in flux-limited samples). These trends are illustrated in part by the multiwavelength spectra of a typical FSRQ (Fig. 4) and a typical HBL and LBL (Fig. 15).

Analyzing the spectra of these and other blazars in terms of synchrotron models, Sambruna (1994) finds that a simple transformation in terms of angle between HBL and LBL cannot explain the differences in their multiwavelength spectra. To account for the shorter peak wavelength of the synchrotron emission in HBL compared to LBL, it is necessary to invoke both higher electron Lorentz factors (not to be confused with the bulk Lorentz factor of the jet) and stronger magnetic fields in the X-ray-emitting region. Similarly, the FSRQ have still lower electron energies and weaker magnetic fields than the RBL. The lower electron energies mean that in the X-ray band, the synchrotron component is relatively less important than any Compton-scattered emission (whether from scattered synchrotron photons or other ambient photons), leading to the flatter X-ray spectra and perhaps the stronger gamma-ray emission.

Thus, it is plausible that all blazars are dominated by synchrotron plus Compton-scattered continuum emission, with mean relativistic electron energies and magnetic fields systematically declining with increasing bolometric luminosity (Sambruna 1994). To establish this connection among BL Lac objects and FSRQ definitively, via analysis of the physical parameters in blazar jets, requires extensive multiwavelength monitoring of complete samples of blazars. Unfortunately, it is difficult to correlate variability between gamma-ray and other wavelengths because current detector sensitivity precludes variability studies for all but a few of the brightest blazars (Kniffen et al. 1993; Hunter et al. 1993).

7.2.3 BL Lac objects as gravitationally microlensed FSRQ

The main differences between BL Lacs and FSRQ are, to first order, that the FSRQ are more distant, more luminous, and have stronger emission lines. Ostriker and Vietri (1985, 1990) have suggested that gravitational microlensing by stars in a foreground galaxy could turn an optically violently variable (OVV) quasar (i.e., an FSRQ, in our terminology) into a BL Lac. Specifically, a distant FSRQ with a compact optical/ultraviolet continuum region and an extended optical/ultraviolet emission-line region, whose line of sight passes nearly through the center of a foreground galaxy, would have the continuum preferentially amplified by microlensing. A factor of $\gtrsim 10$ enhancement could, Ostriker and Vietri estimated, reduce the equivalent widths of the BL Lac emission lines sufficiently. In addition, the BL Lac would appear to lie in the (approximate) center of the (nearby) lensing galaxy. Its redshift, in practice often inferred from the "host" galaxy spectrum, would refer to the lensing galaxy rather than the FSRQ, so the derived luminosity of the BL Lac object would be artificially low.

In this picture, BL Lacs and FSRQ are intrinsically the same objects, and there is no separate low-luminosity blazar class to be unified with FR I radio galaxies. Note that the relativistic jet is probably still required to explain the rapid variability, polarization, and other blazar characteristics of FSRQ, although microlensing could account for some low-amplitude, approximately achromatic, variability in BL Lac objects (Urry et al. 1993; Edelson et al. 1995).

There are a number of arguments against the microlensing hypothesis, albeit none definitive. These include the following.

(1) The optical amplification factors derived from numerical simulations under the microlensing hypothesis, basically comparing the optical continuum fluxes of BL Lacs and FSRQ in the 1 Jy and 2 Jy samples, respectively, are much smaller than the factor of 10 required by Ostriker and Vietri to swamp the emission lines of quasars (Padovani 1992b).

(2) The observed optical number counts of BL Lacs (Padovani and Urry 1991; Hawkins et al. 1991) do not appear to flatten at $B \sim 16-18$, as predicted by Ostriker and Vietri, although the faint counts are still quite uncertain.

(3) When BL Lac "host" galaxies are detected (e.g., Abraham et al. 1991), their nuclei are almost always well-centered on the galaxy (see Stocke et al. 1995 for evidence of de-centering in MS 0205.7+3509, an EMSS BL Lac), whereas the microlensing scenario would allow the background FSRQ to be well off the center of the microlensing galaxy. Existing limits on de-centering may already be sufficient to rule out the presence of even a small number of microlensed sources (Merrifield 1992) and *HST* imaging of complete samples have the potential to decide this issue finally.

(4) At least five of the low-redshift 1 Jy RBL have emission lines and absorption lines at the same redshift (Stickel et al. 1993), indicating that in a substantial number of cases, the absorption line redshifts are from the host galaxy rather than the lensing galaxy.

(5) The systematic differences in VLBI polarization structure for BL Lac objects and FSRQ, notably the 90° difference in mean magnetic field orientation, should not exist if one is simply an amplified version of the other (Gabuzda et al. 1992). Microlensing changes the image position randomly with respect to the direction of polarization (which is unchanged), since the lens mass distribution does not "know" about the orientation of the background jet. Thus, the VLBI polarization in BL Lacs should be relatively uncorrelated with jet morphology compared to FSRQ, whereas they are parallel and perpendicular to the jet, respectively.

[17]The peak wavelength is definitely longer for LBL than HBL, but the comparison for FSRQ and LBL has not yet been done with sufficient statistics. Furthermore, the peak wavelength lies in the far-infrared band, so that this question must really be answered with *ISO*.

(6) Microlensing should cause the radio-to-optical continuum of the "low-luminosity" BL Lac objects (basically, the HBL) to be flatter than that of FSRQ, which is more or less as observed (Stocke et al. 1985; Sambruna 1994); however, the observed difference is larger than expected from microlensing. To shift the wavelength of the peak synchrotron emission in FSRQ, generally in the infrared, to the ultraviolet/EUV/soft X-ray, would require amplifying the short-wavelength continuum by several orders magnitude (see Fig. 15).

The evidence for microlensing in a few individual cases remains unclear. One of the most promising microlensing candidates, 0235+164 (Stickel et al. 1988a), which has multiple absorption systems (Yanny et al. 1989), a de-centered foreground group of galaxies (Abraham et al. 1993), and an extremely high superluminal velocity ($\beta_a \sim 90$; Bååth 1984), is almost certainly weakly amplified by macrolensing (Abraham et al. 1993), but no one has calculated the effects of microlensing by stars in the foreground lens. [Abraham et al. (1993) argued that by analogy to a normal quasar, microlensing could cause significant variability only on time scales of years; however, the relevant source–lens velocity for FSRQ is the superluminal jet velocity rather than the typical stellar velocity in a galaxy core (Gopal-Krishna and Subramanian 1991). Therefore, the variability time scales can be much shorter, quite comparable to those observed in 0235+164.] In the case of PKS 0537−441, another lensing candidate, Falomo et al. (1992) failed to detect the foreground galaxy, the presence of which had been suggested by Stickel et al. (1988b).

In summary, there are a number of arguments against microlensing in large numbers of BL Lac objects, and there are no clear cases of microlensing in any one BL Lac. Still, there are no data that actually falsify the microlensing hypothesis. We suggest a clear and incontrovertible test. As the *HST* Key Project on quasar absorption lines has demonstrated (Bahcall et al. 1993), the ultraviolet spectrum of a distant FSRQ should show multiple absorption lines due to intervening Lyα clouds. Suppose we have a BL Lac object that appears to lie in an elliptical galaxy at a redshift of, say, $z=0.25$, and we want to test whether it is actually a quasar at a redshift of, say, $z=1.9$ (or less) that is microlensed by that galaxy. With an ultraviolet spectrum from ~1500 to 3500 Å (with sufficient signal-to-noise ratio to detect absorption lines with equivalent widths of a few hundred milliangstroms) the presence or absence of unidentified (i.e., Lyα) absorption features answers this question unambiguously. This project is ideal for *HST*.

8. THE VIABILITY OF UNIFIED SCHEMES

On the whole, unified schemes for radio-loud AGN are very successful. But there remain some potential problems, including disturbing trends in the linear sizes of radio galaxies and quasars, a dependence on redshift of the ratio of quasars to radio galaxies, the lack of superluminal motion in radio galaxies, and the un-FR-I-like radio morphologies of some BL Lac objects. A number of complications also exist, like the need to include evolution in unified schemes (the critical angle separating different AGN classes or the ratio of $L_{\rm jet}/\mathscr{L}_{\rm ext}$ may well depend on redshift), even as the relatively simple beaming models adopted so far are underconstrained by existing data. In this section we review known problems for unified schemes and anticipate complications that should be addressed when there are more complete data for larger samples of radio-loud AGN.

8.1 Potential Problems with Unification

8.1.1 Linear sizes of blazars and radio galaxies

In principle, the linear sizes of radio sources can be used to test unification because blazars oriented at small angles to the line of sight should have systematically smaller large-scale radio structures than radio galaxies in the plane of the sky. Right at the start, however, we must say that conclusions regarding the relative linear sizes of blazars and radio galaxies are extremely murky, having been the subject of quite a number of papers, with often contradictory results (Gopal-Krishna and Kulkarni 1992; Barthel 1989; Kapahi 1987; 1989, 1990; Barthel and Miley 1988; Onuora 1989, 1991; Hough and Readhead 1989; Nilsson et al. 1993, and references therein). It turns out that the linear size depends, not unexpectedly, on several factors like radio power and redshift. Even matching these variables, the expected difference in mean linear size is quite modest, only a factor of 2 for an orientation of 30° compared to 90°, while the scatter in intrinsic sizes must be many times that large.

In a recent work, Singal (1993a; see also Singal 1988) studied the linear sizes of a large, heterogeneous sample of radio galaxies (about half of which have redshifts estimated from the magnitude–redshift relation) and quasars. His main result is that both size–luminosity and size–redshift correlations are significantly different for the two classes. In particular, luminosity and size are directly correlated for radio galaxies and inversely correlated for quasars, while the size of radio galaxies falls strongly with redshift and not at all for quasars. According to Singal, the only redshift range for which unification works is $0.5<z<1$, the interval Barthel (1989) used in his original analysis of the 3CR catalog ostensibly because of the better statistics there. Indeed, for the lowest luminosity bin and $z\leqslant 0.4$, Singal (1993a) found that the median linear size of quasars is larger than that of radio galaxies, completely opposite to the predictions of the unified scheme.

These results, however, are uncertain and/or contradict other comparable work. One problem with determining linear sizes is that often the radio source morphology is unclear or the source is poorly resolved. In a similar study limited to sources with clear FR II double structures, which by definition have sharp outer boundaries, Nilsson et al. (1993) found quite different results for the dependence of linear size on redshift and luminosity; in direct contrast to Singal (1993a), the median values of the linear size for quasars are (marginally) smaller than for galaxies in all luminosity bins.

Another issue is the use of complete flux-limited samples. The 3CR catalog is excellent for this purpose because it is largely unbiased by beamed flux. From the luminosity function analysis we found quasars (effectively SSRQ) and radio

galaxies are divided at $\theta_c \sim 38°$ (Table 3); the mean angle for SSRQ (between 14° and ~38°) is therefore 28° and the mean angle for FR IIs is 66°. The ratio of quasar linear size to radio galaxy linear size, 1.9 for these mean angles, is both small and a very weak function of critical angle. Estimating the critical angle from the numbers of quasars and radio galaxies in the 3CR gives $\theta_c = 44.4°$ (Barthel 1989), with a 1σ uncertainty of $\pm 6.6°$; this gives a foreshortening factor of $1.9^{+0.3}_{-0.2}$. The foreshortening factor would be much larger were one to compare only FSRQ and FR IIs, but there are too few FSRQ in the 3CR and using the 2 Jy sample would mean incorporating the selection bias of beaming, which is nontrivial.

Another complication is that even modest misalignments between large-scale radio structure and the obscuring torus are enough to confuse the expected linear size trend (Gopal-Krishna et al. 1994). For example, the distributions of observed linear size and bend angle for a large, heterogeneous sample of quasars and radio galaxies are completely consistent with random orientations within and without a cone angle of ~50°, respectively, assuming only that the jets have small intrinsic bend angles ($\lesssim 25°$) and modest intrinsic arm-length differences (Lister et al. 1994a). In sum, considering the many problems and potential complications, it is remarkable that the analysis of linear sizes of quasars and FR IIs gives any sensible results at all.

The comparison of linear sizes of FR I galaxies and BL Lac objects is even more difficult because the amorphous FR I radio structures have no clear outer boundaries. The largest angular sizes of the EMSS BL Lacs are similar to those of B2 FR Is and of a heterogeneous sample of radio-selected BL Lacs (Perlman and Stocke 1993), in apparent contradiction to their unification. This may be due to substantial misalignments between the parsec- and kiloparsec-scale jets (Perlman and Stocke 1993), which are quite common in BL Lacs (Kollgaard et al. 1992). In that case, a small angle to the line of sight of the VLBI jet does not necessarily imply a very small radio linear size.

In addition, if the bulk Lorentz factors in BL Lac objects are small (Sec. 6.3), the critical angle separating them from FR Is can be quite large. For example, for $\gamma \sim 2$ and $f \sim 0.05$, $\theta_c \sim 19°$ (Table 3). The corresponding ratio of projected lengths of BL Lacs and FR Is, evaluated at the mean angle (ignoring beaming) is ~3; for the XBL fit in Table 3 it is ~2.5.

In the end, consideration of linear sizes of radio sources is not a compelling test of unified schemes. Even the oft-stated problem of large deprojected radio sizes—wherein the lengths of superluminal sources and/or one-sided jets as large as ~1 Mpc in length (like NGC 6251) are thought to be uncomfortably large when deprojected by their orientation angles—vanishes when one thinks about the numbers. Neither superluminal motion nor one-sidedness require a particularly small angle [Fig. 21 and Eq. (A4), Eq. (A8)], and in fact the expected deprojection correction is only a factor of 2 or so.

8.1.2 Dependence of quasar fraction on redshift

In his original unification paper, Barthel (1989) used the ratio of quasars to radio galaxies in the 3CR catalog (essentially SSRQ to FR II) to determine a critical angle separating the two classes. However, Singal (1993b) found that the quasar fraction in the 3CR appears to increase with redshift[18] and noted that Barthel's result depended on choosing the redshift interval $0.5 < z < 1$. Given the small numbers involved, Singal's number ratios are actually within 2σ of no redshift dependence, assuming Poisson statistics (Gehrels 1986). Moreover, once low-excitation 3CR FR II galaxies are excluded (Sec. 5.2), the quasar/radio-galaxy fraction is independent of redshift (Laing et al. 1994).

The number ratios of quasars to radio galaxies binned by redshift imply a set of critical angles which in turn correspond to predicted ratios of mean linear sizes for the two classes. These size ratios agree with the observed values to within $\sim 2\sigma$, contrary to Singal's conclusions, once the associated uncertainties in the predicted values are taken into account (Saikia and Kulkarni 1994).

Even taking Singal's numbers at face value, any inconsistencies can be explained easily by allowing for a moderate misalignment (~20°–30°) between the radio axis and the axis of the optically thick torus hiding the broad emission-line region in radio galaxies (Gopal-Krishna et al. 1994). Finally, as Singal (1993b) noted, a modest dependence of quasar fraction on redshift might be explained by an evolution in the opening angle of the obscuring torus, as it might by anything causing a correlation between opening angle and luminosity (Lawrence 1991; Sec. 8.2.1).

8.1.3 Absence of superluminal motion in radio galaxies

The subrelativistic kiloparsec-scale jet velocities in FR I galaxies, typically of the order of 1000–10,000 km s^{-1} (Bicknell et al. 1990), used to represent a problem for the FR I/BL Lac unification, which requires relativistic speeds at least on small scales. It was not clear that FR Is were relativistic even on the smallest scales, and if they were, it was not clear how they were decelerated or what the observational signature of that deceleration would be. Now, new observational (Venturi et al. 1993; Feretti et al. 1993; Giovannini et al. 1994) and theoretical results (Laing 1994; Bicknell 1994) supporting the presence of relativistic motion on parsec scales in these sources have changed our understanding of FR Is. Physically reasonable models have also been proposed for the required deceleration (Laing 1994; Bicknell 1994).

If FR Is are relativistic on small scales, they should show superluminal motion, even near the plane of the sky. A jet with a Lorentz factor of 5 would have apparent transverse speeds $\beta_a \simeq 2.3$ and 1 for viewing angles of 45° and 90°, respectively [Eq. (A4)]. The few measurements of jet proper motions with VLBI, however, suggest that presently studied FR I radio galaxies display relativistic but still subluminal

[18] In a related study with a largely overlapping sample, Lawrence (1991) found the fraction of broad-line objects increased with radio power and possibly *decreased* with redshift.

speeds. Using the data compiled by Vermeulen and Cohen (1994), we obtain an average value $\langle\beta_a\rangle\sim0.5$ (converting to our adopted value of $H_0=50$ km s^{-1} Mpc^{-1}) for four FR Is (NGC 315, M87, Centaurus A, and NGC 6251). The speeds for FR IIs seem to be no different: $\beta_a\simeq0.5-1.0$ for Cygnus A (Carilli et al. 1994).

These results may imply that radio galaxies have smaller Lorentz factors than BL Lacs and radio quasars. It is important to remember, however, that detection of VLBI components in radio galaxies is hampered by relativistic deamplification and dilution by unbeamed emission. For $\gamma=5$, for example, jets are deamplified for orientation angles $\theta\gtrsim35°$ (Appendix A), which would include basically all radio galaxies (see Table 3); for larger Lorentz factors, the angle is even smaller and the deamplification larger. (The jet-to-counterjet ratio remains significantly larger than unity even at large angles; Fig. 22.) Similarly, at these angles the ratio of transverse jet luminosity to unbeamed luminosity is $\lesssim10^{-2}$ for $\gamma=5$ and $f=0.01$ [Eq. (C6)] and equals $\sim10^{-4}$ at 90° [Eq. (C7)]. Thus, the bulk of the emission may well appear to be stationary even if a transverse relativistic jet is present. Another consideration is that significant beaming can be reconciled with subluminal motion of knots if these are reverse shocks advected by the jet; their motion would then give a misleading indication of the flow velocity (Bicknell 1994).

In the end, either FR Is are intrinsically different from BL Lacs or they will exhibit superluminal motion on small scales. Surveys of FR Is with the Very Long Baseline Array (VLBA) should help decide this question. It is extremely interesting that in one nearby FR I galaxy, M87, which has been extremely well mapped in the radio, superluminal motion has been detected on kiloparsec scales, with β_a up to 2.5 (Biretta et al. 1995). At least one FR I, then, must have an appreciable bulk flow on both parsec and kiloparsec scales.

8.1.4 The parent population of BL Lac objects

There are some potential mismatches in the properties of FR I radio galaxies and BL Lac objects, although these are far from demonstrated conclusively. First, the narrow emission-line strengths of BL Lacs, where measured, barely overlap with the distribution for FR Is (Sec. 5.4.2, Fig. 11), although this is complicated by the lack of complete samples and uniform coverage, not to mention the extreme difficulty of detecting very weak lines (and the lack of published upper limits) in BL Lac objects.

Second, broad Mg II lines are quite strong in some high-redshift BL Lacs (Sec. 7.1, Fig. 19), while there is little evidence for similarly strong broad lines in nearby FR Is. In part, this could be due to the lack of sensitive UV measurements of FR Is or to a correlation with continuum luminosity (and therefore redshift); both effects would limit the observation of Mg II in existing, very local, samples of FR Is.

Third, the diffuse radio emission of BL Lac objects displays FR II morphology in some cases (Sec. 5.4.1) and sometimes quite high unbeamed luminosity (Fig. 10). There may also be a deficit of twin-jet morphologies in BL Lacs, depending on the true value of the critical angle. It may well be that the parent population of BL Lac objects includes at least some FR II radio galaxies, presumably those with low-excitation optical spectra. We expect that the beaming calculation under this hypothesis would show this scheme to be viable and that the derived Lorentz factor(s) will not change much. Certainly this would be an interesting calculation to do once the optical spectra of the 2 Jy sample are sufficient to separate the low-excitation and high-excitation FR IIs.

8.2 Possible Complications for Unification

8.2.1 Properties of the obscuring torus

The opening angle of the obscuring torus may well be a function of source power. For example, the inner radius of the torus could be determined by the evaporation temperature of dust, $\mathscr{R}_{\rm in}\sim0.06(L_{\rm bol}/10^{45}{\rm erg\ s^{-1}})^{0.5}$ pc (Lawrence 1991; Netzer and Laor 1994). Since more distant quasars are more luminous, this would produce a positive dependence of the quasar fraction on redshift. There are claims in the literature that the ratio of broad- to narrow-line objects depends on redshift (Lawrence 1991; Singal 1993b), but at least in the 3CR sample this trend disappears once the low-excitation FR IIs are excluded (Sec. 8.1.2). The misclassification of some quasars as NLRG could also confuse the issue (Sec. 6.1.1).

An interesting distinction between high- and low-luminosity unified schemes for radio-loud AGN is that the high-luminosity AGN include transition objects, the SSRQ, which are relatively unbeamed in terms of radio emission but "beamed" (i.e., unobscured) in terms of optical spectrum. The analog of SSRQ for the low-luminosity AGN—broad-line radio galaxies with FR I morphologies—is not seen (with the exception of the BLRG 3C 120); surveys find either narrow-line FR I or BL Lacs (with occasional broad lines). If FR I galaxies do have broad emission lines at some level, the lack of broad lines could be explained if the opening angle of the torus depended on luminosity (Falcke et al. 1995; Sec. 5.4.2). This would mean the torus opening angle in FR Is is much smaller than in FR IIs. To eliminate broad-line FR Is, it must be comparable to or smaller than the radio beaming angle, whereas in quasars the torus opening angle is much larger than the critical angle for relativistic beaming of the radio emission. Sensitive infrared spectroscopy and spectropolarimetry of FR Is will address this issue by detecting or putting interesting limits on the broad-line luminosities of FR I radio galaxies. *ISO* observations of radio galaxies, BL Lac objects, and quasars will constrain the relative amounts of obscuring matter in each class.

Direct mapping of the torus may be possible with high spatial resolution spectroscopic observations of water masers. Recent VLBI imaging of water masers in NGC 4258, a nearby galaxy with low-level AGN activity, provides evidence of rotating molecular gas in a region less than 0.13 pc from the center (Miyoshi et al. 1995). This is important direct evidence for molecular gas in the nuclei of galaxies, as implied by the obscuring torus hypothesis. The case of NGC 4258 is not yet the desired demonstration of a molecular torus in AGN, however, because the molecular gas is distributed in a very thin disk rather than a torus. Using the results of Miyoshi et al. (1995), we find the ratio of disk height to inner radius is $\lesssim0.02$, corresponding to an opening angle of $\sim90°$, which will clearly not obscure the central

source very effectively. In addition, masers do not automatically signal the presence of a torus; in NGC 1068, there are masers in the southern radio component with locations and velocities approximately commensurate with rotation, but there is also a maser to the north that apparently arises in molecular gas shocked by the radio jet (Gallimore et al. 1995).

8.2.2 Cosmic evolution of radio-loud AGN

Cosmic evolution could be an important aspect of unified schemes. Realistically, one should probably expect evolution in the Lorentz factor (γ), in the ratio of beamed to unbeamed flux (R), and in the intrinsic fraction of luminosity radiated by the jet (f). But evolution has been largely ignored in unified schemes (cf. Vagnetti and Spera 1994) because of the poor statistics when existing samples are divided into multiple redshift bands.

In most cases, one finesses the evolution of AGN by parameterizing it with a smooth function and extrapolating evolving properties to zero redshift. For example, comparisons between beamed and observed LFs were done assuming exponential luminosity evolution (Sec. 6). The preferred approach, statistics permitting, is to derive the LFs at different redshifts and apply the beaming formalism to the single-epoch LFs. This would allow, for example, the study of evolutionary trends of the beaming parameters.

The well-identified radio-selected samples currently available—the 3CR, the 1 Jy, the 2 Jy samples—are quite shallow. For a typical radio-loud AGN spectrum, optical and X-ray surveys are much deeper, in many cases the equivalent of 1 mJy or fainter at 5 GHz. Deep radio surveys, optically identified and classified morphologically in the radio, would greatly improve our understanding of unified schemes but represent a substantial technical challenge.

Another important aspect is the evolution of individual sources and the potential consequences for their radio morphologies. For example, the observed correlation between core-to-extended radio flux and linear size (e.g., Lister et al. 1994b) can be explained by a model wherein the radio source starts out as a luminous core that fades with time as the lobes brighten (Hutchings et al. 1988). If this evolutionary effect dominates over beaming and orientation, it could complicate considerably the use of this flux ratio as a beaming indicator.

8.2.3 Parametrization of relativistic beaming

The adopted beaming model (Sec. 5.6; Appendix B) is undoubtedly too simple. Jets are almost certainly complicated, more so than usually assumed in the statistical tests (Lind and Blandford 1985; Bridle et al. 1994). They are likely to be bent, have variable bulk Lorentz factors, have hot spots at local shocks, and so on, rather than being a well-behaved, ideal confluence of particles, photons, and fields in equipartition. This is borne out by the complex morphologies and trajectories of superluminal components in blazars. Jet velocities probably decrease or increase with increasing distance from the nucleus, whereas we have assumed they are fixed; observed superluminal motion in well-monitored sources is definitely complex (e.g., Biretta et al. 1986). Finally, there is always the problem of flow vs. pattern velocity (Sec. 4.2), with only the former causing Doppler boosting.

Moreover, it is not clear how jets form and propagate. By what physical process is matter accelerated to Lorentz factors $\sim$5, and sometimes as much as an order of magnitude higher? How is the balance between kinetic and radiative energy determined? Jet formation and motion is almost certainly affected by the local gas environment, which might explain in part the differences between FR I and FR II radio galaxies (De Young 1993; Bicknell 1994), and perhaps why the parsec-scale magnetic field configurations differ in quasars and BL Lac objects. Jet motion is probably also affected by competition between gravitational force and radiation pressure, which moderates the accretion rate. If so, the Lorentz factor could depend on the source Eddington ratio ($\dot{m}_{\rm Edd} \propto L/M$, where M is the mass of the central black hole; Abramowicz 1992).

Unified schemes for radio-loud objects can also be complicated if the beaming is wavelength-dependent. Although this is probably not the case for BL Lacs (Sambruna 1994), it could be important in quasars (Impey et al. 1991, but see also Hough and Readhead 1989). The dependence of beaming on wavelength occurs naturally for an obscuring torus because its transparency is wavelength dependent, or for an inhomogeneous jet model with variable Lorentz factor along its length.

8.2.4 Compact steep-spectrum and gigahertz peaked-spectrum sources

The place of Compact Steep-Spectrum Sources (CSS) and the possibly related Gigahertz Peaked-Spectrum Sources (GPS) in the unified scheme for high-power radio sources is an open question. CSS and GPS include both quasars and radio galaxies. Their most striking feature is their compact radio structure ($\lesssim$15 and $\lesssim$1 kpc, respectively; see Fanti et al. 1990a and O'Dea et al. 1991 for reviews of their properties). In terms of the definitions in Sec. 1 (Table 1), we include them in the SSRQ/FSRQ and NLRG classes, as appropriate.

The CSS and GPS sources constitute a non-negligible part of radio samples; for example, CSS represent approximately 13% of the 3CR sample (Fanti et al. 1990a) and $\sim$20% of the 2 Jy sample (Morganti et al. 1993). For our statistical analysis in Sec. 6, we removed the galaxies (because they were not classified as either FR I or FR II by their radio morphologies) but included the quasars; this might have increased the critical angles slightly.

Statistical considerations exclude the possibility that most CSS and GPS are intrinsically large radio sources seen at small angles to the line of sight. Instead, they are probably inherently compact (Fanti et al. 1990b). At the same time, the size distribution and relative numbers of CSS quasars and galaxies are consistent with the former being the latter viewed at angles smaller than $\sim$45° (Fanti et al. 1990b), although the different radio morphologies of the two classes are not entirely explained by orientation. CSS and GPS could represent an early stage of radio source evolution (Fanti et al.

1990b) and if so, probably should be included in unification. Alternatively, they may lie in unusual environments (O'Dea et al. 1991). In either case, unified schemes bear on their origin, and it is important to understand how they fit into the present paradigm.

8.2.5 Selection effects in the identification of quasars

If quasar unification schemes are correct, all quasars are oriented at a preferred angle from which the broad-line region is visible. This undoubtedly has strong effects on other quasar properties. For example, it could explain why no Lyα edges are seen in the ultraviolet spectra of quasars (Koratkar et al. 1992; Kinney 1994) even though they are expected from accretion disks, an important element in the current AGN paradigm (Fig. 1). That is, assuming that the axes of accretion disks and obscuring matter coincide, no edge-on disks would be seen and so no Lyα edges should be seen.

Other secondary effects are also possible. If the accretion disks in quasars are thick, as expected for high-luminosity AGN, then their radiation patterns can be anisotropic independent of the obscuring torus (Madau 1988). Because its radiation pattern is narrower than the opening angle of the obscuring torus, the thick disk can by itself introduce mild selection effects (Urry et al. 1991b) wherein quasars are more face-on than implied by their emission-line properties (assuming the axes of the thick disk and torus are aligned). In that case, the optical-through-ultraviolet continuum emission from quasars will appear bluer and more luminous than if it were emitted isotropically.

8.2.6 Extended continuum emission in Type 2 AGN

Spectropolarimetry has indicated an interesting complication in a number of Type 2 AGN; specifically, the scattered broad-line flux is sometimes more polarized than the continuum (Tran 1995). This implies that in addition to the nuclear power-law continuum source there must be an extended continuum source in the scattering region which dilutes the polarized flux of the scattered nuclear continuum. The *in situ* extended featureless continuum must be similar to the nuclear power law, and in some ways the match between the nuclear and extended properties is a bit mysterious. The details of the spectral shapes depend on very high signal-to-noise spectropolarimetric data, however, available only for a few of the brightest sources, and so remain to be determined for the Type 2 AGN as a class.

The presence of an extended optical continuum component can also be inferred from the uniformity of Hβ equivalent widths in AGN types from Seyferts to radio-loud Type 2 AGN to quasars (Binette et al. 1993). According to unification, the intensity of the narrow Hβ line should be relatively orientation independent while the broad line and the nuclear continuum are not, meaning the equivalent width should differ strongly between Type 1 and Type 2 AGN. The lack of a difference can be explained if appreciable continuum emission is generated in or near the line-emitting cloud, roughly in proportion to the incident photoionizing continuum, in which case the equivalent width will not depend strongly on orientation.

Locally generated continuum, such as shock-excited emission from a jet interacting with the interstellar medium (Sutherland et al. 1993), could also explain the similar reddening seen in lines and continuum (Binette et al. 1993), as well as the association of optical emission-line gas with extended radio structure (Sec. 3.1). Extended optical/UV continuum associated with emission-line regions has in fact been seen in some nearby Seyfert 2 galaxies (Pogge and De Robertis 1993) and in Cygnus A (Pierce and Stockton 1986; Antonucci et al. 1994). To first order, an extended continuum source should mitigate the selection effects of beaming in the optical band; the degree to which this is the case depends critically on its luminosity relative to the nuclear continuum.

9. THE TEN MOST IMPORTANT QUESTIONS

Strong anisotropy in AGN is well established (Secs. 3 and 4). This means some form of unification through orientation must be valid. The first step in understanding AGN, then, is to unify the principal classes of radio-loud AGN as described in this review. The next step is to untangle the effects of cosmic evolution, which causes the luminosity, morphology, and/or number of AGN to change with time (redshift). With an ensemble of AGN for which orientation and evolutionary effects have been removed, we will finally be able to approach the more physically interesting issues of black hole mass, black hole spin, accretion rate, formation and evolution of the individual radio source, etc.

For radio-loud AGN—radio galaxies, quasars, and blazars—relativistic beaming is likely to be very important, on both small and large scales. This has an enormous effect on the observed properties. Two schemes, one unifying low-luminosity (FR I) radio galaxies with weak-lined blazars (BL Lac objects) and the other unifying high-luminosity (FR II) radio galaxies with strong-lined blazars (OVV, HPQ, FSRQ), and SSRQ, are both consistent with essentially all available data (Secs. 5, 6, and 7). There are some remaining problems or complications that require further analysis (Sec. 8), but these are far from falsifying the concept of unification.

From today's vantage point, we identify the ten most important issues for unification and ultimately for understanding AGN. That unification works quite well with very simple models means we do understand something important about AGN. As we learn more and more about radio sources, and the simplicity of present unified schemes inevitably gives way to increasing complexity, we will doubtless discover even more about what it is that we do not know. As an anonymous person (who was surely a scientist) said: *The greater the sphere of our knowledge, the larger is the surface of its contact with the infinity of our ignorance.*[19] In that spirit, recognizing that the questions we ask today, which we believe will lead to fundamental understanding of AGN, may not be the questions asked or answered tomorrow, we put forward the following list:

(1) Is there evidence for BL Lacs or obscured quasars in all radio galaxies?

[19]Anonymous quotation in *A Short History of Astronomy*, A. Berry (New York, Dover).

(2) What is the relation between HBL, LBL, and FSRQ?

(3) Are the observed distributions of β_a, R, and jet/counterjet ratios commensurate with beaming?

(4) Is the Lorentz factor higher in the high-luminosity radio sources (quasars and FR II radio galaxies) than in low-luminosity radio sources (BL Lac objects and FR I radio galaxies)?

(5) Do FR Is have broad emission-line regions?

(6) What is the relation between FR Is and FR IIs?

(7) How do jets form and propagate?

(8) What is the physical cause of the radio loud–radio quiet distinction?

(9) Where are the narrow-line (Type 2) radio-quiet quasars?

(10) What are the fundamental parameters governing the central engine, and is it powered by a black hole?

We thank many of our colleagues for helpful comments and discussions, including Ski Antonucci, Stefi Baum, John Biretta, Howard Bond, Sperello di Serego Alighieri, James Dunlop, Mike Eracleous, Carla Fanti, Roberto Fanti, Bob Fosbury, Gabriele Ghisellini, Paolo Giommi, Bob Goodrich, Gopal-Krishna, Ann Gower, Tim Heckman, John Hutchings, Buell Jannuzi, Ken Kellermann, Ron Kollgaard, Robert Laing, Andy Lawrence, Laura Maraschi, Raffaella Morganti, Chris O'Dea, Frazer Owen, Joe Pesce, Eric Perlman, Rita Sambruna, Chris Simpson, Ashok Singal, John Stocke, Steve Unwin, and Paul Wiita. We further thank Jim Braatz, James Dunlop, John Hutchings, Raffaella Morganti, Frazer Owen, Geoffrey Taylor, and Andrew Wilson for providing data, images, and figures; Joe Pesce, John Godfrey, and Dave Paradise for help producing figures; Sarah Stevens-Rayburn for library assistance; and the Space Telescope Science Institute, the STScI Visitor Program, Christina Padovani, and Andrew Szymkowiak for support of the collaborative visits which made completion of this work possible.

APPENDIX A: RELATIVISTIC BEAMING PARAMETERS

We discuss here the various beaming parameters and how they are related to one another. Many of the equations can be found in Ghisellini et al. (1993).

The kinematic Doppler factor of a moving source is defined as

$$\delta \equiv [\gamma(1-\beta\cos\theta)]^{-1}, \tag{A1}$$

where β is its bulk velocity in units of the speed of light, $\gamma=(1-\beta^2)^{-1/2}$ is the corresponding Lorentz factor, and θ is the angle between the velocity vector and the line of sight. The Doppler factor has a strong dependence on the viewing angle (as shown in Fig. 20), which gets stronger for larger Lorentz factors. For $0°\leqslant\theta\leqslant 90°$, δ ranges between $\delta_{\min}=\delta(90°)=\gamma^{-1}$ and $\delta_{\max}=\delta(0°)=(1+\beta)\gamma\sim 2\gamma$ for $\gamma\gg 1$. Moreover, $\delta=1$ for $\theta_\delta=\arccos\sqrt{(\gamma-1)/(\gamma+1)}$ (e.g., for an angle $\theta_\delta\simeq 35°$ if $\gamma=5$), and for decreasing θ_δ with increasing γ (Fig. 20); for angles larger than θ_δ relativistic *deamplification* takes place.

Given a value of δ, a lower limit to the Lorentz factor is given by the condition $\delta\leqslant\delta_{\max}$; that is,

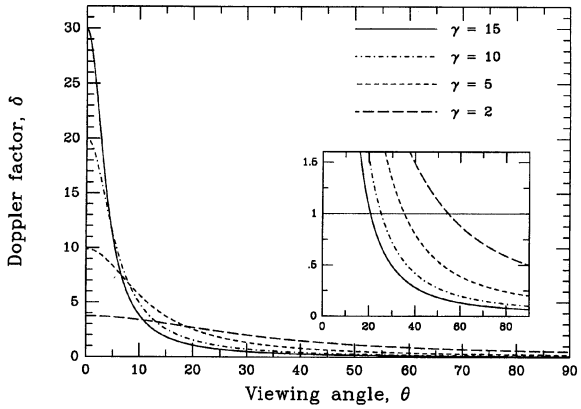

FIG. 20—The dependence of the Doppler factor on the angle to the line of sight. Different curves correspond to different Lorentz factors: from the top down, $\gamma=15$, 10, 5, 2. The expanded scale on the inset shows the angles for which $\delta=1$.

$$\gamma\geqslant\frac{1}{2}\left(\delta+\frac{1}{\delta}\right). \tag{A2}$$

When δ is a lower limit, as in the SSC case, this expression is valid only for $\delta>1$, since for $\delta<1$, $\delta+1/\delta$ decreases for increasing δ. It can also be shown that for any value of γ,

$$\sin\theta\leqslant\frac{1}{\delta}, \tag{A3}$$

which gives a useful upper limit to θ if $\delta>1$.

In the relativistic beaming model, the observed transverse velocity of an emitting blob, $v_a=\beta_a c$, is related to its true velocity, $v=\beta c$, and the angle to the line of sight by

$$\beta_a=\frac{\beta\sin\theta}{1-\beta\cos\theta}. \tag{A4}$$

It can be shown that if $\beta>1/\sqrt{2}\simeq 0.7$, then for some orientations superluminal motion is observed. The maximum value of the apparent velocity, $\beta_{a,\max}=\sqrt{\gamma^2-1}$, occurs when $\cos\theta=\beta$ or $\sin\theta=\gamma^{-1}$; for this angle, $\delta=\gamma$. This implies a minimum value for the Lorentz factor $\gamma_{\min}=\sqrt{\beta_a^2+1}$ (see Fig. 21). For example, if one detects superluminal motion in a source with $\beta_a\sim 5$, the Lorentz factor responsible for it has to be at least 5.1. It is also apparent from Fig. 21 that superluminal speeds are possible even for large angles to the line of sight; sources oriented at $\theta\sim 50°$, have $\beta_a\gtrsim 2$ if $\gamma\gtrsim 5$, and sources in the plane of the sky ($\theta=90°$) have $\beta_a=\beta\sim 1$ for $\gamma\gtrsim 3$.

The apparent velocity in terms of γ and δ is

$$\beta_a=\sqrt{2\delta\gamma-\delta^2-1}. \tag{A5}$$

We find from equations (A1) and (A4), $\beta_a=\delta\gamma\beta\sin\theta$, and for the angle that maximizes the apparent velocity, $\sin\theta=\gamma^{-1}$, $\beta_a=\delta\beta=\gamma\beta=\sqrt{\gamma^2-1}\simeq\gamma\simeq\delta$.

With a measurement of superluminal velocity and an independent estimate of the Doppler factor (for example, from an SSC calculation), one can combine Eqs. (A1) and (A4) to obtain two equations in four unknowns. That is, under the hypothesis that the "bulk" and "pattern" speeds are the

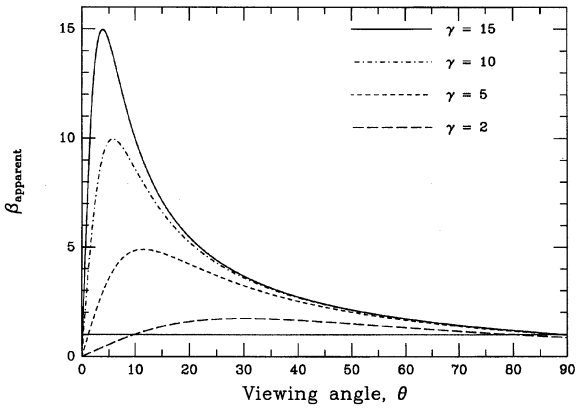

FIG. 21—The apparent velocity relative to the speed of light vs. angle to the line of sight for an emitter approaching at relativistic speed. Different curves correspond to different Lorentz factors: from the top down, γ=15, 10, 5, 2. The dotted line corresponds to $\beta_a=1$. Note that β_a is essentially independent of γ at large angles.

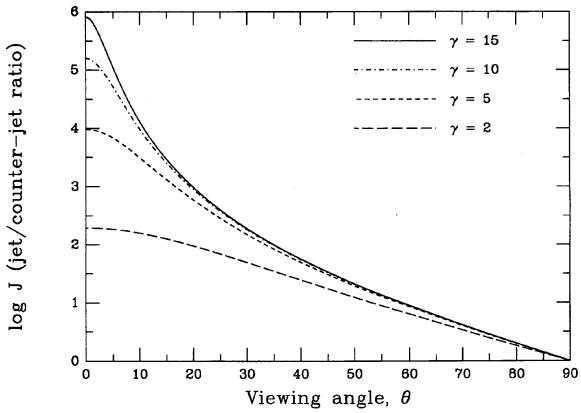

FIG. 22—The jet to counterjet ratio, J, vs. angle to the line of sight for $p=2$. Different curves correspond to different Lorentz factors: from the top down, γ=15, 10, 5, 2. Note that the ratio is essentially independent of γ at large angles.

same, one can derive the value of the Lorentz factor and the angle to the line of sight:

$$\gamma=\frac{\beta_a^2+\delta^2+1}{2\delta}, \tag{A6}$$

$$\tan\theta=\frac{2\beta_a}{\beta_a^2+\delta^2-1}. \tag{A7}$$

Note that γ reaches its minimum value when $\delta=\sqrt{\beta_a^2+1}\equiv\gamma_{\min}$. If δ is a lower limit (as when it is derived from an SSC calculation) and $\delta<\sqrt{\beta_a^2+1}$, then the γ estimated from Eq. (A6) is an upper limit (of course always bound to be $\geq\gamma_{\min}$), while if $\delta>\sqrt{\beta_a^2+1}$, it is a lower limit. For $\delta\gg\sqrt{\beta_a^2+1}$, $\gamma\simeq\delta/2$, while if $\delta\ll\sqrt{\beta_a^2+1}$, $\gamma\simeq\gamma_{\min}/2\delta$. As for Eq. (A7), when δ is a lower limit, the inferred θ is always an upper limit.

The predicted jet/counterjet ratio (i.e., the ratio between the approaching and receding jets), can be expressed in terms of δ and β_a as

$$J=\left(\frac{1+\beta\cos\theta}{1-\beta\cos\theta}\right)^p \tag{A8}$$

$$=(\beta_a^2+\delta^2)^p. \tag{A9}$$

In the simplest cases, $p=2+\alpha$ or $3+\alpha$ (Appendix B). Figure 22 shows the jet/counterjet ratio as a function of the viewing angle for various values of the Lorentz factors and for $p=2$ (which minimizes the effect, as p is likely to be larger). The dependence on orientation is very strong, since $J\approx\delta^{2p}$. From the jet/counterjet ratio alone [Eq. (A8)], we obtain

$$\beta\cos\theta=\frac{J^{1/p}-1}{J^{1/p}+1}, \tag{A10}$$

from which an upper limit to θ (since $\beta\leq1$) and a lower limit to β (since $\cos\theta\leq1$) can be derived.

It is useful to calculate the angular parameters relevant to tests of unified schemes. For sources randomly oriented within the angular range θ_1 to θ_2, the mean orientation angle is

$$\langle\theta\rangle\equiv\frac{\int_{\theta_1}^{\theta_2}\theta\sin\theta\,d\theta}{\int_{\theta_1}^{\theta_2}\sin\theta\,d\theta} \tag{A11}$$

$$=\frac{\theta_1\cos\theta_1-\theta_2\cos\theta_2+\sin\theta_2-\sin\theta_1}{\cos\theta_1-\cos\theta_2}. \tag{A12}$$

The linear size of extended sources is proportional to $\sin\theta$, for which the mean value is

$$\langle\sin\theta\rangle\equiv\frac{\int_{\theta_1}^{\theta_2}\sin^2\theta\,d\theta}{\int_{\theta_1}^{\theta_2}\sin\theta\,d\theta} \tag{A13}$$

$$=\frac{\theta_2-\theta_1+\cos\theta_1\sin\theta_1-\cos\theta_2\sin\theta_2}{2(\cos\theta_1-\cos\theta_2)}. \tag{A14}$$

Finally, the mean value of $\cos\theta$ is given by

$$\langle\cos\theta\rangle\equiv\frac{\int_{\theta_1}^{\theta_2}\cos\theta\sin\theta\,d\theta}{\int_{\theta_1}^{\theta_2}\sin\theta\,d\theta} \tag{A15}$$

$$=\frac{1}{4}\frac{\cos(2\theta_1)-\cos(2\theta_2)}{\cos\theta_1-\cos\theta_2}. \tag{A16}$$

APPENDIX B: DOPPLER ENHANCEMENT

The Doppler factor, δ (Appendix A), relates *intrinsic* and *observed* flux for a source *moving* at relativistic speed $v=\beta c$. For an approaching source, time intervals measured in the observer frame are shorter than in the rest frame (even allowing for time dilation) because the emitter "catches up" to its own photons:

$$t=\delta^{-1}t', \tag{B1}$$

where primed quantities refer to the rest frame of the source. Since the number of wavefronts per unit time is constant, the

emission is blue-shifted (essentially the inverse relation):

$$\nu = \delta \nu'. \tag{B2}$$

The intensity enhancement ("Doppler boosting") is an even more dramatic effect. Because I_ν/ν^3 is a relativistic invariant, the transformation of specific intensity is

$$I_\nu(\nu) = \delta^3 I'_{\nu'}(\nu') \tag{B3}$$

(Rybicki and Lightman 1979). One power of δ comes from the compression of the time interval [Eq. (B1)] and two come from the transformation of the solid angle, $d\Omega = \delta^2 d\Omega'$.

If the emission is isotropic in the source rest frame (i.e., $I'_{\nu'}$ is not a function of angle), the flux density, F_ν, transforms in the same way as the specific intensity. For a power-law spectrum of the form $F'_{\nu'} \propto (\nu')^{-\alpha}$, Eq. (B3) becomes

$$F_\nu(\nu) = \delta^{3+\alpha} F'_{\nu'}(\nu); \tag{B4}$$

δ^α is just the ratio of the intrinsic power-law fluxes at the observed and emitted frequencies.

Broadband fluxes are obtained from integrating Eq. (B3) over frequency, and since $d\nu = \delta\, d\nu'$ [Eq. (B2)], these are boosted by another factor of δ

$$F = \delta^4 F'. \tag{B5}$$

The degree of variability in AGN is frequently measured by the change in flux over a given period of time, which from Eqs. (B1) and (B5) is

$$\frac{\Delta F}{\Delta t} = \delta^5 \frac{\Delta F'}{\Delta t'}. \tag{B6}$$

Equations (B4), (B5), and (B6) assume that the emission comes from a moving source, so they apply to the case of discrete, essentially point-like, components. For a smooth, continuous jet, the observed emitting volume is decreased by one power of the Doppler factor because of Lorentz contraction, so that the exponents in Eqs. (B4), (B5), and (B6) become $2+\alpha$, 3, and 4, respectively (Begelman et al. 1984; Cawthorne 1991; Ghisellini et al. 1993).

Relaxing the assumption of isotropic emission in the rest frame can also change the relationship between intrinsic and observed flux. If the source is an optically thin jet with magnetic field parallel to its axis, then in the rest frame $F'_{\nu'}(\theta') \propto (\sin\theta')^{1+\alpha}$. Since $\sin\theta' = \delta \sin\theta$, Eq. (B4) becomes $F_\nu(\nu) = \delta^{(3+2\alpha)} (\sin\theta)^{1+\alpha} F'_{\nu'}(\nu)$ (Cawthorne 1991; Begelman 1993).

So far we have assumed power-law emission in the rest frame. Strictly speaking, for synchrotron emission this would mean the jet is either completely optically thin ($F_\nu \propto \nu^{-\alpha}$, $\alpha \gtrsim 0.5$) or completely optically thick ($F_\nu \propto \nu^{5/2}$). Real jets are probably inhomogeneous and have flat spectra caused by the superposition of individual synchrotron components with different self-absorption frequencies. Relativistic beaming distorts these components differentially because of the dependence of optical depth and F_ν on δ, so the overall spectral shape should change. For a standard conical jet with tangled magnetic field, the integrated flux transforms approximately as $\delta^{2+\alpha}$, where α refers to the observed integrated spectrum rather than the spectral index of the local emission (Cawthorne 1991).

Additional complications in the evaluation of the amplification factor include the lifetimes of the emitting components, the radial dependence of the their emissivities, and the presence of shocks (Lind and Blandford 1985). In the following we will hide all these possibilities in a single parameter, p, by assuming that the observed luminosity, L_j, of a relativistic jet is related to its intrinsic luminosity, $\mathscr{L}_j$, via

$$L_j = \delta^p \mathscr{L}_j, \tag{B7}$$

with $p = 3+\alpha$ for a moving, isotropic source and $p = 2+\alpha$ for a continuous jet (other values are certainly possible).

The recent detection of superluminal motion within our own galaxy (Mirabel and Rodríguez 1994) permits for the first time a direct estimate of p. Since proper motions are measured for both the approaching and receding components, $\beta \cos\theta$ is uniquely determined to be 0.323 ± 0.016 (where β refers to the pattern speed; Mirabel and Rodríguez 1994). Using the observed jet/counterjet ratio, $F_j/F_{cj} = 8 \pm 1$, and assuming the bulk speed in Eq. (A8) is equal to the pattern speed, we find $p = 3.10 \pm 0.25$. One might expect $p = 3+\alpha$ because the components are discrete blobs, whereas our estimate implies $p \approx 2+\alpha$ since the measured spectral index is $\alpha = 0.8$. Alternatively, $p \sim 3.8$ is allowed if the bulk speed is actually lower than the pattern speed, with a ratio $\beta_{\rm bulk}/\beta_{\rm pattern} \sim 0.8$ (cf. Bodo and Ghisellini 1995).

Regardless of the precise value of p, relativistic beaming has a very strong effect on the observed luminosity. A relativistic jet has $\gamma \lesssim \delta \lesssim 2\gamma$ for $\theta \lesssim \arcsin \gamma^{-1}$ (Appendix A), meaning a modest bulk Lorentz factor of $\gamma = 10$ amplifies the intrinsic power by 2–5 orders of magnitude (depending on p). The Doppler boosted radiation is strongly collimated and sharply peaked: at $\theta \sim 1/\gamma \sim 6°$, the observed jet power is already $\sim$4–16 times fainter than at $\theta = 0°$ (for $p = 2$–4). At 90°, the reduction is huge, a factor of $\sim 10^4$–10^8. Although this is a very large ratio, it is actually much smaller than the inferred extinction at optical wavelengths caused by an obscuring torus, which can be up to a factor of 10^{20} (Djorgovski et al. 1991).

APPENDIX C: RATIO OF CORE TO EXTENDED FLUX

The ratio between core and extended flux is an important beaming indicator. We use the observed luminosity ratio, $R = L_{\rm core}/L_{\rm ext}$, which is related to the observed flux ratio via a K correction:

$$R = \frac{F_{\rm core}}{F_{\rm ext}} (1+z)^{\alpha_{\rm core} - \alpha_{\rm ext}} \tag{C1}$$

$$\sim \frac{F_{\rm core}}{F_{\rm ext}} (1+z)^{-1}. \tag{C2}$$

We do not correct for the fact that $F_{\rm ext}$ diminishes faster with redshift than $F_{\rm core}$, as this depends on the source morphology. [In any case it is not a large effect. The corrections calculated by Perlman and Stocke (1993) for 14 BL Lac

objects with redshifts from 0.2 to 0.5 are roughly proportional to $(1+z)^{1.2}$.]

We associate the core with the relativistically beamed jet and the extended power with the unbeamed emission. In terms of the beaming formalism,

$$R=L_j/\mathscr{L}_u=f\delta^p, \tag{C3}$$

where L_j is the observed jet luminosity [Eq. (B7)], $\mathscr{L}_u$ is the unbeamed luminosity, $f\equiv\mathscr{L}_j/\mathscr{L}_u$ is the ratio of intrinsic jet to unbeamed luminosity, δ is the Doppler factor, and p is the appropriate exponent (Appendix B). We call sources "beamed" when $R>R_{\rm min}\sim 1$.

The largest angle between the jet and the line of sight for beamed objects is a critical angle, θ_c, defined by the condition $R_{\rm min}\equiv f\delta^p_{\rm min}$, where $\delta_{\rm min}=\delta(\theta_c)$. That is,

$$\theta_c=\arccos\left\{\frac{1}{\beta}-\frac{1}{\beta\gamma}\left(\frac{f}{R_{\rm min}}\right)^{1/p}\right\}. \tag{C4}$$

Conversely, the largest ratio, $R_{\rm max}\equiv f\delta^p_{\rm max}$, will occur at the smallest angle, $\theta_{\rm min}$. If $\theta_{\rm min}=0°$, as is usually the case, then

$$f=\frac{R_{\rm max}}{[\gamma(1+\beta)]^p}. \tag{C5}$$

If there is a range of Lorentz factors, $R_{\rm max}$ is evaluated at $\gamma_{\rm max}$. If $\theta_{\rm min}\neq 0°$, as is the case for SSRQ, R will be maximum for $\gamma=1/\sin\theta_{\rm min}$.

For large angles ($\theta\gtrsim\arccos[0.5/\beta]$), emission from the receding jet is no longer negligible and Eq. (C3) is replaced by

$$R=f\{[\gamma(1-\beta\cos\theta)]^{-p}+[\gamma(1+\beta\cos\theta)]^{-p}\}. \tag{C6}$$

The relationship between our parameter f and $R_T\equiv R(90°)$ used by other authors (e.g., Orr and Browne 1982) is given by

$$R_T=\frac{2f}{\gamma^p}. \tag{C7}$$

For $\theta_{\rm min}=0°$, $R_{\rm max}=f[\gamma(1-\beta)]^{-p}\simeq f(2\gamma)^p$, so that $R_{\rm max}/R_T\simeq 2^{p-1}\gamma^{2p}$. This implies

$$\gamma\simeq[(R_{\rm max}/R_T)/2^{p-1}]^{1/2p}. \tag{C8}$$

Combining the maximum value of R for a set of beamed objects, $R_{\rm max,b}$, and the minimum value of R for the parent population, $R_{\rm min,unb}$, gives a lower limit to the value of γ (since $R_{\rm max}/R_T\gtrsim R_{\rm max,b}/R_{\rm min,unb}$). In the case of a distribution of γs, the Lorentz factor derived from this argument is the largest one, since that will be responsible both for $R_{\rm max}(\propto\gamma^p)$ and $R_T(\propto\gamma^{-p})$.

APPENDIX D: GLOSSARY OF ACRONYMS

Here we list all the acronyms defined in the text and the section in which they are first found.

AGN: Active Galactic Nuclei, Sec. 1.
BAL: Broad Absorption Line (Quasars), Sec. 2.
BLRG: Broad-Line Radio Galaxies, Sec. 2.
CDQ: Core-Dominated Quasars, Sec. 2.
CSS: Compact-Steep Spectrum, Sec. 6.1.1.
EMSS: (*Einstein* Observatory) Extended Medium Sensitivity Survey, Sec. 5.4.1.
FR I: Fanaroff–Riley Type I, Sec. 2.
FR II: Fanaroff–Riley Type II, Sec. 2.
FSRQ: Flat-Spectrum Radio Quasars, Sec. 2.
FWHM: Full Width Half Maximum, Sec. 5.4.2.
GPS: Gigahertz-Peaked Spectrum, Sec. 6.1.1.
HBL: High (-Energy Cutoff) BL Lacs, Sec. 6.2.6.
HGLS: (*EXOSAT*) High Galactic Latitude Survey, Sec. 6.2.1.
HPQ: Highly Polarized Quasars, Sec. 2.
KS: Kolmogorov–Smirnov, Sec. 5.3.1.
LASS: (*HEAO-1*) Large Area Sky Survey, Sec. 5.4.1.
LBL: Low (-Energy Cutoff) BL Lacs, Sec. 6.2.6.
LF: Luminosity Function, Sec. 5.6.
NELG: Narrow-Emission-Line X-ray Galaxies, Sec. 2.
NLRG: Narrow-Line Radio Galaxies, Sec. 2.
OVV: Optically Violently Variable (Quasars), Sec. 2.
RBL: Radio (Selected) BL Lacs, Sec. 5.4.1.
SSC: synchrotron-self-Compton, Sec. 4.1.
SSRQ: Steep-Spectrum Radio Quasars, Sec. 2.
VLBA: Very Long Baseline Array, Sec. 8.1.3.
VLBI: Very Long Baseline Interferometry, Sec. 4.2.
XBL: X-ray (Selected) BL Lacs, Sec. 5.4.1.

REFERENCES

Abraham, R. G., Crawford, C. S., and McHardy, I. M. 1992, ApJ, 401, 474
Abraham, R. G., Crawford, C. S., Merrifield, M. R., Hutchings, J. B., and McHardy, I. M. 1993, ApJ, 415, 101
Abraham, R. G., McHardy, I. M., and Crawford, C. S. 1991, MNRAS, 252, 482
Abramowicz, M. A. 1992, in Extragalactic Radio Sources: From Beams to Jets, eds. J. Roland, H. Sol, and G. Pelletier (Cambridge, Cambridge University Press), p. 206
Angel, J. R. P., and Stockman, H. S. 1980, ARAA, 8, 321
Antonucci, R. 1984, ApJ, 278, 299
Antonucci, R. 1993, ARAA, 31, 473
Antonucci, R., and Barvainis, R. 1990, ApJ, 363, L17
Antonucci, R., Hurt, T., and Kinney, A. 1994, Nature, 371, 313
Antonucci, R., and Miller, J. S. 1985, ApJ, 297, 621
Antonucci, R., and Ulvestad, J. S. 1985, ApJ, 294, 158
Arnaud, K. A., Johnstone, R. M., Fabian, A. C., Crawford, C. S., Nulsen, P. E. J., Shafer, R. A., and Mushotzky, R. F. 1987, MNRAS, 227, 241
Avni, Y., and Bahcall, J. N. 1980, ApJ, 235, 694
Axon, D. J., Pedlar, A., Unger, S. W., Meurs, E. J. A., and Whittle, D. M. 1989, Nature, 341, 631
Bååth, L. B. 1984, in VLBI and Compact Radio Sources, eds. R. Fanti et al. (Dordrecht, Kluwer), p. 127
Bade, N., Fink, H. H., and Engels, D. 1994, A&A, 286, 381
Bahcall, J. N., et al. 1993, ApJS, 87, 1
Bahcall, J. N., Kirhakos, S., and Schneider, D. P. 1995, ApJ (in press)
Bailey, J., Sparks, W., Hough, J., and Axon, D. 1986, Nature, 322, 150
Barthel, P. D. 1989, ApJ, 336, 606
Barthel, P. D., and Miley, G. K. 1988, Nature, 333, 319
Baum, S. A., and Heckman, T. M. 1989, ApJ, 336, 681
Baum, S. A., Zirbel, E. L., and O'Dea, C. P. 1995, ApJ, 451 (in press)
Begelman, M. C. 1993, in Jets in Extragalactic Radio Sources, eds.

H.-J. Röser, K. Meisenheimer, R. A. Perley, and P. A. G. Scheuer (Berlin, Springer), p. 145
Begelman, M. C., Blandford, R. D., and Rees, M. J. 1984, Rev. Mod. Phys., 56, 255
Bicknell, G. V. 1994, ApJ, 422, 542
Bicknell, G. V., de Ruiter, H. R., Parma, P., Morganti, R., and Fanti, R. 1990, ApJ, 354, 98
Binette, L., Fosbury, R. A. E., and Parker, D. 1993, PASP, 105, 1150
Biretta, J. A., Moore, R. L., and Cohen, M. H. 1986, ApJ, 308, 93
Biretta, J. A., Zhou, F., and Owen, F. N. 1995, ApJ, 447, 582
Blandford, R. D. 1990, in Active Galactic Nuclei, eds. T. J.-L. Courvoisier and M. Mayor (Saas-Fee Advanced Course 20) (Berlin, Springer), p. 161
Blandford, R. D., and Rees, M. J. 1978, in Pittsburgh Conference on BL Lac Objects, ed. A. N. Wolfe (Pittsburgh, University of Pittsburgh Press), p. 328
Bodo, G., and Ghisellini, G. 1995, ApJ, 441, L69
Bridle, A. H. 1992, in Testing the AGN Paradigm, eds. S. S. Holt, S. G. Neff, and C. M. Urry (New York, AIP), p. 386
Bridle, A. H., Hough, D. H., Lonsdale, C. J., Burns, J. O., and Laing, R. A. 1994, AJ, 108, 766
Bridle, A. H., and Perley, R. A. 1984, ARAA, 22, 319
Browne, I. W. A. 1983, MNRAS, 204, 23p
Browne, I. W. A. 1989, in BL Lac Objects, eds. L. Maraschi, T. Maccacaro, and M.-H. Ulrich (Berlin, Springer), p. 401
Browne, I. W. A., and Marchã, M. J. M. 1993, MNRAS, 261, 795
Browne, I. W. A., and Murphy, D. W. 1987, MNRAS, 226, 601
Burbidge, G., and Hewitt, A. 1989, in BL Lac Objects, ed. L. Maraschi, T. Maccacaro, and M.-H. Ulrich (Berlin, Springer), p. 412
Carilli, C. L., Bartel, N., and Diamond, P. 1994, AJ, 108, 64
Cawthorne, T. V. 1991, in Beams and Jets in Astrophysics, ed. P. A. Hughes (Cambridge, Cambridge University Press), p. 187
Celotti, A., Maraschi, L., Ghisellini, G., Caccianiga, A., and Maccacaro T. 1993, ApJ, 416, 118
Chambers, K. C., Miley, G. K., and van Breugel, W. 1987, Nature, 329, 604
Cimatti, A., di Serego Alighieri, S., Fosbury, R. A. E., Salvati, M., and Taylor, D. 1993, MNRAS, 264, 421
Della Ceca, R. 1993, Ph.D. Thesis, University of Bologna
Della Ceca, R., Zamorani, G., Maccacaro, T., Wolter, A., Griffiths, R., Stocke, J., and Setti, G. 1994, ApJ, 430, 533
de Ruiter, H. R., Parma, P., Fanti, C., and Fanti, R. 1990, A&A, 227, 351
De Young, D. S. 1993, ApJ, 405, L13
di Serego Alighieri, S., Binette, L., Courvoisier, T. J.-L., Fosbury, R. A. E., and Tadhunter, C. N. 1988, Nature, 334, 591
di Serego Alighieri, S., Cimatti, A., and Fosbury, R. A. E. 1994a, ApJ, 431, 123
di Serego Alighieri, S., Danziger, J., Morganti, R., and Tadhunter, C. 1994b, MNRAS, 269, 998
di Serego Alighieri, S., Fosbury, R. A. E., Quinn, P. J., and Tadhunter, C. N. 1989, Nature, 341, 307
Djorgovski, S., Weir, N., Matthews, K., and Graham, J. R. 1991, ApJ, 372, L67
Dondi, L., and Ghisellini, G. 1995, MNRAS, 273, 583
Dunlop, J. S., and Peacock, J. A. 1990, MNRAS, 247, 19
Dunlop, J. S., Taylor, G. L., Hughes, D. H., and Robson, E. I. 1993, MNRAS, 264, 455
Economou, F., Lawrence, A., Ward, M. J., and Blanco, P. R. 1995, MNRAS, 272, L5
Edelson, R. A., et al. 1995, ApJ, 438, 120
Elvis, M., Plummer, D., Schachter, J., and Fabbiano, G. 1992, ApJS, 80, 257
Evans, I. N., Ford, H. C., Kinney, A. L., Antonucci, R. R. J., Armus, L., and Caganoff, S. 1991, ApJ, 369, L27
Fabbiano, G., Miller, L., Trinchieri, G., Longair, M. S., and Elvis, M. 1984, ApJ, 277, 115
Fabbiano, G., Willner, S. P., Carleton, N. P., and Elvis, M. 1986, ApJ, 304, L37
Falcke, H., Gopal-Krishna, and Biermann, P. L. 1995, A&A (in press)
Falomo, R., Melnick, J., and Tanzi, E. G. 1992, A&A, 255, L17
Falomo, R., Pesce, J. E., and Treves, A. 1993, ApJ, 411, L63
Falomo, R., Pesce, J. E., and Treves, A., 1995, ApJ, 438, L9
Fanaroff, B. L., and Riley, J. M. 1974, MNRAS, 167, 31p
Fanti, C., Fanti, R., de Ruiter, H. R., and Parma, P. 1987, A&AS, 69, 57
Fanti, C., Fanti, R., O'Dea, C. P., and Schilizzi, R. T. (eds.) 1990a, Compact Steep-Spectrum and GHz-Peaked Radio Sources (Bologna, Istituto di Radioastronomia-CNR)
Fanti, R., Fanti, C., Schilizzi, R. T., Spencer, R. E., Nan Rendong, Parma, P., van Breugel, W. J. M., and Venturi, T. 1990b, A&A, 231, 333
Feretti, L., Comoretto, G., Giovannini, G., Venturi, T., and Wehrle, A. E. 1993, ApJ, 408, 446
Feretti, L., Giovannini, G., Gregorini, L., Parma, P., and Zamorani, G. 1984, A&A, 139, 55
Fleming, T. A., Green, R. F., Jannuzi, B. T., Liebert, J., Smith, P. S., and Fink, H. 1993, AJ, 106, 1729
Franceschini, A., Danese, L., De Zotti, G., and Toffolatti, L. 1988, MNRAS, 233, 157
Fried, J. W., Stickel, M., and Kühr, H. 1993, A&A, 268, 53
Fugmann, W. 1989, A&A, 205, 86
Gabuzda, D. C., Cawthorne, T. V., Roberts, D. H., and Wardle, J. F. C. 1992, ApJ, 388, 40
Gabuzda, D. C., Kollgaard, R. I., Roberts, D. H., and Wardle, J. F. C. 1993, ApJ, 410, 39
Gabuzda, D. C., Mullan, C. M., Cawthorne, T. V., Wardle, J. F. C., and Roberts, D. H. 1994, ApJ, 435, 140
Gallimore, J. F., Baum, S. A., O'Dea, C. P., Brinks, E., and Pedlar, A. 1995, in preparation
Garrington, S. T., and Conway, R. G. 1991, MNRAS, 250, 198
Gehrels, N. 1986, ApJ, 303, 336
Ghisellini, G. 1987, Ph.D. Thesis, SISSA, Trieste
Ghisellini, G., and Maraschi, L. 1989, ApJ, 340, 181
Ghisellini, G., Padovani, P., Celotti, A., and Maraschi, L. 1993, ApJ, 407, 65
Giommi, P., Ansari, S. G., and Micol, A. 1995, A&AS, 109, 267
Giommi, P., et al. 1991, ApJ, 378, 77
Giommi, P., and Padovani, P. 1994, MNRAS, 268, L51
Giovannini, G., Feretti, L., Gregorini, L., and Parma, P. 1988, A&A, 199, 73
Giovannini, G., Feretti, L., Venturi, T., Lara, L., Marcaide, J., Rioja, M., Spangler, S. R., and Wehrle, A. E. 1994, ApJ, 435, 116
Goodrich, R. W., and Cohen, M. H. 1992, ApJ, 391, 623
Gopal-Krishna, and Kulkarni, V. K. 1992, A&A, 257, 11
Gopal-Krishna, Kulkarni, V. K., and Mangalam, A. V. 1994, MNRAS, 268
Gopal-Krishna, and Subramanian, K. 1991, Nature, 349, 766
Gopal-Krishna, and Wiita, P. J. 1993, Nature, 363, 142
Grandi, S. A., and Osterbrock, D. A. 1978, ApJ, 220, 783
Green, R. F., Schmidt, M., and Liebert, J. 1986, ApJS, 61, 305
Halpern, J. P., Impey, C. D., Bothun, G. D., Tapia, S., Skillman, E. D., Wilson, A. S., and Meurs, E. J. 1986, ApJ, 302, 711
Harms, R. J., et al. 1994, ApJ, 435, L35
Hawkins, M. R. S., Véron, P., Hunstead, R. W., and Burgess, A. M. 1991, A&A, 248, 421

Heckman, T. M., O'Dea, C. P., Baum, S. A., and Laurikainen, E. 1994, ApJ, 428, 65
Hes, R., Barthel, P. D., and Fosbury, R. A. E. 1993, Nature, 362, 326
Hes, R., Barthel, P. D., and Hockstra, H. 1995, A&A (in press)
Hill, G. J., Goodrich, R. W., and DePoy, D. L. 1995, ApJ (submitted)
Hill, G. J., and Lilly, S. J. 1991, ApJ, 367, 1
Hine, R. G., and Longair, M. S. 1979, MNRAS, 188, 111
Hjellming, R. M., and Rupen, M. P. 1995, preprint
Holt, S. S., Neff, S. G., and Urry, C. M. (eds.) 1992, Testing the AGN Paradigm (New York, AIP)
Hough, J. H., Brindle, C. B., Axon, D. J., Bailey, J., and Sparks, W. B. 1987, MNRAS, 224, 1013
Hough, J. H., Brindle, C. B., Wills, B. J., Wills, D., and Bailey, J. 1991, ApJ, 372, 478
Hough, D. H., and Readhead, A. C. S. 1989, AJ, 98, 1208
Hoyle, F. R. S., Burbidge, G. R., and Sargent, W. L. W. 1966, Nature, 209, 751
Hunter, S. D., et al. 1993, ApJ, 409, 134
Hutchings, J. B. 1987, ApJ, 320, 122
Hutchings, J. B., Holtzman, J., Sparks, W. B., Morris, S. C., Hanisch, R. J., and Mo, J. 1994, ApJ, 429, L1
Hutchings, J. B., and Morris, S. L. 1995, preprint
Hutchings, J. B., and Neff, S. G. 1992, AJ, 104, 1
Hutchings, J. B., Price, R., and Gower, A. C. 1988, ApJ, 329, 122
Impey, C. D., Lawrence, C. R., and Tapia, S. 1991, ApJ, 375, 46
Inglis, M. D., Brindle, C., Hough, J. H., Young, S., Axon, D. J., Bailey, J. A., and Ward, M. J. 1993, MNRAS, 263, 895
Isobe, T., Feigelson, E. D., Akritas, M. G., and Babu, G. J. 1990, ApJ, 364, 104
Jackson, N., and Browne, I. W. A. 1990, Nature, 343, 43
Jackson, N., and Tadhunter, C. N. 1993, A&A, 272, 105
Jannuzi, B. T., Smith, P. S., and Elston, R. 1994, ApJ, 428, 130
Jones, P. A., McAdam, W. B., and Reynolds, J. E. 1994, MNRAS, 268, 602
Jones, T. W., O'Dell, S. L., and Stein, W. A. 1974, ApJ, 188, 353
Kapahi, V. K. 1987, in Observational Cosmology, eds. A. Hewitt, G. Burbidge, and L. Z. Fang (Dordrecht, Reidel), p. 251
Kapahi, V. K. 1989, AJ, 97, 1
Kapahi, V. K. 1990, in Parsec Scale Radio Jets, eds. J. A. Zensus and T. J. Pearson (Cambridge, Cambridge University Press), p. 304
Kapahi, V. K., Athreya, R. M., Subrahmanya, C. R., McCarthy, P. J., van Breugel, W., Hunstead, R. W., and Baker, J. C. 1994, in Astronomy Posters of the XXII IAU, ed. H. van Woerden (Sliedrecht, Twin), p. 195
Kellermann, K. I., and Pauliny-Toth, I. I. K. 1969, ApJ, 155, L71
Kellermann, K. I., Sramek, R., Schmidt, M., Shaffer, D. B., and Green, R. 1989, AJ, 98, 1195
Kinney, A. L. 1994, in The Physics of Active Galaxies, eds. G. V. Bicknell, M. A. Dopita, and P. J. Quinn, ASP Conf. Series, 54, p. 61
Kniffen, D. A., et al. 1993, ApJ, 411, 133
Kollgaard, R. I. 1994, Vistas Astron., 38, 29
Kollgaard, R. I., Wardle, J. F. C., and Roberts, D. H. 1990, AJ, 100, 1057
Kollgaard, R. I., Wardle, J. F. C., Roberts, D. H., and Gabuzda, D. C. 1992, AJ, 104, 1687
Koratkar, A., Kinney, A. L., and Bohlin, R. C. 1992, ApJ, 400, 435
Kristian, J., Sandage, A. R., and Westphal, J. A. 1978, ApJ, 221, 383
Kurfess, J. D., Johnson, W. N., and McNaron-Brown, K. 1994, in The Gamma Ray Sky Seen with CGRO and SIGMA (in press)
La Franca, F., Gregorini, L., Cristiani, S., de Ruiter, H., and Owen, F. 1994, AJ, 108, 1548
Laing, R. A. 1988, Nature, 331, 149
Laing, R. A. 1994, in The Physics of Active Galaxies, eds. G. V. Bicknell, M. A. Dopita, and P. J. Quinn, ASP Conf. Series, 54, p. 227
Laing, R. A., Jenkins, C. R., Wall, J. V., and Unger, S. W. 1994, in The Physics of Active Galaxies, eds. G. V. Bicknell, M. A. Dopita, and P. J. Quinn, ASP Conf. Series, 54, p. 201
Laing, R. A., Jenkins, C. R., Wall, J. V., and Unger, S. W. 1995, in preparation
Laing, R. A., Riley, J. M., and Longair, M. S. 1983, MNRAS, 204, 151
Laurent-Muehleisen, S. A., Kollgaard, R. I., Moellenbrock, G. A., and Feigelson, E. D. 1993, AJ, 106, 875
Lawrence, A. 1987, PASP, 99, 309
Lawrence, A. 1991, MNRAS, 252, 586
Lawrence, A. 1993, in The Nearest Active Galaxies, eds. J. Beckman, L. Colina, and H. Netzer (Consejo Superior de Investigationes Cientificas), p. 3
Lawrence, A., and Elvis, M. 1982, ApJ, 256, 410
Lawrence, A., et al. 1995, in preparation
Ledden, J. E., and O'Dell, S. L. 1985, ApJ, 298, 630
Lehnert, M. D., Heckman, T. M., Chambers, K. C., and Miley, G. K. 1992, ApJ, 393, 68
Lind, K. R., and Blandford, R. D. 1985, ApJ, 295, 358
Lister, M., Hutchings, J. B., and Gower, A. C. 1994a, ApJ, 427, 125
Lister, M., Gower, A. C., and Hutchings, J. B. 1994b, AJ, 108, 821
Madau, P. 1988, ApJ, 327, 116
Madau, P., Ghisellini, G., and Persic, M. 1987, MNRAS, 224, 257
Madejski, G. M., and Schwartz, D. A. 1983, ApJ, 275, 467
Maraschi, L., et al. 1994a, ApJ, 435, L91
Maraschi, L., Fossati, G., Tagliaferri, G., and Treves, A. 1995, ApJ, 443, 578
Maraschi, L., Ghisellini, G., and Boccasile, A. 1994b, in The Nature of Compact Objects in AGN, eds. A. Robinson and R. J. Terlevich (Cambridge, Cambridge University Press), p. 381
Maraschi, L., Ghisellini, G., and Celotti, A. 1992, ApJ, 397, L5
Maraschi, L., Ghisellini, G., Tanzi, E., and Treves A. 1986, ApJ, 310, 325
Maraschi, L., and Rovetti, F. 1994, ApJ, 436, 79
Marscher, A. P., Marshall, F. E., Mushotzky, R. F., Dent, W. A., Balonek, T. J., and Hartman, M. F. 1979, ApJ, 233, 498
McCarthy, P. J. 1989, Ph.D. thesis, University of California at Berkeley
McCarthy, P. J., van Breugel, and Kapahi, V. K. 1991, ApJ, 371, 478
McCarthy, P. J., Spinrad, H., van Breugel, W., Liebert, J., Dickinson, M., Djorgovski, S., and Eisenhardt, P. 1990, ApJ, 365, 487
McCarthy, P. J., van Breugel, W., Spinrad, H., and Djorgovski, S. 1987, ApJ, 321, L29
McHardy, I. M., Merrifield, M. R., Abraham, R. G., and Crawford, C. S. 1994, MNRAS, 268, 681
Merrifield, M. R. 1992, AJ, 104, 1306
Miller, J. S., Goodrich, R. W., and Mathews, W. G. 1991, ApJ, 378, 47
Mirabel, I. F., and Rodríguez, L. F. 1994, Nature, 371, 46
Miyoshi, M., Moran, J., Herrnstein, J., Greenhill, L., Nakai, N., Diamond, P., and Inoue, M. 1995, Nature, 373, 127
Morganti, R., Fosbury, R. A. E., Hook, R. N., Robinson, A., and Tsvetanov, Z. 1992, MNRAS, 256, 1p
Morganti, R., Killeen, N. E. B., and Tadhunter, C. N. 1993, MNRAS, 263, 1023

Morganti, R., Oosterloo, T. A., Fosbury, R. A. E., and Tadhunter, C. N. 1995, MNRAS (in press)
Morganti, R., Robinson, A., Fosbury, R. A. E., di Serego Alighieri, S., Tadhunter, C. N., and Malin, D. F. 1991, MNRAS, 249, 91
Morris, S. L., Stocke, J. T., Gioia, I. M., Schild, R. E., Wolter, A., Maccacaro, T., and Della Ceca, R. 1991, ApJ, 380, 49
Mulchaey, J. S., Mushotzky, R. F., and Weaver, K. A. 1992, ApJ, 390, L69
Murphy, D. W., Browne, I. W. A., and Perley, R. A. 1993, MNRAS, 264, 298
Mushotzky, R. F., Serlemitsos, P. J., Boldt, E. A., Holt, S. S., and Becker, R. H. 1978, ApJ, 220, 790
Mushotzky, R. F. 1982, ApJ, 256, 92
Netzer, H., and Laor, A. 1994, ApJ, 404, L51
Nilsson, K., Valtonen, M. J., Kotilainen, J., and Jaakkola, T. 1993, ApJ, 413, 453
O'Dea, C. P., Baum, S. A., and Stanghellini, C. 1991, ApJ, 380, 660
Onuora, L. I. 1989, Ap&SS, 162, 343
Onuora, L. I. 1991, ApJ, 377, 36
Orr, M. J. W., and Browne, I. W. A. 1982, MNRAS, 200, 1067
Osterbrock, D. E. 1989, Astrophysics of Gaseous Nebulae and Active Galactic Nuclei (Mill Valley, University Science Books)
Ostriker, J. P., and Vietri, M. 1985, Nature, 318, 446
Ostriker, J. P., and Vietri, M. 1990, Nature, 344, 45
Owen, F. N., and Laing, R. A. 1989, MNRAS, 238, 357
Owen, F. N., and Ledlow, M. J. 1994, in The Physics of Active Galaxies, eds. G. V. Bicknell, M. A. Dopita, and P. J. Quinn, ASP Conf. Series, 54, p. 319
Owen, F. N., Ledlow, M. J., and Keel, W. C. 1995, ApJ (in press)
Owen, F. N., and White, R. A. 1991, MNRAS, 249, 164
Padovani, P. 1992a, A&A, 256, 399
Padovani, P. 1992b, MNRAS, 257, 404
Padovani, P. 1993, MNRAS, 263, 461
Padovani, P., Ghisellini, G., Fabian, A. C., and Celotti, A. 1993, 260, L21
Padovani, P., and Giommi, P. 1995a, ApJ, 444, 567
Padovani, P., and Giommi, P. 1995b, in preparation
Padovani, P., and Urry, C. M. 1990, ApJ, 356, 75
Padovani, P., and Urry, C. M. 1991, ApJ, 368, 373
Padovani, P., and Urry, C. M. 1992, ApJ, 387, 449
Parma, P., et al. 1992, in Astrophysical Jets, Poster Papers from the Space Telescope Science Institute Symposium, eds. D. Burgarella, M. Livio, and C. O'Dea (Baltimore, Space Telescope Science Institute), p. 30
Parma, P., Fanti, C., Fanti, R., Morganti, R., and de Ruiter, H. R. 1987, A&A, 181, 244
Peacock, J. A. 1987, in Astrophysical Jets and Their Engines, ed. W. Kundt (Dordrecht, Reidel), p. 185
Pearson, T. J., and Readhead, A. C. S. 1988, ApJ, 328, 114
Pérez-Fournon, I., and Biermann, P. 1984, A&A, 130, L13
Perlman, E. S., and Stocke, J. T. 1993, ApJ, 406, 430
Perlman, E. S., Stocke, J. T., Shaffer, D. B., Carilli, C. L., and Ma, C. 1994, ApJ, 424, L69
Perlman, E. S., et al. 1995, ApJ (submitted)
Pesce, J. E., Falomo, R., and Treves, A. 1994, AJ, 107, 494
Phillips, M. M., Jenkins, C. R., Dopita, M. A., Sadler, E. M., and Binette, L. 1986, AJ, 91, 1062
Piccinotti, G., Mushotzky, R. F., Boldt, E. A., Holt, S. S., Marshall, F. E., Serlemitsos, P. J., and Shafer, R. A. 1982, ApJ, 253, 485
Pier, E. A., and Krolik, J. H. 1992, ApJ, 399, L23
Pier, E. A., and Krolik, J. H. 1993, ApJ, 418, 673
Pierce, M. J., and Stockton, A. 1986, ApJ, 305, 204
Pogge, R. 1988, ApJ, 328, 519
Pogge, R. W., and De Robertis, M. M. 1993, ApJ, 404, 563
Polatidis, A. G., Wilkinson, P. N., Xu, W., Readhead, A. C. S., Pearson, T. J., Taylor, G. B., and Vermeulen, R. C. 1995, ApJS, 98, 1
Prestage, R. M., and Peacock, J. A. 1988, MNRAS, 230, 131
Quirrenbach, A., Witzel, A., Krichbaum, T. P., Hummel, C. A., Wegner, R., Schalinski, C., Ott, M., Alberdi, A., and Rioja, M. 1992, A&A, 258, 279
Rawlings, S., and Saunders, R. 1991, Nature, 349, 138
Rawlings, S., Saunders, R., Eales, S. A., and Mackay, C. D. 1989, MNRAS, 240, 701
Readhead, A. C. S. 1994, ApJ, 426, 51
Rees, M. J. 1966, Nature, 211, 468
Robinson, A., Binette, L., Fosbury, R. A. E., and Tadhunter, C. N. 1987, MNRAS, 227, 97
Romanishin, W. 1992, ApJ, 401, L65
Rowan-Robinson, M. 1968, MNRAS, 138, 445
Rowan-Robinson, M. 1977, ApJ, 213, 638
Rybicki, G., and Lightman, A. 1979, Radiation Processes in Astrophysics (New York, Wiley)
Saikia, D. J., and Kulkarni, V. K. 1994, MNRAS, 270, 897
Sambruna, R. 1994, Ph.D. thesis, SISSA, Trieste
Sambruna, R., et al. 1995, in preparation
Sanders, D. B., Phinney, E. S., Neugebauer, G., Soifer, B. T., and Matthews, K. 1989, ApJ, 347, 29
Sanders, D. B., Soifer, B. T., Elias, J. H., Madore, B. F., Matthews, K., Neugebauer, G., and Scoville, N. Z. 1988, ApJ, 325, 74
Sarazin, C. L., and Wise, M. W. 1993, ApJ, 411, 55
Scarrott, S. M., Rolph, C. D., and Tadhunter, C. N. 1990, MNRAS, 243, 5P
Schachter, J. F., et al. 1993, ApJ, 412, 541
Scheuer, P. A. G. 1987, in Superluminal Radio Sources, eds. J. A. Zensus and T. J. Pearson (Cambridge, Cambridge University Press), p. 104
Scheuer, P. A. G., and Readhead, A. C. S. 1979, Nature, 277, 182
Schmidt, M. 1968, ApJ, 151, 393
Schneider, D. P., Gunn, J. E., and Hoessel, J. G. 1983, ApJ, 268, 476
Schwartz, D. A., Brissenden, R. J. V., Tuohy, I. R., Feigelson, E. D., Hertz, P. L., and Remillard, R. A. 1989, in BL Lac Objects, eds. L. Maraschi, T. Maccacaro, and M.-H. Ulrich (Berlin, Springer), p. 64
Schwartz, D. A., and Ku, W. H.-M. 1983, ApJ, 266, 459
Singal, A. K. 1988, MNRAS, 233, 87
Singal, A. K. 1993a, MNRAS, 263, 139
Singal, A. K. 1993b, MNRAS, 262, L27
Singal, A. K., and Gopal-Krishna 1985, MNRAS, 215, 383
Smith, E. P., Heckman, T. M., Bothun, G. D., Romanishin, W., and Balick, B. 1986, ApJ, 306, 64
Smith, E. P., and Heckman, T. M. 1989, ApJ, 341, 658
Smith, E. P., and Heckman, T. M. 1990, ApJ, 348, 38
Smith, E. P., O'Dea, C. P., and Baum, S. A. 1995, ApJ, 441, 113
Sparks, W. B., Fraix-Burnet, D., and Macchetto, F. 1992, Nature, 355, 804
Spinrad, H., Djorgovski, S., Marr, J., and Aguilar, L. 1985, PASP, 97, 932
Stiavelli, M., Biretta, J., Møller, P., and Zeilinger, W. W. 1992, Nature, 355, 802
Stickel, M., Fried, J. W., and Kühr, H. 1988a, A&A, 198, L13
Stickel, M., Fried, J. W., and Kühr, H. 1988b, A&A, 206, L30
Stickel, M., Fried, J. W., and Kühr, H. 1993, A&AS, 98, 393
Stickel, M., and Kühr, H. 1993, A&AS, 97, 483
Stickel, M., and Kühr, H. 1994, A&AS, 103, 349
Stickel, M., Meisenheimer, K., and Kühr, H. 1994, A&AS, 105, 211

Stickel, M., Padovani, P., Urry, C. M., Fried, J. W., and Kühr, H. 1991, ApJ, 374, 431
Stocke, J. T., Liebert, J., Schmidt, G., Gioia, I. M., Maccacaro, T., Schild, R. E., Maccagni, D., and Arp, H. C. 1985, ApJ, 298, 619
Stocke, J. T., Morris, S. L., Gioia, I. M., Maccacaro, T., Schild, R., Wolter, A., Fleming, T. A., and Henry, J. P. 1991, ApJS, 76, 813
Stocke, J. T., Wurtz, R., and Perlman, E. S. 1995, ApJ (submitted)
Stocke, J. T., Wurtz, R., Wanf, Q., Elston, R., and Jannuzi, B. T. 1992, ApJ, 400, L17
Sutherland, R. S., Bicknell, G. V., and Dopita, M. A. 1993, ApJ, 414, 510
Tadhunter, C. N., Fosbury, R. A. E., and di Serego Alighieri, S. 1989, in BL Lac Objects, eds. L. Maraschi, T. Maccacaro, and M.-H. Ulrich (Berlin, Springer), p. 79
Tadhunter, C. N., Morganti, R., di Serego Alighieri, S., Fosbury, R. A. E., and Danziger, I. J. 1993, MNRAS, 263, 999
Tadhunter, C. N., Scarrott, S. M., and Rolph, C. D. 1990, MNRAS, 246, 163
Tadhunter, C. N., and Tsvetanov, Z. 1989, Nature, 341, 422
Taylor, G. B., Vermeulen, R. C., Pearson, T. J., Readhead, A. C. S., Henstock, D. R., Browne, I. W. A., and Wilkinson, P. N. 1994, ApJS, 95, 345
Taylor, G. L., Dunlop, J. S., and Hughes, D. H. 1995, MNRAS, in preparation
Teräsranta, H., and Valtaoja, E. 1994, A&A, 283, 51
Thakkar, D. D., Xu, W., Readhead, A. C. S., Pearson, T. J., Taylor, G. B., Vermeulen, R. C., Polatidis, A. G., and Wilkinson, P. N. 1995, ApJS, 98, 33
Tingay, S., et al. 1995, Nature, 374, 141
Tran, H. D. 1995, ApJ, 440, 597
Tribble, P. C. 1992, MNRAS, 256, 281
Turnshek, D. A. 1984, ApJ, 280, 51
Turnshek, D. A. 1988, in QSO Absorption Lines: Probing the Universe, eds. J. C. Blades, D. A. Turnshek, and C. A. Norman (Cambridge, Cambridge University Press), p. 17
Ueno, S., Koyama, K., Nishida, M., Yamauchi, S., and Ward, M. J. 1994, ApJ, 431, L1
Ulrich, M.-H. 1981, A&A, 103, L1
Ulrich, M.-H. 1989, in BL Lac Objects, eds. L. Maraschi, T. Maccacaro, and M.-H. Ulrich (Berlin, Springer), p. 45
Ulvestad, J., Johnston, K., Perley, R., and Fomalont, E. 1981, AJ, 86, 1010
Urry, C. M. 1984, Ph.D. thesis, The Johns Hopkins University
Urry, C. M., et al. 1993, ApJ, 411, 614
Urry, C. M., et al. 1995, ApJ (submitted)
Urry, C. M., Marziani, P., and Calvani, M. 1991b, ApJ, 371, 510
Urry, C. M., and Padovani, P. 1991, ApJ, 371, 60
Urry, C. M., Padovani, P., and Stickel, M. 1991a, ApJ, 382, 501
Urry, C. M., and Shafer, R. A. 1984, ApJ, 280, 569
Vagnetti, F. 1995, in preparation
Vagnetti, F., Giallongo, E., and Cavaliere, A. 1991, ApJ, 368, 366
Vagnetti, F., and Spera, R. 1994, ApJ, 436, 611
Valtaoja, E., Teräsranta, H., Urpo, S., Nesterov, N. S., Lainela, M., and Valtonen, M. 1992, A&A, 254, 80
Venturi, T., Giovannini, G., Feretti, L., Comoretto, G., and Wehrle, A. E. 1993, ApJ, 408, 81
Vermeulen, R. C., and Cohen, M. H. 1994, ApJ, 430, 467
Véron-Cetty, M.-P., and Woltjer, L. 1990, A&A, 236, 69
Véron-Cetty, M.-P., and Véron, P. 1993, A Catalogue of Quasars and Active Nuclei, ESO Scientific Report No. 13, 1993
von Montigny, C., et al. 1995, ApJ, 440, 525
Wall, J. V., and Peacock, J. A. 1985, MNRAS, 216, 173
Ward, M. J., Blanco, P. R., Wilson, A. S., and Nishida, M. 1991, ApJ, 382, 115
Wardle, J. F. C., Moore, R. L., and Angel, J. R. P. 1984, ApJ, 279, 93
Wilkes, B. J. 1986, MNRAS, 218, 331
Wills, B. J., Wills, D., Breger, M., Antonucci, R., and Barvainis, R. 1992a, ApJ, 398, 454
Wills, B. J., Wills, D., Evans, N. J., Natta, A., Thompson, K. L., Breger, M., and Sitko, M. L. 1992b, ApJ, 400, 96
Wilson, A. S., Braatz, J., Heckman, T. M., Krolik, J. H., and Miley, G. K. 1993, ApJ, 419, L61
Wilson, A. S., and Colbert, E. J. M. 1995, ApJ, 438, 62
Wolter, A., Caccianiga, A., Della Ceca, R., and Maccacaro, T. 1994, ApJ, 433, 29
Worrall, D. M., and Birkinshaw, M. 1994, ApJ, 427, 134
Worrall, D. M., and Wilkes, B. J. 1990, ApJ, 360, 396
Wurtz, R., Ellingson, E., Stocke, J. T., and Yee, H. K. C. 1993, AJ, 106, 869
Yanny, B., York, D. G., and Gallagher, J. S. 1989, ApJ, 338, 735
Yates, M. G., Miller, L., and Peacock, J. A. 1989, MNRAS, 240, 129
Yee, H. K. C., and Ellingson, E. 1993, ApJ, 411, 43
Zirbel, E. L., and Baum, S. A. 1995, ApJ, 448, 521